# SYNTHESIS AND APPLICATIONS OF POLYPYRROLE BASED TERNARY NANOCOMPOSITE FOR ELECTROCHEMICAL DETECTION AND REMOVAL OF HEAVY METAL

Thesis Submitted for the Award of the Degree of

## **DOCTOR OF PHILOSOPHY**

in

**Chemistry** 

By

Goverdhan Singh

12014932

Supervised by Dr. Harish mudila (19331)

Associate professor

**Department of Chemistry** 

Lovely professional university Jalandhar, (p.b), india Co-Supervised by
Dr. Anil kumar (22056)
Assistant professor
Department of Chemistry
Lovely Professional University

Jalandhar, (P.B), India



LOVELY PROFESSIONAL UNIVERSITY, PUNJAB 2025 **DECLARATION** 

I, hereby declared that the presented work in the thesis entitled "SYNTHESIS AND

APPLICATIONS OF POLYPYRROLE BASED TERNARY NANOCOMPOSITE

FOR ELECTROCHEMICAL DETECTION AND REMOVAL OF HEAVY

METAL" in fulfilment of degree of Doctor of Philosophy (Ph. D.) is outcome of research

work carried out by me under the supervision of Dr. Harish Mudila and Dr Anil Kumar,

Department of Chemistry, Lovely Professional University, Punjab, India. In keeping with

general practice of reporting scientific observations, due acknowledgements have been

made whenever work described here has been based on findings of another investigator.

This work has not been submitted in part or full to any other University or Institute for the

award of any degree.

Goverdlan Singh

(Signature of Research Scholar)

Goverdhan Singh

Registration No: 12014932

Department of Chemistry,

School of Chemical Engineering and Physical Sciences,

Lovely Professional University, Punjab, India

I

# **CERTIFICATE**

This is to certify that the work reported in the Ph. D. thesis entitled "SYNTHESIS AND APPLICATIONS OF POLYPYRROLE BASED TERNARY NANOCOMPOSITE FOR ELECTROCHEMICAL DETECTION AND REMOVAL OF HEAVY METAL" submitted in fulfillment of the requirement for the reward of degree of Doctor of Philosophy (Ph.D.) in Chemistry, is a research work carried out by Goverdhan Singh, 12014932, is bonafide record of his original work carried out under my supervision and that no part of thesis has been submitted for any other degree, diploma or equivalent course.

Signature of Supervisor

Dr. Harish Mudila
Associate Professor
Department of Chemistry
School of Chemical Engineering
and Physical Sciences, Lovely
Professional University, Punjab,
India Punjab, India

Signature of Co-Supervisor

Dr. Anil Kumar
Assistant Professor
Department of Chemistry
School of Chemical Engineering
and Physical Sciences, Lovely
Professional University, Punjab,
India Punjab, India

#### **ABSTRACT**

Nowadays with increase in the population as well as rapid industrialization leads to affects the quality of the environment. Various pollutants are released into the surroundings that have an adverse effect on the life existing on this planet. A variety of pollutants are present in the environment (inorganic, organic, biological, etc.), but heavy metals due to their nonbiodegradable nature and toxicity are imposing serious threats to the life of this ecosystem. As heavy metals (HM) are released from various anthropogenic and natural processes into the environment, their excess concentration in the environment leads to retard the environment's ability to promote life, which leads to threatening the health of plants, animals, and humans. The contamination of environment by the heavy metals (including Pb<sup>2+</sup>, Cd<sup>2+</sup>, Cu<sup>2+</sup>, etc.) is a serious concern nowadays and hence their determination and removal from the environment to monitor its quality is of supreme importance. A variety of techniques ranging from analytic to electrochemical are employed for the detection of these heavy metal contaminants from various sources. The electrochemical technique because of its simple instrumentation, low cost, and rapid analysis gives extra benefits over other techniques. In spite of the electrochemical technique the type of the electrode material also plays a significant role in detecting the heavy metal ions. A number of electrodes like screen-printed carbon electrodes, gold electrodes, glassy carbon electrodes, carbon paste electrodes, etc. have been employed over the past for the sensing of heavy metal ions. The sensitivity and selectivity of these electrodes can be further enhanced by fabricating them with different types of materials. Therefore, researchers are in demand to improve the electrochemical performance of electrode materials used as HM sensors.

Various types of electroactive materials have been identified to enhance the sensitivity and selectivity of the bare electrodes for heavy metal detection. These are mainly classified as organic materials like conducting polymer (CPs, viz. PPY, PANI, PTH), etc. carbonaceous materials (Graphene/reduced Graphene oxide, Graphene oxide (GO), graphite, CNTs, activated charcoal/carbon, quantum dots, fullerenes, etc.), non-carbonaceous materials like Transition metals (their oxides, halides, carbides, nitrides, hydroxides, etc.) PPY-based electroactive materials have emerged as the potential class for

electrochemical sensing of Pb<sup>2+</sup> ions, which includes PPY-based binary and ternary composite. PPY because of its biocompatibility, high conductivity, low cost, and ease of preparation acts as one of the most reliable materials for the preparation of electrochemical sensors. Certain limitations of PPY like affinity towards agglomerations, poor solubility in water difficulty in their extraction from different mediums render their applications in various fields. To overcome these drawbacks and to improve its electrochemical performance PPY is fabricated using certain Carbonaceous and non-carbonaceous (viz., GO and ZnO respectively) based materials.

The present work focuses mainly on the preparation of the PPY-based binary and then ternary composites in different weight ratios by ex-situ method. The binary composites of PPY with GO at % ratios (mg) as (4:1, 2:1, 1:1, and 1:2) are prepared and the optimized binary composite is then fabricated with ZnO or MnO<sub>2</sub> to synthesize the ternary composites at % ratios (mg) as (2:1, 1:1 and 1:2) using the above-mentioned method. The electrochemical techniques Cyclic voltammetry (CV) and electron impedance spectroscopy (EIS) were used to study the electrochemical behavior of the individual and prepared composites as well as for the optimization of the binary and ternary composite for further studies. The individual as well as composite material was characterized using FTIR, XRD, SEM, XPS and TGA to study its structural, morphological, and thermal properties. The sensing of Pb<sup>2+</sup> ion has been carried out using the DPASV technique on the PG 1 and the ternary PGZ 2 and PGM 1 composite. Electrochemical studies reveal that polypyrrolebased composites exhibit superior detection capabilities for Pb2+ ions at trace levels due to their high surface area, excellent charge transport properties, and specific metal-binding interactions. The electrode material (PGZ 2) shows a linear response ( $R^2 = 0.97$ ) with a limit of detection of  $0.05 \mu M$  for  $Pb^{2+}$  ions within the concentration range of 0.3 to  $3.0 \mu M$ . Similarly, the electrode material PGM 1 shows a linear response ( $R^2 = 0.99$ ) with a limit of detection of 0.03  $\mu M$  for  $Pb^{2+}$  ions within the concentration range of 0.3 to 3.0  $\mu M$ . The interference study of the electrodes (PGZ 2 and PGM 1) in the presence of other metal ions (Cd<sup>2+</sup> and Cu<sup>2+</sup>) shows a good response. These results show that the prepared electrodes can be employed for the detection of other heavy metal ions from various aqueous sources.

Despite the detection of the Pb<sup>2+</sup> ions by the prepared electrodes, these are also helpful in the removal of Pb<sup>2+</sup> ions which has been carried out by UV-visible spectroscopy. PGZ 2 and PGM 1 electrodes show a removal efficiency of 86.92 and 84.89 percent for Pb<sup>2+</sup> ions after 24 hours of contact.

Overall, these PPY-based ternary composites (PGXs) exhibit immense potential as advanced functional materials for the dual detection and removal of toxic metal pollutants. Their synergistic properties arising from composite engineering make them highly efficient, selective, and reusable, addressing key challenges in environmental remediation. Future research will focus on the large-scale production, cost-effectiveness, and integration of these materials into practical sensing and filtration devices for industrial applications. The development of smart, self-healing, and responsive polypyrrole-based composites can further revolutionize environmental monitoring and water purification technologies, ensuring a cleaner and safer ecosystem

### **ACKNOWLEDGEMENT**

I would like to begin by sincerely expressing my gratitude to the Almighty Kul Devta for His abundant blessings, which have guided and supported me throughout my research endeavors, ultimately leading to the successful completion of this academic journey.

I would like to extend my sincere appreciation and heartfelt gratitude to my supervisor, **Dr. Harish Mudila**, Associate Professor at the School of Chemical Engineering and Physical Sciences, Department of Chemistry, Lovely Professional University, Punjab (India). He has been an exceptional mentor, offering unwavering support, especially during the challenging days of the COVID-19 pandemic when I was deeply concerned about my work. This Ph.D. would not have been possible without his invaluable guidance and continuous feedback. I am truly grateful for his encouragement, which has nurtured my research journey and allowed me to grow as a researcher. I am also deeply indebted to my co-supervisor, **Dr. Anil Kumar**, Assistant Professor at the School of Chemical Engineering and Physical Sciences, Department of Chemistry, Lovely Professional University, Punjab (India), for sharing his immense knowledge and vast experience, which greatly inspired my academic pursuits. The unconditional support from Dr. Harish Mudila and Dr. Anil Kumar has been instrumental in making this achievement a reality, and I consider it a true blessing to have pursued my Ph.D. under their mentorship.

I extend my thanks and a deep sense of gratitude to the members of the End Term presentation panel members for providing their valuable suggestions and comments during the research work.

I extend my thanks to the Centre Instrumentation Facility of Lovely Professional University for helping to characterize samples. I also express my thanks to the non-teaching staff of the School of Chemical Engineering and Physical Sciences for their cooperation and assistance in my thesis work.

I want to say words of thanks to my senior, **Dr. Navneet Kour**, for her invaluable suggestions, unwavering support, and companionship throughout this Ph.D. journey. Her words of advice and discussions are always valuable to me throughout this work.

Words are not enough to express my thanks to my juniors cum friends **Adfar Rashid** and **Ankita**. They formed the core of my research time. They have been a true and great supporter and have supported me unconditionally throughout this work.

I would like to dedicate this thesis to my parents. First and foremost, I extend my deepest gratitude to my father, Mr. **Gorkh Nath**, whose unconditional love, unwavering support, and endless sacrifices have made this journey possible. Your words of encouragement and belief in me have been the pillars of my strength, guiding me through every challenge and triumph. I am short of words to express my sincere gratitude to my mother, Mrs. **Pardeso Devi.** From the very beginning, she instilled in me the values of perseverance, integrity, and curiosity, qualities that have shaped both my academic and personal growth. I cannot weigh my feelings in words that lie deep in my heart for my mother. I am profoundly grateful to my parents for their unwavering patience, wisdom, and continuous encouragement. They have been my greatest source of inspiration, constantly reminding me that no dream is beyond reach when pursued with dedication and perseverance.

I would like to express my deepest gratitude to my bestie, **Heema Kumari**, for her unwavering love, patience, and support throughout this journey. Your encouragement, understanding, and belief in me have been my greatest sources of strength and motivation that kept me going. Thank you for being my rock, my inspiration, in this adventure. I am forever grateful to have you by my side.

I also express my regards, love, and affection to my brother **Naresh Singh** and sister **Monika Thakur**, who stood by me through thick and thin and always provided me with cooperation, moral support, and encouragement.

At the end, I would like to thank all the people who contributed to the success of this research work, without whom this research would not have been possible.

Mr. Goverdhan Singh

Research Scholar

## **TABLE OF CONTENTS**

CHAPTER 1	INTRODUCTION			
1.1.	Introduction to heavy metals			
1.2.	Techniques for heavy metal detection			
1.2.1	Spectroscopic techniques			
1.2.2	Optical technique	5		
1.2.3	Electrochemical techniques	5		
1.3	Conducting Polymers (CPs)	7		
1.3.1	Polypyrrole	7		
1.4.	Objectives of the research work	11		
CHAPTER 2				
2.1.	Conducting polymers and CP-based materials for heavy metal sensing	12		
2.2.	PPY as Sensing Material	14		
2.3.	Binary Composites as Sensing Materials	17		
2.3.1.	PPY-based Binary Composites	17		
2.3.2.	TMO-based binary electrode material	20		
2.4.	Ternary composite as sensing material	24		
2.4.1.	PPY-based Ternary Composites	24		
2.4.2.	PANI-based electrode material			
CHAPTER 3	MATERIALS AND METHODS			
3.	Materials and Methods	27		
3.1.	Materials	27		
3.2.	Preparation of Electroactive Materials	27		
3.2.1.	Preparation of Polypyrrole (PPY)	27		
3.2.2.	Preparation of Graphene Oxide (GO)	27		
3.2.3.	Preparation of Polypyrrole/Graphene Oxide (PPY/GO) Binary Composites	29		
3.2.4.	Preparation of Polypyrrole/Graphene Oxide/ZnO	30		
	(PPY/GO/ZnO) Ternary Composites			
3.2.5.	Preparation of Polypyrrole/Graphene Oxide/ MnO2	30		
	(PPY/GO/MnO2) Ternary Composites			
3.3.	Preparation of working electrodes			
3.4	Characterization of PPY, GO, and prepared Composites (PGs and PGXs)	31		
3.4.1.	FT-IR (Fourier Transform Infrared Spectroscopy)	31		
3.4.2.	XRD (X-ray Diffractometry	32		

2.4.2	V 1 4 1 4 (VDC)	32		
3.4.3.	X-ray photoelectron spectroscopy (XPS)			
3.4.4.	SEM (Scanning Electron Microscopy)			
3.4.5.	TGA (Thermogravimetric Analysis)			
3.4.6	UV-Visible Spectroscopy			
3.5.	Electrochemical measurements			
3.5.1	Cyclic Voltammetry (CV) studies	33		
3.5.2.	Differential Pulse Anodic Stripping Voltammetry (DPASV)	34		
3.6.	measurements Probable Mechanism for Heavy Metal Sensing:	34		
3.0.	1 Todadic McChanishi for Ticavy Mctar Schsing.	34		
CHAPTER 4	RESULTS AND DISCUSSION			
4.	Characterization	37		
4.1.	FT-IR of PPY, GO, PG, ZnO, and PGZ Ternary Composite	37		
4.2.	XRD spectra of PPY, GO, PG, ZnO, and PGZ	39		
4.3.	Morphological analysis	41		
4.3.1	XPS Studies of PGZ composite	44		
4.4	Thermal Studies	45		
4.5.	Electrochemical measurements using Cyclic Voltammetry	47		
4.6.	Electrochemical impedance spectroscopy (EIS) studies	50		
4.7.	Electrochemical detection of Pb <sup>2+</sup> using the DPASV technique	52		
4.7.1.	DPASV measurements of different electrodes	52		
4.7.2.	Electrochemical performance of the Electrode material	53		
4.7.3.	Selectivity of the PGZ electrode for sensing Pb <sup>2+</sup> ions	57		
4.7.4.	Reproducibility and stability of the PGZ electrode for sensing Pb <sup>2+</sup> ions			
4.8.	Removal of the Pb <sup>2+</sup> metal ion using PGZ 2 composite	60		
4.9.	FT-IR of PPY, GO, PG, MnO2, and PGM Ternary Composite	62		
4.10.	XRD spectra of PPY, GO, PG, MnO2, and PGM	65		
4.11.	Morphological studies	67		
4.11.1	XPS Studies of PGM composite	69		
4.12.	Thermal Studies	71		
4.13.	Electrochemical measurements using Cyclic Voltammetry	73		
14.	Electrochemical impedance spectroscopy (EIS) studies			
4.15.	Electrochemical detection of Pb <sup>2+</sup> using the DPASV technique			
4.15.1	DPASV measurements of different electrodes			
4.15.2.	Electrochemical performance of the Electrode material	78 80		
4.15.3	Selectivity of the PGM 1 electrode for sensing Pb <sup>2+</sup> ions			
4.15.4	Reproducibility and stability of the PGM 1 electrode for			
	sensing Pb <sup>2+</sup> ions			
4.16.	Removal of the Pb <sup>2+</sup> metal ion using PGM 1 composite			
	· · · · · · · · · · · · · · · · · · ·	88		

5.1.	Conclusion	88
5.2.	Future work	90

# LIST OF FIGURES

Figure No.	Figure Title	Page No.
Figure 1	Typical representation of an electrochemical cell	6
Figure 2	Adsorption of HM ion on the surface of composite materials	10
Figure 3.	ure 3. Scheme showing the synthesis process of polypyrrole	
Figure 4.	Scheme depicting the synthesis process of GO.	29
Figure 5.	Chemical representation of the detection of Pb <sup>2+</sup> ion on PGXs	35
Figure 6.	Graphical representation of the detection of Pb <sup>2+</sup> ion on PGX	36
Figure 7.	FTIR spectra of PPY, GO, PG, ZnO, and PGZ	38
Figure 8.	XRD of PPY, GO, PG, ZnO, and PGZ	40
Figure 9.	SEM micrograph of PPY (A), GO (B), ZnO (C), and PGZ	42
	(D)	
Figure 10.	Mixed elemental mapping of PGZ	43
Figure 11.	Average particle size of PGZ ternary composite	43
Figure 12.	XPS spectral analysis of PGZ Ternary composite	44
Figure 13.	Deconvolution spectra of C 1s, N 1s, O 1s, and Zn 2p of PGZ	45
Figure 14.	TGA of PPY, GO, ZnO, PG, and PGZ (A), Graphical representation of TGA parameter (Tonset, Td, and Char%) of all the samples (B).	47
Figure 15.	CV curves of PPY, GO, and PGs in 5 mM K <sub>3</sub> [Fe(CN) <sub>6</sub> ] and 0.1M KCl	48
Figure 16	CV curves of CPE, ZnO, and PGZs in 5 mM K <sub>3</sub> [Fe(CN) <sub>6</sub> ] and 0.1M KCl	49
Figure 17	Comparative CV graphs of different electrodes at 0.05 V/s scan in 5 mM K3[Fe(CN) <sub>6</sub> ] and 0.1M KCl	50
Figure 18		
Figure 19	Comparative DPASV of CPE, PPY, GO, PG 1, and PGZ 2 at 3.0 µM Pb <sup>2+</sup> ion	52
Figure 20	DPASV curves of PG at various concentrations of Pb <sup>2+</sup> (0.3 to 3.0 μM)	54
Figure 21	Calibration curve of PG 1 at various concentrations of Pb <sup>2+</sup> (0.3 - 3.0 µM)	55
Figure 22	DPASV curves of PGZ 2 at various concentrations of Pb <sup>2+</sup> (0.3 to 3.0 μM)	56

Figure 23	Calibration curve of PGZ 2 composites at various concentrations of Pb <sup>2+</sup> (0.3 - 3.0 µM)			
Figure 24	DPASV results of PGZ 2 composite in the presence of 3.0	58		
	$\mu$ M Pb <sup>2+</sup> ions and in the presence of interference, 1.2 and 3.0 $\mu$ M Cd <sup>2+</sup> and Cu <sup>2+</sup> ions			
Figure 25	Representation of the reproducibility of PGZ 2 electrodes in			
8	$3.0\mu M \text{ Pb}^{2+}$ ion solution.			
Figure 26	Representation of the stability of PGZ 2 electrodes in 3.0µM	60		
C	Pb <sup>2+</sup> ion concentration			
Figure 27	UV-Vis spectra representing the detection and removal of	61		
C	Pb <sup>2+</sup> ions in aqueous solution			
Figure 28	FTIR spectra PPY, GO, MnO2, PG, and PGM.	64		
Figure 29	XRD of PPY, GO, PG, MnO2, and PGM	66		
Figure 30	SEM micrograph of PPY (A), GO (B), MnO2 (C), and PGM	67		
_	(D			
Figure 31	Mixed elemental mapping of PGM	68		
Figure 32	Average particle size of PGZ ternary composite.	69		
Figure 33	XPS spectral analysis of PGM Ternary composite	70		
Figure 34	Deconvolution spectra of C 1s, N 1s, O 1s, and Mn 2p of PGM			
Figure 35	TGA of PPY, GO, ZnO, PG, and PGM (A), Graphical	73		
υ	representation of TGA parameter (Tonset, Td, and Char%) of			
	all the samples (B).			
Figure 36	CV curves of PPY, GO, and PGs in 5 mM K3[Fe(CN) <sub>6</sub> ] and	74		
_	0.1M KCl			
Figure 37	CV curves of CPE, MnO2, and PGMs in 5 mM K3[Fe(CN) <sub>6</sub> ]	75		
_	and 0.1M KCl			
Figure 38	Comparative CV graphs of different electrodes at the scan of	76		
	0.05 V/s 5 mM K3[Fe(CN) <sub>6</sub> ] and 0.1M KCl			
Figure 39	EIS spectra of CPE, PPY, GO, PG 1, and PGM 1 in 5 mM	77		
	k3[Fe(CN) <sub>6</sub> ] an electrolytic solution containing 0.1 M KCl			
Figure 40	Comparative DPASV of CPE, PPY, GO, PG 1, and PGM 1	79		
	at 3.0 $\mu$ M Pb <sup>2+</sup> ion			
Figure 41	DPASV curves of PG at various concentrations of Pb <sup>2+</sup> (0.3	80		
	to 3.0 μM)			
Figure 42	Calibration curve of PG 1 at various concentrations of Pb <sup>2+</sup>	81		
	(0.3 - 3.0 μΜ)			
Figure 43	DPASV curves of PGM 1 at various concentrations of Pb <sup>2+</sup>	82		
	(0.3 to 3.0 μM)			
Figure 44	Calibration curve of PGM 1 at various concentrations of Pb <sup>2+</sup>	82		
	$(0.3 - 3.0 \mu\text{M})$			

Figure 45	DPASV results of PGM 1 in the presence of 3.0 µM Pb <sup>2+</sup> and	83
	in the presence of interference, 1.2 and 3.0 $\mu$ M Cd <sup>2+</sup> and Cu <sup>2+</sup>	
	ions.	
Figure 46	Representation of the reproducibility of PGM 1 in 3.0 μM	85
	Pb <sup>2+</sup> ion solution	
Figure 47	Representation of the stability of PGM 1 in 3.0 µM Pb <sup>2+</sup> ion	86
	solution	
Figure 48	UV-visible spectra representing detection and removal of	87
	Pb <sup>2+</sup> ion in aqueous solution	

# LIST OF TABLES

Table No.	Table Title	Page No.
Table 1	A list of HMs present in potable water with permissible	3
	limits, sources, and probable side effects.	
Table 2	Amount of PPY and GO, corresponding to the ratio for	29
	preparation of PPY/GO composites (PGs)	
Table 3	Amount of PG 1 and ZnO, corresponding to the ratio for	30
	preparation of PPY/GO/ZnO composites (PGZs)	
Table 4	Amount of PG and MnO2, corresponding to the ratio for	31
	preparation of PPY/GO/ MnO2 composites (PGMs)	
Table 5	Important FT-IR peaks of PPY, GO, ZnO, PG, and PGZ	39
Table 6	The removal efficiency of Pb <sup>2+</sup> ion by PGZ composite	62
	with time	
Table 7	Important FT-IR peaks of PPY, GO, MnO2, PG, and	65
	PGM	
Table 8	Removal efficiency of Pb <sup>2+</sup> ion by PGM composite with	87
	time	
Table 9	Results for the sensing of Pb <sup>2+</sup> ions by PGZ 2 and PGM 1	89

# LIST OF ABBREVIATIONS

PPY	Polypyrrole		
OPPY	Overoxidized Polypyrrole		
IIP	Ion-imprinted PPy		
PANI	Polyaniline		
CPE	Carbon paste electrode		
GCE	Glassy carbon electrode		
CNFs	Carbon nanofibers		
SPCE	Screen-printed carbon electrode		
ITO	Indium tin oxide		
LOD	Limit of detection		
Pct	Pectin		
GO	Graphene oxide		
sGO	Cysteine-functionalized graphene		
SGO	oxide		
rGO	Reduced graphene oxide		
ErGO	Electrochemically reduced GO		
ZnO	Zinc oxide		
$MnO_2$	Manganese Dioxide		
PA	Phytic acid		
MWCNT	Multiwalled Carbon Nanotube		
PACh <sup>2-</sup>	2(2-pyridylazo)chromotropic acid		
FACII <sup>2</sup>	anion		
Au	Gold electrode		
WHO	World Health Organization		
EPA	U.S. Environmental Protection Agency		
CV	Cyclic voltammetry		
DPASV	Differential pulse anodic stripping		
DIASV	voltammetry		
FT-IR	Fourier transform infrared		
1.1-11	spectroscopy		
SEM Scanning electron microsc			
XRD	X-ray diffractometry		
TGA	Thermogravimetric Analysis		
XPS	X-ray photoelectron spectroscopy		
LOD	Limit of Detection		
$\mu g L^{-1}$ Microgram per liter			
μΑ	Micro ampere		
·	-		

$\mu\mathrm{M}^{-1}$	Micro perMolar	
PPb	Parts per billion	

CHAPTER 1 INTRODUCTION

\_\_\_\_\_

1.1. Introduction to heavy metals: Heavy metals (HMs) are natural constituents having high atomic mass and density in the range of 5 g cm<sup>-3</sup> compared to other lighter metals. Heavy metals have high electrical conductivity and show a tendency to form cations by the loss of their valence shell electrons. Heavy metals are distributed in various environmental spheres (atmosphere, lithosphere, hydrosphere, and biosphere) in varying amounts and concentrations. (Koller, M., and Saleh, H. M., 2018; Azeh E. G., et al., 2019). Due to the presence of HMs in trace concentrations (ppb range to less than 10 ppm) in various environmental segments, these are also known as trace elements. (Tchounwou, P. B., et al., 2012). Although HMs are the natural constituents distributed on the earth's crust, a large number of anthropogenic activities (agricultural activities, industrial processes, fossil fuel combustion, etc.) and natural processes like soil erosion, volcanic eruptions, etc., are also responsible for their distribution on the earth's crust. During the extraction of HMs from their ores, these are left behind in the soil, spread in large amounts in the environment, and transported to other parts by air and water (Tchounwou, P. B., et al., 2012; Azeh E. G., et al., 2019).

HMs exist in varying amounts and concentrations in the environmental sphere and hence are taken by animals, plants, etc., residing in the contaminated areas. These are also accumulated in the human body through the consumption of these plants, animals, or by using contaminated water. (Ding, R., et al., 2021). Some of the heavy metals, iron, zinc, nickel, etc., when present in required amounts, function as essential nutrients needed for the normal functioning of the human anatomy. Their defect and the excess amount in the body may also lead to adverse effects. Certain HMs like lead, arsenic, mercury, cadmium, copper, etc., even when present in minute concentrations, lead to adverse effects on various biological processes. (Tchounwou, P. B., et al., 2012; Koller, M., and Saleh, H. M., 2018). These HMs are carried and distributed in the body cells and tissues of various organisms through binding with proteins, nucleic acids, etc., leading to the destruction and

alteration of the normal functioning of these macromolecules. The toxicity of heavy metals has several adverse effects on plants, animals, and human beings. In the human body, their toxicity leads to several disorders, and damage to the lungs, kidneys, and blood constituents, leading to several diseases. The accumulation of heavy metals for a long time in the body weakens the neurological, muscular, and physical processes, causing diseases like Alzheimer's, Parkinson's, etc. (Masindi, V., and Muedi, K. L., 2018; Azeh E. G., et al., 2019). Although the mechanism of carcinogenicity and toxicity induced by heavy metals is not elucidated, their toxicological mechanisms of action depend on their unique physicochemical properties. (Tchounwou, P.B., et al., 2012; Sing, G., et al., 2022). As HMs are released from various anthropogenic and natural processes into the environment, their excess concentration in the environment leads to retard the environment's ability to promote life. This leads to threatening the health of plants, animals, and humans. The presence of heavy metals in different environmental segments (air, soil, and water) above their permissible amount alters the system's normal function, which in turn affects the life of this ecosystem. (Ding, R., et al., 2021). The ecosystem can tolerate a limited range of heavy metals, above which they become pollutants in the environment. HMs, like As, Cr, Cu, Hg, Pb, and Zn, are reported in **Table 1**, which shows the contamination source, side effects, and permissible limits of these HMs. The most prevailing pollutants in the environment by States Environmental Protection Agency (USEPA) report. (Verma, S., et al., 2021; Mitra, S., et al., 2022).

Table 1. A list of HMs present in potable water with permissible limits, sources, and probable side effects.

Heavy metals	Permissible limit (mg/L, WHO)	Sources from where they contaminate water	Side effects	Reference
Pb	0.05	PVC pipes, natural and household plumbing systems, etc.	Anemia, learning and behavioral disturbances, etc.	Puri and Kumar (2012), Sanyal et al (2020)
Cd	0.005	Industrial, household, vehicular, and other wastes, etc.	It affects the CNS, teratogenesis, carcinogenesis, numerous body parts, etc.	Mudila et al (2018), Sanyal et al (2020)
Hg	0.001	Use of fertilizers etc.	Depression, carcinogenic, etc.	Mudila et al (2018), Sanyal et al (2020)
Fe	0.1	Industrial processes, sewage discharges, etc.	Haemorrhagicnecrosis. Hemochromatosis etc.	Mudila et al (2018), Sanyal et al (2020)
Cr	0.1	Use of fertilizers, industrialization, etc.	Organ failure, liver damage, carcinogenic effects, etc.	Puri and Kumar (2012), Sanyal et al (2020)
As	0.01	Natural and anthropogenic sources.	Leucomelanosis, keratosis, skin cancer. CNS disturbance etc.	Mudila et al (2018), Sanyal et al (2020)

The contamination of the environment by heavy metals is a serious concern nowadays, and hence their determination and removal from the environment to monitor its quality is very important. (Masindi, V., and Muedi, K. L., 2018; Ding, R., et al., 2021). Various organizations like the Environmental Protection Agency (EPA), World Health Organization (WHO), etc., have set certain permissible limits of concentrations of heavy metals to be present in various samples in the environment. Therefore, the detection and removal of their quantities present in the various samples is of supreme importance in monitoring environmental quality. The determination of these HMs is not possible through sight, smell, or taste; highly selective and sensitive techniques are required for their detection from the various samples of air, food, water, soil, etc. (Bansod, B., et al., 2017; Mudila, H., et al., 2018)

- **1.2. Techniques for heavy metal detection:** Different types of techniques are employed for the determination of these heavy metal contaminants from various sources. These include spectroscopic, optical, and **electrochemical** techniques, each having its own benefits and limitations.
- 1.2.1. Spectroscopic techniques: A large number of spectroscopic methods like Inductively coupled plasma mass spectroscopy (ICP-MS), Neutron activation analysis (NAA), X-ray Fluorescence Spectrometry (XRF), etc. are used detection/determination of HMs from various intricate mediums present in the environments (Bansod, B., et al., 2017). These analytical techniques are fast operating, sensitive, and highly selective, and used for the determination of a variety of trace and ultra-trace elements with low detection limits, having good accuracy, and with a minimum level of interference from other elements present in the sample. Although these techniques are convenient, have broad applications, but have a high cost and a complex operating system, which requires an expert to operate. Due to the heavy operating system used in these techniques, these are not carried to the field for analysis purposes. For the analysis of multiple elements, these techniques require changing the light source and coupling with other chromatographic techniques for quantitative analysis. These techniques require the

sample to be pre-transformed into a solution, and the risk of sample storage and handling increases. (Jin, M., et al., 2020)

- **1.2.2.** Optical technique (Spectrophotometric measurements) is also used for the determination of heavy metal ions. These techniques are also not the most reliable for infield applications because of their multipart equipment, including photodetectors, lasers, and high power required for their operations, and the high cost of the equipment. All these require extra care and precision for their operation in the determination of heavy metals.
- **1.2.3. Electrochemical techniques:** as compared to other techniques employed for heavy metal detection, they are simple, reliable, low-cost, suitable for short analytical time for insitu and on-line measurements, and hence are employed largely in the area of research. A large number of techniques are available for the determination of HMs. Some of these techniques involve Cyclic voltammetry (CV), Differential pulse anodic stripping voltammetry (DPASV), Linear sweep voltammetry (LSV), and square wave anodic stripping voltammetry (SWASV). These techniques require a simple procedure, in which the contaminated samples of interest to be monitored are fabricated even on small circuits. Although electrochemical methods are the most reliable and are being used by researchers, these methods also have some drawbacks. These methods have poor sensitivity, lower value of the limit of detection (LOD), and poor reproducibility and stability; therefore are not useful in the detection/determination of HMs in real samples and complex matrices. Due to the interference of some materials like quantum dots and mercury, these methods require consideration before they are applied to Heavy metals in real water samples and other environmental spheres. The LOD and sensitivity of these techniques are enhanced by the fabrication of different sensing electrodes with these techniques. (Bansod, B., et al.,2017; Ramalechume, C., et al.,2020)

The instrument/cell employed for the detection of heavy metals electrochemically consists of three electrode systems i. The reference electrode (**RE**), ii. Working electrode (**WE**), and iii. Counter electrode (**CE**). **Fig. 1**.

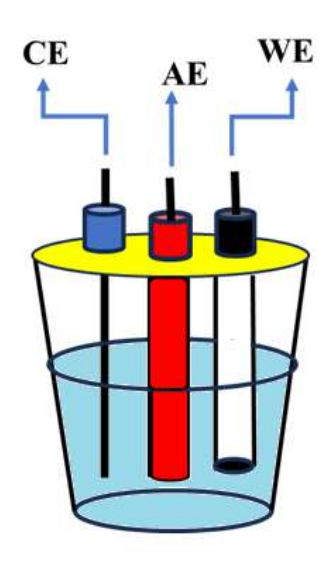


Figure 1: Typical representation of an electrochemical cell

All three electrodes are placed in an electrolytic cell containing an electrolytic solution. The surface of the **WE** is modified with different materials to provide a better surface area for HM ions. During the operation of the cell, oxidation or reduction of HM by the loss or gain of electrons takes place on the surface of the working electrode. As a result, the current flows between **WE** and the **CE**, and the relationship between the concentration/amount of HM ions and the current is obtained. A high input impedance device is used to measure the potential between **WE** and **RE** and to stop the reversal of current from the working electrode. (**Bansod**, **B.**, et al., 2017; WU, Q., et al., 2021).

The results obtained during the electrochemical process largely depend on the category of electrode employed as the WE. The limitations of bare electrodes, like slow charge transfer kinetics, low selectivity and sensitivity, overpotential for surface reactions, and poor current signal in the electrochemical process, render their applicability in sensing. To overcome these limitations, researchers are exploring various binding materials on the surface of bare electrodes to increase their sensitivity and selectivity. Various methods like drop-casting, electro-polymerization, doping, and chemical layer-by-layer methods are employed to modify the conventional electrode surface. A variety of materials, ranging from conducting polymers, carbon-based materials, and transition metal oxides etc., have

been employed by the researcher to enhance the electrochemical activity of the unmodified electrode. (Islam, S., et al.,2021; WU, Q., et al.,2021)

- 1.3. Conducting Polymers (CPs): CPs are also named synthetic metals because of their similarities in properties (electrical and electrochemical) with traditional semiconductors and metals. The addition/removal of electrons from the  $\pi$ -bonded polymer results in the generation of charge carriers, promoting the charge transfer reactions. The conductivity can be improved by many factors, like alteration in temperature, doping, etc. CPs are used in the applicable field of capacitors, actuators, sensors, biosensors, etc. (Le, T.H., et al., 2017). Conducting polymers like Polypyrrole (PPY), Polyaniline (PANI), Polyacetylene (PACE), Polythiophene (PTH), etc. have specific properties viz. physical, mechanical, chemical, electrical, environmental stability, low cost, easy formation (via chemical or electrochemical processes), tunable charge transfer ability (via copolymerization or structural derivations), and adaptability which make them suitable to be used for different application including sensors (Bai, H., and Shi, G., 2007).
- 1.3.1. Polypyrrole (PPY): PPY, likewise other CPs, has a conjugated system of  $\pi$ -electron cloud that can be prepared by an oxidative polymerization process by deposition at the electrode surface chemically or electrochemically. PPY is considered an important CP due to its good electrical/electrochemical properties, better stability to exist in the environment in ambient conditions, and lesser toxicological harms. Likewise, other CPs PPY can also conduct electricity owing to their conjugated system and thus find their explicit technological application in supercapacitors, corrosion inhibition, light-weight batteries, EMI shielding, and a variety of sensors. (**Kumar A., et al., 2020**). PPY, because of its low cost, high conductivity, and ease of preparation, acts as a reliable material for the fabrication of electrochemical sensors. Numerous research works on PPY (and functionalized PPY) show that it is used for the sensing of large numbers of heavy metals. PPY exhibits a high electrical conductivity of  $10^2$  S/cm (comparable to In and Sn). PPY (bound with epoxy, Opuntia Ficus Extract) based heavy metal sensor has been employed for the determination of HMs (Pb<sup>2+</sup>, Cd<sup>2+</sup>, Cu<sup>2+</sup>, and Zn<sup>2+</sup> ions). (Quintana, H., et al., 2013). Conductive PPY NPs were successfully synthesized using CQAS (chitosan

quaternary ammonium groups) and LSN (lignosulfonate) as dispersants. A PPY NPs-modified on GCE was designed as an electrode material, enabling highly sensitive detection/determination of Pb<sup>2+</sup> with a low LOD of 0.055 μmolL<sup>-1</sup> in the concentration range of 0.1–50 μmolL<sup>-1</sup> (**Xu, T., et al., 2020**). PPY coated with Sulphur-containing carboxy methyl ion-imprinted polymers (S-IIPs) modified on GCE was used for the detection of Hg<sup>2+</sup> in water using SWASV. The developed sensor has a LOD of 0.1 μgL<sup>-1</sup> within the concentration range of 20-800 μgL<sup>-1</sup> for Hg<sup>2+</sup> ions. (**Velempini, T.,et al., 2018**)

Both the performance and properties of PPY, like other CPs, are enhanced with the introduction of nano dimensions to it and hence are of significant importance in diverse fields of research. PPY nanomaterials have increased surface area as compared to simple PPY and hence are a potent component for the fabrication of various sensing materials used in the detection of heavy metals and other analytes. (Harlin, A., and Ferenets, M., 2006). New developments in the fields of nanotechnology and nanoscience have been achieved over the last few years by the combination of different carbon nanomaterials (graphene, CNTs, carbon nanofillers, etc.). These carbon nanomaterials are combined with PPY and are employed as sensing materials in diverse fields. Due to the enlarged surface area and large penetration depth of these nanostructured PPY, they facilitate the diffusion of the analyte to a much greater extent. The use of these nanostructured PPY also results in the improvement of the detection limits. Nanostructured PPY used as sensing material includes nanowires, nanofibers, nanotubes, etc. (Fourati, N., et al., 2016; Oularbi, L., et al.,2017). Some unique and advantageous physical, chemical, and electronic properties of PPY and its composites with Graphene, MWCNTs, metal, metal oxide NPs, etc., allow it to be a potent material in electrochemical sensing of HMs present in various samples. (Naveen, M. H., et al., 2017). A PPY/rGO hydrogel composite was employed by (Suvina., V., et al., 2018) for the sensing of HMs (Hg<sup>2+</sup>, Cu<sup>2+</sup>, Cd<sup>2+</sup>, and Pb<sup>2+</sup>). The sensor shows the detection limits much lower than the limits given by the WHO and other polymer-based heavy metal sensors. From their studies, they concluded that the high surface area (21.48 m<sup>2</sup> g<sup>-1</sup>) and increased pore volume of PPY/rGO hydrogel composite result in the accumulation of large metal ions on its surface and hence enhance the sensitivity of the

material for HMs sensing. A low LOD (0.3 nM) for Pb<sup>2+</sup> metal ions was reported in their studies. An ion-imprinted polypyrrole (IIP) and reduced graphene oxide (IIP/rGO) based binary composite was employed by (Hu, S., et al., 2019) to detect Cd<sup>2+</sup> in water. The increased surface area of (IIP/rGO) results in the fast electron transfer kinetics among Cd<sup>2+</sup> and the electrode surface. A LOD of 0.26 µg/L was reported for the trace level of Cd<sup>2+</sup> in water samples. A rapid, sensitive, and selective electrochemical sensor for Pb2+ ions detection was fabricated by (Rong., R., et al., 2017) employing PPY/rGO nanocomposite. Because of its polyporous structure, and ease of synthesis, the sensor renders decent reproducibility, selectivity, and long-term stability it acts as a potent material for the determination of Pb2+ ions. The result of Pb2+ on the PPY/rGO modified electrode was linear, with a LOD of 4.7× 10<sup>-11</sup> mol/L. (Zhuang., Y., et al., 2018) reported a high electrochemical response for Hg<sup>2+</sup> using PPY/rGO/ZnO composite with an interference barrier. The physical barrier acts as a shield for the electroactive material and as a driving force for electrochemical detection with outstanding anti-interference capacity because of the Schottky barrier. Differential pulse voltammetry (DPV) was used for detecting the Hg<sup>2+</sup> electrochemical behavior with varying concentrations, and a sensitive and high response was obtained with a change in the concentration of Hg<sup>2+</sup> using PPY/rGO/ZnO composite in comparison to the PPY/rGO and PPY/ ZnO composites under the same conditions.

Likewise, the detection of heavy metals involves various detection technique, numerous methods have also been employed for the removal of HMs ions from aqueous sources. These methods include adsorption, membrane filtration, ion exchange, electrodeposition, coagulation–flocculation, and chemical precipitation. Each method has its own mechanism, benefits, and loopholes compared to others. Among the various treatment methods for HM–contaminated effluents, adsorption and ion reduction emerge as the two most prominent mechanisms.

Adsorption-based technologies are extensively applied in environmental remediation to mitigate industrial pollution, particularly in the purification of wastewater, potable water, and other aqueous effluents. Fundamentally, adsorption is a surface-driven phenomenon in which HM ions or atoms interact through physical or chemical forces with

the surface of the adsorbent. Surface atoms possess higher energy than those within the bulk material because they are not fully coordinated by neighboring atoms, thereby facilitating adsorption. The process becomes more pronounced as the number of active sites on the adsorbent surface increases. Consequently, a thin layer of adsorbate is formed over the active surface of the adsorbent. The key advantages of this technique include its simple operation, versatility, time efficiency, and cost-effectiveness (depending on the adsorbent used). Additionally, the adsorbent can often be recovered and reused for multiple cycles, while maintaining a high capacity for capturing heavy metal ions. (Yadav, V. B., et al 2019; Sosa Lissarrague, M. H., et al, 2023).

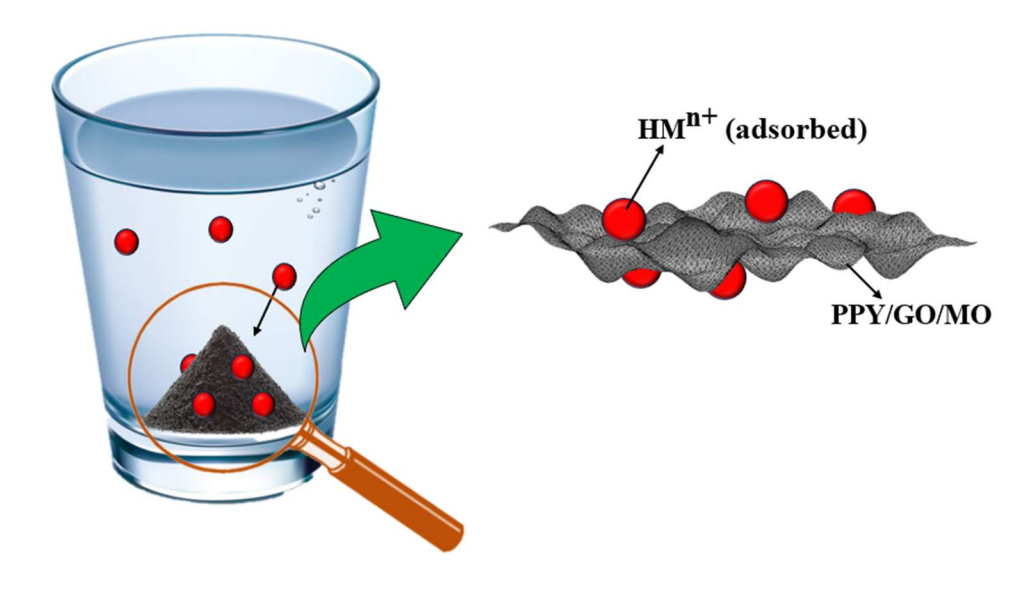


Figure 2: Adsorption of HM ion on the surface of composite materials

In this work, the adsorbent used for removing Pb<sup>2+</sup> metal ions from aqueous sources is the ternary composite of PPY/GO/ZnO and PPY/GO/MnO<sub>2</sub>. The presence of PPY, GO, and TMOs (ZnO and MnO<sub>2</sub>) leads to the synergistic effect in the ternary composite. the improved structural framework, enhanced surface area, conductivity, and redox behavior of the composite material facilitate the adsorption and fast adsorption kinetics on its surface. The improved surface area and the presence of different oxygen functionalities in the ternary composite result in the adsorption of Pb<sup>2+</sup> ions from the aqueous sources through Electrostatic attractions, surface complexation, π-π stacking etc.

Though a number of materials had been used for effective determination and decontamination of aqueous sources from a variety of heavy metals, but still a significant material with maximum efficiency and minimum hazard is to be searched. Researchers employed various types of materials for the same (as mentioned in the previous section), individual, binary, and ternary components with their certain benefits, which had been considered. However, most of them are set back with limited efficiency, high cost, environmental hazards, and time-consuming, so a more perfect material is to be sought. In this direction, we proposed a ternary material of PPY/Graphene/TMO for effectively detecting these heavy metals from water wastes. This proposed material will have the essence of all three components, which have their benefits and can overcome certain loopholes.

### 1.4. Objectives of the research work

The specific objectives of the research topic are

- 1. Preparation of polypyrrole, and Graphene oxide/Graphene using graphite
- 2. Fabrication of Polypyrrole (PPY) based ternary nanocomposites using transition metal oxides (TMO) and Graphene oxide /graphene in varying concentrations
- 3. Detection and removal of heavy metals with electrochemical techniques using Polypyrrole based nanocomposites

\_\_\_\_\_

2.1. Conducting polymers (CPs) and CP-based materials for heavy metal sensing: In contrast to conventional organic polymers, conducting or conjugated polymers are a new class of materials with fewer monomer units. Conducting polymers consist of alternate single and double bonds in which the delocalization of the  $\pi$ -bonds results in the generation of a variety of charge carriers, like bipolarons, solitons, polarons, etc. The exceptional physical properties of conducting polymers, largely dependent on their size and length, include low cost and lightweight, corrosion resistance, and exceptional optical, electrical, mechanical, and conducting properties. Some of the CPs include polypyrrole (PPY), polyaniline (PANI), poly(para-phenylene) (PPP), polyacetylene (PA), polythiophene (PTH), etc. (Naveen, M. H., et al., 2017; K, N., and Rout, C. S., 2021)

PPY, likewise, other CPs have a conjugated system of  $\pi$ -electron cloud that can be prepared by an oxidative polymerization process by deposition at the electrode surface, chemically or electrochemically, both involving electron transfer. The chemical oxidative method is most frequently preferred to the electrochemical method because of the better structural feature and higher mass of the resulting polymer. (Fourati, N., et al., 2016). The effect of oxidants (ferric chloride and ammonium persulfate) on the morphology of PPY and hence on the conductivity and stability was studied by (Yussuf, A., et al., 2018). The conductivity of PPY synthesized using ferric chloride as an oxidant is higher than that of ammonium persulfate. This enhancement in conductivity may be ascribed to the difference in structures and the mode of interaction of oxidants with monomer pyrrole during PPY synthesis. The stability, melting point, glass transition temperature, etc., of the PPY are also influenced by the ratio of monomer to oxidant.

PPY is considered an important CP due to its good electrical/electrochemical properties, better stability to exist in the environment in ambient conditions, and lesser toxicological harms. The mechanical properties, processability, and other physiological characteristics of PPY can be enhanced by amalgamating it with other CPs or by forming copolymers of PPY. These PPY-based composites/nanocomposites possess electrical

properties similar to those of metals or semiconductors and thus have found their application in diverse fields. PPY, because of its great conductivity, cost effectiveness, and simple preparation, acts as a reliable material for the fabrication/generation of electrochemical sensors. Many studies on the PPY (and functionalized PPY) show that it is used for the detection of large numbers of heavy metals from various sources (Harlin, A., and Ferenets, M., 2006; Yussuf, A., et al., 2018). Despite numerous advantages of PPY structural degradation, like agglomeration of such materials during the charging/discharging process can seriously disrupt the cyclability and rate capability performance of PPY towards the sensing of HMs. To overcome these limitations, certain materials like carbonaceous-based and metal nanoparticles have been used by the researcher in combination with the PPY to improve the stability and the electrochemical performance of the employed modified electrodes toward the detection of HMs (Cui, L., et al., 2015).

Graphene oxide (GO), a 2D carbonaceous material synthesized from graphite, results in a layered structure having oxygen functionalities (carbonyl, carboxyl, epoxide, and hydroxyl groups, etc.) present on its edges as well as on the basal planes. These oxygen functionalities on the surface of GO act as an active center for the redox reactions to take place and binding sites for its surface modifications making it a potent material to detect the presence of analytes in various samples and for surface modifications of electrodes (Chang, J., et al., 2014; Islam, S., et al.,2021). With certain remarkable properties (high surface area, mechanical stiffness, etc.,) GO is an excellent material for developing high-performance platforms across various applications. However, its tendency to restack and irreversibly agglomerate—driven by  $\pi$ - $\pi$  interactions and weak physical forces—can lead to the formation of graphite. To enhance graphene's sensing capabilities and mitigate this aggregation, surface functionalization or the incorporation of other components is necessary. (Akhtar, M., et al., 2020). Integrating graphene oxide (GO) with other components, like conducting polymers (CPs) and metal oxides (TMOs), enhances its electrochemical performance. This improvement is due to a synergistic effect that stabilizes

the structure, reduces the ion diffusion path, and facilitates rapid electron transport on their surface. (Ghanbari, K., and Bonyadi, S.,2018).

TMOs are the most important class of materials that have found their potential in various areas, including their use as adsorbent for the removal of heavy metals pollutants from various sources. TMOs have certain remarkable properties that enable them to find wide applications in electrochemical sensing, electrode materials in metal ion batteries, etc. The roughened surface and small size (nanoscale) of these TMOs allows them to modify a variety of electrodes and in the determinations of various analytes electrochemically. A wide area of bio and electrochemical sensing, catalysis, etc., is enhanced by the use of these TMOs because of their fast electron kinetics. The better sensitivity and selectivity in enhancing catalytic activity depend on the morphological shapes of TMOs (Agnihotri, A. S., et al., 2021; Seisenbaeva, G. A., et al., 2014).

2.2. PPY as Sensing Material: Oularbi, L., et al., (2017) developed a nanocomposite of PPY and carbon nanofibers (CNF) modified on the carbon paste electrode (CPE) (PPY/CNF/CPE) for determining Pb<sup>2+</sup>. The unique properties of both PPY and CNF were fabricated on the surface of CPE by dispersion of functionalized CNFs and electropolymerization of PPY using galvanostatic mode. The electro-polymerization of the PPY on CPE and CNF/CPE was carried out using CV in LiClO<sub>4</sub> (0.25 M) electrolyte at 0.05 V/s scan rate. Well-defined redox peaks in PPY/CPE and PPY/CNF/CPE were obtained. The enhancement of the redox peaks and decreased peak separation in PPY/CNF/CPE compared to PPY/CPE were reported, which is attributed to the presence of CNF that improves the electron transfer ability of the PPY in the composite. The interfacial behavior of the respective electrode material was further studied using EIS studies. In the case of PPY/CNF/CPE the charge transfer resistance is found to be lower as compared to the CPE, CNF/CPE, and PPY/CNF electrode which is credited to the synergetic influence of both CNF and PPY that facilitates the fast electron transfer reaction of [Fe(CN)6] <sup>3-/4-</sup> SWASV was employed for the Pb <sup>2+</sup> detection in acetate buffer having acidic pH (4.5). An anodic stripping peak with enlarged intensity due to the oxidation of Pb to Pb<sup>2+</sup> ion was encountered on the modified electrode (PPY/CNF/CPE). The improved intensity of stripping peak value on PPY/CNF/CPE compared to the other electrodes resulted from the improved/enhanced surface area, decent electrical conductivity, and the chelating effect of PPY for Pb in the composite material. A LOD of 0.05 µgL<sup>-1</sup> for the Pb<sup>2+</sup> ions was reported.

**Zhang, H., et al. (2023).** developed a PPY functionalized by phytic acid (PA/PPY) electrode fabricated on SPCE for the electrochemical sensing of Pb<sup>2+</sup> ion using Differential pulse anodic stripping voltammetry (DPASV) within the concentration range of 10 to 600 nM. The sensor (PA/PPY/SPCE) exhibits decent stability with a relative standard deviation (RSD) of 3.1%, repeatability RSD of < 2%, and a low LOD of 0.43 nM, demonstrating exceptional detection capabilities. Additionally, the sensor has a high recovery rate (>93%) and exhibits promising findings in the sensing of Pb<sup>2+</sup> ions in water samples. **Lo, M., et al., (2018)** employed PPY bonded with benzene sulfonic acid (BSA) modified with aminobenzenediazonium-based ITO electrode (PPY/ ITO-AP) for the determination of HMs (viz., Cd<sup>2+</sup>, Cu<sup>2+</sup>, and Pb<sup>2+</sup>) by DPV. LODs of 0.99, 8.95, and 11.6 nM Pb<sup>2+</sup>, Cd<sup>2+</sup>, and Cu<sup>2+</sup> were reported, which are lower than the reported by WHO. The electrode film shows greater selectivity with distinguishable and remarkable peaks of interfering metal ions at same and different concentrations. Diazonium salt plays a key role in sticking PPY films to the ITO's surface, thus constructing the electrode (PPY/ ITO-AP) useful for the sensing of HMs in an aqueous medium.

Wanekaya, A., and Sadik, O. A., (2002) prepared an overoxidized Polypyrrole (OPPY) doped with 2(2-pyridylazo) chromotropic acid anion (PACh<sup>2-</sup>) electrode for the sensing of Pb<sup>2+</sup> ion using the DPASV technique. Comparative CV studies were performed in the presence of Pb<sup>2+</sup> ions using PPY/PACh<sup>2-</sup> and OPPY/PACh<sup>2-</sup> electrodes. Voltammograms reveal that OPPY/ PACh<sup>2-</sup> electrode shows well-defined and sharp peaks of Pb<sup>2+</sup> ion compared to PPY/ PACh<sup>2-</sup>. This may be occurring because of the strong complexing tendency of the HM ions with the anion PACh<sup>2-</sup> and the elimination of the background as observed in the case of the PPY/ PACh<sup>2-</sup> electrode. well-defined stripping peaks with a LOD of 10 ng/ml for Pb<sup>2+</sup> ion on OPPY/ PACh<sup>2-</sup> electrode were reported using DPASV measurements. The results of both measurements (CV and DPASV) for the sensing of Pb<sup>2+</sup> ion using PACh<sup>2-</sup> based electrode are in agreement with each other. The

electrochemical response of the Pb<sup>2+</sup> ion on PPY doped with iminodiacetic acid (IDA) modified on CPE has been studied by Joseph, A., et al., (2014) using DPASV. CPE/PPY-IDA modified electrode shows better electrochemical response for the sensing of Pb<sup>2+</sup> ion compared to the bare CPE electrode. This occurs as a result of the binding of Pb2+ ions to the surface of PPY-IDA containing carboxyl groups, thus leading towards the accumulation of a large number of metal ions on its surface, resulting in a higher peak response when compared to the bare electrode. The stripping peak response for other divalent metal ions (Zn<sup>2+</sup>, Cd<sup>2+</sup>, Co<sup>2+</sup>, Hg<sup>2+</sup>, Ni<sup>2+</sup>, and Cu<sup>2+</sup>) was also studied within the working concentration of  $Pb^{2+}$  (1 × 10<sup>-6</sup> M or less). Studies show that only  $Cu^{2+}$  and  $Cd^{2+}$ show stripping behavior at this concentration. The stability constant of Cu<sup>2+</sup> is higher compared to Cd<sup>2+</sup>, also the response of Pb<sup>2+</sup> is lower than both Cu<sup>2+</sup> and Cd<sup>2+</sup> ions. The sensitivity of the CPE/PPY-IDA electrode material is also influenced due to foreign metal ions. Studies show that the current response of the Pb<sup>2+</sup> ion reduces in presence of  $1 \times 10^{-5}$ M interference metal ion (Cu<sup>2+</sup> and Cd<sup>2+</sup>) whereas in the presence of Hg<sup>2+</sup> ion response increases compared to that of an individual Pb<sup>2+</sup> stripping response in the absence of interfering ions. CPE/PPY-IDA electrode shows a good correlation for the sensing of Pb<sup>2+</sup> ion within the range of  $1 \times 10^{-6}$  M to  $5 \times 10^{-9}$  M with LOD of  $9.6 \times 10^{-9}$  M.

EIS studies were carried out to study the reaction kinetics at the electrode and the solution interface. The results depict that the rate of electron transfer at GCE/PPY is higher than at GCE/PPY/S-IIPs. The higher charge transfer resistance of GCE/PPY/S-IIPs is due to the presence of non-conductive S-IIP that slows the rate of the electron-transfer process in the composite material. The peak current response for the detection of Hg<sup>2+</sup> using SWASV for the electrode material (GCE/PPY/S-IIPs) is higher as compared to the other electrodes which may be result of strong binding of metal ions (Hg<sup>2+</sup>) with the nitrogen of PPY and the presence of higher number of active sites for the deposition of Hg<sup>2+</sup> on the GCE/PPY/S-IIPs surface. **Velempini, T., et al. (2018)** reported a LOD of 0.1 μgL<sup>-1</sup> for Hg<sup>2+</sup> ion using GCE/PPY/S-IIPs which is less compared to those reported by WHO (1 μgL<sup>-1</sup>) and EPA (μgL<sup>-1</sup>).

The electrochemical performance of the PPY Multiwalled carbon nanotube (MWCNT) modified on a gold (Au) electrode was analyzed using CV, showing a higher current response for PPY/MWCNT as compared to PPY/Au and Bare Au electrodes. This enhancement is because of the improved surface area available post-modification of the electrode (Au) with PPY/MWCNT allowing smooth transfer of electrons between Fe(CN)<sub>6</sub> <sup>3-/4-</sup> and the electrode material. A higher peak current response for the detection of Pb<sup>2+</sup> at low concentration on PPY/MWCNT was observed in comparison to the bare Au electrode, which may be attributed to the strong affinity of MWCNT towards Pb<sup>2+</sup> ions. A LOD of 0.65 μgL-<sup>1</sup> for Pb<sup>2+</sup> was reported by **Zhu**, **X.**, et al., (2017) in their studies.

- 2.3. Binary Composites as sensing materials: While individual materials often exhibit limitations in selectivity and sensitivity, the synergy between conducting polymers and other materials (Carbonaceous and non-carbonaceous) has demonstrated significant improvements in electrochemical performance. The enhanced catalytic activity, conductivity, rapid electron transfer kinetics, large surface area, and high sensitivity of these composites make them promising candidates for water quality monitoring (Diedhiou, I., et al., 2023)
- 2.3.1. PPY-based Binary Composites: Smarzewska, S., and Ciesielski, W., (2014) developed a GO/CPE electrode, for the detection of Pb<sup>2+</sup> ions in real water samples. Due to the greater stability, reproducibility, and other promising properties of the electrode, it is employed for lead determination. The peak current values (maximum current value) of Pb<sup>2+</sup>ions on the surface of GO/CPE are higher than those on the bare CPE, which is ascribed to the increased conductivity, surface area, and strong affinity for the metal ion, allowing fast reaction kinetics. A LOD of 2.18× 10<sup>-8</sup> mol L<sup>-1</sup> was reported. Seenivasan, R., et al., (2015) employed cysteine-functionalized graphene oxide (sGO)/PPY composite to detect and remove Pb<sup>2+</sup> ions in aqueous solution using DPV. The current value of the redox peaks in GO is less compared to PPY because of the presence of oxygen functionalities on GO surface, which hindered the electron transfer process. The enhancement in the peak current of the Pb<sup>2+</sup> ion on the (sGO)/PPY electrode compared to that of individual PPY and GO electrodes improved conductivity and surface area

facilitating fast electron transfer on the surface of the electrode. The sensor had a measurable detection limit of 0.07 ppb, below the WHO's 10 ppb threshold.

Cd<sup>2+</sup> sensing using three-dimensional porous PGO/PPY was developed by Song, Y., et al., (2019) for environmental applications. The sensing of Cd<sup>2+</sup> on the PGO/PPY electrode was performed using SWSV and DPSV techniques. Both techniques follow the same procedure that involves the accumulation of Cd on the electrode's surface at a potential of -1.1 V in 0.1M acetate buffer, followed by oxidation to the metal ions by sweeping in the potential range of -1.1 V to -0.5 V. The results show a better sensitivity and stable deviation for the Cd<sup>2+</sup> detection in the case of DPSV compared to the SWSV technique. The sensor demonstrated a LOD of 0.05 µgL<sup>-1</sup>, lower than the WHO standard limit, and was suitable for tap, pond, and river water, minimizing electroactive ions. Dai, H., et al., (2016) introduced an electrochemical sensor for determining HMs ions (Cd<sup>2+</sup>, and Pd2+) on a PPY functionalized with phytic acid (PA) and GO-modified electrode (PA/PPY/GO). The sensor, which measured Pd<sup>2+</sup> and Cd<sup>2+</sup> with a working range of 5–150 μgL<sup>-1</sup>, showed an appreciable electrochemical conductivity with a significant increase in peak current when compared to other modified electrodes (PPY/GO and PA/GO). The peak current values obtained using the DPV technique show that current intensity is proportional to the amount/concentration of Pd<sup>2+</sup> and Cd<sup>2+</sup> ions and the obtained LODs for these metal ions are  $0.41 \,\mu g L^{-1}$  and  $2.13 \,\mu g L^{-1}$ .

Suvina, V., et al., (2018) reported a LOD of 0.3 nM for Pb<sup>2+</sup> ions which is lower than reported by WHO using PPY/rGO hydrogel composite material. The increase in surface area (21.48 m<sup>2</sup>/g) and pore volume of the composite material, as compared to the PPY (5.89 m<sup>2</sup>/g) enhances the interaction of HM ions with the composite material. This increased area in the PPY/rGO binary composite by the presence of rGO on the PPY's surface facilitates efficient adsorption and detection of metal ions, leading to enhanced sensitivity of the electrode for Pb<sup>2+</sup> ions. An electrochemical sensor made of ion-imprinted PPY and rGO modified on GCE (IIP/rGO/GCE) was developed by Hu, S., et al., (2019) for the trace-level determination of Cd<sup>2+</sup> in water. SWASV technique was applied for the determination of Cd<sup>2+</sup>, showing a substantial difference in the Cd<sup>2+</sup> peak current variation

between IIP/rGO/GCE and NIP/rGO/GCE electrodes. A sharp and higher peak current of  $Cd^{2+}$  in the case of IIP/rGO/GCE is observed. This is due to the enhanced strong binding affinity of  $Cd^{2+}$  ions on the surface of IIP/rGO/GCE which has now enhanced surface area. The electrode material shows greater stability reproducibility and a LOD of 0.26  $\mu g L^{-1}$  within the concentration range of 1- 100  $\mu g L^{-1}$ .

Li, S., et al., (2012) synthesized the PPY/GO composite for the removal of Cr<sup>+6</sup> from the aqueous solutions. The removal efficiency of Cr<sup>+6</sup> ion by PPY/GO is 5.644 mmol/g and the individual PPY electrode is 2.715 mmol/g, which is two times less compared to the binary composite. The improved surface area (84.8 m²/g) of the composite material compared to PPY (41.3 m²/g) creates more adsorption sites on the surface of PPY/GO composite that enhances its removal efficiency. The removal efficiency of the Cr<sup>+6</sup> ion also depends on the initial concentration of the metal ion. The binary composite shows higher percentage removal (adsorption efficiency) for Cr<sup>+6</sup> ion at concentrations of 0.38 mmolL<sup>-1</sup> and its removal percentage decreases at a concentration of 1.97 mmolL<sup>-1</sup>. This may be due to a decrease in the number of active sites on the surface of the composite material at higher concentrations. Rong, R., et al., (2017) developed a PPy/rGO nanocomposite electrode material for the rapid, selective, and sensitive Pb²+ detection. A highly linear response of Pb²+ on the nanocomposite-modified electrode (PPY/GO) with a LOD of 4.7× 10<sup>-11</sup> molL<sup>-1</sup> was encountered.

Palanisamy, S., et al., (2017)., designed a PPY decorated with graphene/β-cyclodextrin (PPY /Gr/CD) modified on SPCE electrode for the detection of Hg<sup>2+</sup> in water. A sharp anodic peak due to the oxidation of Hg<sup>0</sup> to Hg<sup>2+</sup> with enhanced current value was observed in the case of the composite as compared to the electrodes of PPY, Gr/CD, and Gr. The formation of a stable complex of Hg<sup>2+</sup> by binding with the nitrogen of PPY and the Gr-CD's enhanced surface area, which provides more number of active sites for Hg<sup>2+</sup> adsorption in PPY /Gr/CD composite, ensuing a rapid electron transfer kinetics and improving the sensitivity for Hg<sup>2+</sup> sensing. A low detection limit of 0.47 nM L<sup>-1</sup> for Hg<sup>2+</sup> ions was reported, which is lower than that reported by WHO and USEPA). An electrochemical sensor constructed with PPY, pectin, Gr (PPy/Pct/Gr) for Hg<sup>2+</sup> ions

determination in femtomolar concentration was developed by **Arulraj**, **A.D.**, **et al.**, **(2016)**. The electrode achieved a sensitivity of 28.64  $\mu$ A  $\mu$ M<sup>-1</sup> and a LOD of 4 fM, nearly 6 orders of magnitude lower than the recommended concentration in drinking water.

**2.3.2. TMOs-based binary electrode material:** The electrochemical behavior of the prepared electrodes rGO, rGO/ZnO, and Co/ rGO/ZnO was studied using CV. The current values of the prepared electrodes follow the sequence as rGO < rGO/ZnO < Co/rGO/ZnO suggesting the better electrochemical response of the latter electrode. This may be attributed to the incorporation of Co in the composite that facilitates the faster diffusion of ions between electrode and electrolyte. Distinct and sharp anodic stripping peaks of HMs (Cd<sup>2+</sup> and Pb<sup>2+</sup>) with increased current values compared to other electrodes were observed using DPV. LODs of 0.94  $\mu$ gL<sup>-1</sup> for Cd<sup>2+</sup> and 0.83  $\mu$ gL<sup>-1</sup> for Pb<sup>2+</sup> within the concentration range of 10 - 90  $\mu$ gL<sup>-1</sup> were reported using Co/ZnO/rGO electrode were reported by **Karthik, R., and Thambidurai, S., (2017).** The improved selectivity and sensitivity of the Co/ZnO/rGO electrode is due to the reduction in the band gap resulting after the formation of a fused alloy of ZnO when doped with cobalt ion.

ZnO/ polyvinyl alcohol (PVA) nanocomposite incorporated with Graphene was employed for the detection of Cd<sup>2+</sup> ions. The conductivity of ZnO/PVA/Gr composite was found to be higher than ZnO/PVA composite, which may be the result of the synergetic effect of both polymer and Gr that provides a conductive network and increased surface area for charge storage and its transportation. Furthermore, the photocatalytic properties of the ZnO/PVA/Graphene composite were also enhanced, which may be ascribed to the interaction between ZnO and graphene resulting in the reduction of band energy in modified ZnO compared to that of pure ZnO that improves the absorption of the composite material. A enhanced current response than the ZnO/PVA composite, LOD of 9.88 ppm, and accuracy in the range of 0 to 80 ppm for the Cd<sup>2+</sup> ions using ZnO/PVA/Gr composite was reported by **Ismardi, A., et al., (2024).** They reported that the presence of -OH group on the surface of ZnO firstly provides the negative surface in the case of ZnO/PVA/Gr, then acts as the binding site for the positively charged metal ion from the.

Yukird, J., et al., (2018) synthesized a ZnO/Gr composite for the simultaneous detection of HMs ions (Pb<sup>2+</sup> and Cd<sup>2+</sup>) using an ASV technique. ZnO was prepared from zinc acetate by the decomposition method, and then it was employed for the preparation of ZnO/Gr composite by a colloidal coagulation effect at room temperature. The stripping peak current values for both metal ions increase with the increase in the amount of Gr (10-20%), and above 20% it decreases, which is due to the agglomeration of Gr sheets. Similarly, the electrochemical response of the ZnO/Gr firstly increases with the concentration of the suspension (1 - 2 mg/mL). Then it declines with an increase in the concentration (> 2 mg/mL) of the suspension. A LOD of 0.8 and 0.6 μgL<sup>-1</sup> for Pb<sup>2+</sup> and Cd<sup>2+</sup>, respectively, within the 10-100 μgL<sup>-1</sup> concentration range was reported.

A GCE modified with MnO<sub>2</sub> and GO (MnO<sub>2</sub>/GO/GCE) was reported by Sun, H., et al., (2019) for the effective detection of HMs (Cu<sup>2+</sup> and Pb<sup>2+</sup>) ions in the water. The structural and morphological studies show the uniformity of MnO<sub>2</sub> on the surface of GO in the composite. The electrochemical response of the working electrodes was analyzed using techniques like EIS and CV. The resistance to charge transfer in the case of bare GCE and MnO<sub>2</sub>/GCE is higher compared to that of MnO<sub>2</sub>/GO/GCE. The higher charge transfer resistance in MnO<sub>2</sub>/GCE is due to the low conductivity of MnO<sub>2</sub>, thus hindering the smooth transfer of electrons. The surface area as well as the conductivity of MnO<sub>2</sub>/GO/GCE is improved by the incorporation of GO, which acts as a carrier facilitating the fast transfer of electrons, resulting in higher redox peaks when compared to the GCE and MnO<sub>2</sub>/GCE electrodes. The detection of both Cu<sup>2+</sup> and Pb<sup>2+</sup> metal ions on MnO<sub>2</sub>/GO/GCE was studied using the SWASV technique. The stripping peak currents for Cu<sup>2+</sup> and Pb<sup>2+</sup> (-0.07 V and -0.56 V) increase with an increase in the concentration of these metal ions. The synergetic effect of GO and MnO<sub>2</sub> in the composite material provides a porous surface for the adsorption and improves the conductivity, this enhances the overall electrochemical performance of the electrode for the determination of HM ions. The prepared electrode showed greater stability, repeatability, and anti-interference properties with LOD of 19 nM and 17 nM for Pb<sup>2+</sup> and Cu<sup>2+</sup> within the concentration range of 0.05  $\mu$ M to 1  $\mu$ M.

MnO<sub>2</sub> nanoflower after surface modification with the oxygen functionalities and phosphate ions (PO<sub>4</sub>)<sup>3-</sup> (p- MnO<sub>2</sub>) was employed by Liao, J., et al., (2021) for the detection of Pb<sup>2+</sup> ion using the SWASV technique. The electrochemical performance of the MnO<sub>2</sub> and surface-modified p-MnO<sub>2</sub> on the GCE was studied using EIS and CV. The results show that p-MnO<sub>2</sub> based electrode shows higher electrochemical performance compared to unmodified MnO<sub>2</sub>. This may be ascribed to the increased conductivity and specific surface area of the p-MnO<sub>2</sub> electrode allowing the fast redox process to take place on its surface thus enhancing the redox peaks current values compared to the MnO<sub>2</sub> electrode. The results of their studies show that the p-MnO<sub>2</sub> electrode has a sensitivity that is 2 times and lower LOD compared to that of a better MnO<sub>2</sub>-based electrode. The presence of phosphite ion (PO<sub>4</sub>)<sup>3-</sup> binds to the metal ion and acts as a bridge for the redox process to take place on the surface of the p-MnO<sub>2</sub> electrode. A inferior LOD of 0.0012 μM compared to the LOD of 0.025 for the MnO<sub>2</sub> electrode within the concentration range of 0.2 to 1.4 was reported for p-MnO<sub>2</sub>. The p-MnO<sub>2</sub> electrode shows greater stability and reproducibility, offering a promising strategy in diverse applications.

The electrochemical determination of Pb<sup>2+</sup>, Zn<sup>2+</sup>, and Cd<sup>2+</sup>, along with their interference studies with each other, was studied on the different morphologies (MnO<sub>2</sub>/nanoparticle, MnO<sub>2</sub>/nano bowls, and MnO<sub>2</sub>/ nanotube) of MnO<sub>2</sub>-based nanocrystals by **Zhang, Q.X., et al., (2015).** The individual peak current response of all these metal ions (Pb<sup>2+</sup>, Zn<sup>2+</sup>, and Cd<sup>2+</sup>) varies linearly with the concentration of respective metal ions on different MnO<sub>2</sub>-based electrode materials in the absence of any interfering metal ions. The stripping peak behavior of Cd<sup>2+</sup> ions within the concentration range (0.1 to 1.6 μM) in the presence of Zn<sup>2+</sup> (2.0 μM) as an interfering ion was studied on different MnO<sub>2</sub>. based modified electrodes (MnO<sub>2</sub>/nanoparticles/Bi MnO<sub>2</sub>/nano bowl/Bi and MnO<sub>2</sub>/nanotubes/Bi). The Cd<sup>2+</sup> peak current response increases linearly with concentration in the presence of 2.0 μM as an interfering ion. However, the stripping current of Zn<sup>2+</sup> ion firstly increases and then becomes saturated with an increase in the concentration of Cd<sup>2+</sup> ion. The increase in the current response of Zn<sup>2+</sup> is due to the development of a favorable Cd film and Cd-Zn intermetallic compound, whereas at high concentration of Cd<sup>2+</sup> ion surface saturation of

the Cd film takes place which levels off the stripping peak of Zn<sup>2+</sup> ion. The sensitivity of Cd<sup>2+</sup> ion detection in the presence of Zn<sup>2+</sup> as the interference ion is 29.73, 26.28, 23.46 µA  $\mu M^{-1}$  and 18.05 18.69, 12.36  $\mu A$   $\mu M^{-1}$  in the absence of interference for MnO<sub>2</sub>/nanoparticle/Bi MnO<sub>2</sub>/nano bowl/Bi and MnO<sub>2</sub>/nanotubes/Bi electrodes. An increase in the sensitivity values for Cd<sup>2+</sup> (in the presence of Zn<sup>2+</sup>) shows the dependence of Cd<sup>2+</sup> ion detection on the interference Zn<sup>2+</sup> ion because of the formation of favorable intermetallic Cd-Zn film during the deposition step. Similar studies were carried out for the detection of Zn<sup>2+</sup> ion in the presence of Cd<sup>2+</sup> ion (2.0 µM) on these three MnO<sub>2</sub>-based modified electrodes. The stripping peak response of the interference Cd<sup>2+</sup> ion increases and then decreases with further addition of Zn<sup>2+</sup> ion on the surface of both MnO<sub>2</sub>/nano bowl/Bi and MnO<sub>2</sub>/nanotubes/Bi electrodes. However, the peak response on the surface of MnO<sub>2</sub>/nanoparticles/Bi decreases with the addition of Cd<sup>2+</sup> metal ions. This behavior is due to the competition between Cd<sup>2+</sup> and Zn<sup>2+</sup> for the deposition (reduction) on the active sites of the electrode surface. The sensitivity of 1.61, 4.20 and 2.50 µA µM<sup>-1</sup>. for the determination of Zn<sup>2+</sup> in the presence of Cd<sup>2+</sup> ion were reported on the three elctrodes (MnO<sub>2</sub>/nanoparticle/Bi MnO<sub>2</sub>/nanobowl/Bi and MnO<sub>2</sub>/nanotubes/Bi electrodes). A similar value of sensitivity 1.67, 5.17 and 2.56 μA μM<sup>-1</sup>. for the determination of Zn<sup>2+</sup> in absence of Cd<sup>2+</sup> interference was reported showing the no effect of interference on the detection of Zn<sup>2+</sup> metal ion on all the three-electrode material.

ZnO/ErGO-modified on GCE was developed by **Luyen**, **N.D.**, **et al.**, **(2024)** to investigate the electrochemical behavior of HMs (Pb<sup>2+</sup> and Cd<sup>2+</sup>). They reported a LOD of 0.45 and 1.69 ppb for Pb<sup>2+</sup> and Cd<sup>2+</sup>. Stripping peak current values of both Pb<sup>2+</sup> and Cd<sup>2+</sup> largely depend on the volume of ZnO/ErGO added on the glassy carbon electrode. A 5  $\mu$ L volume of ZnO/ErGO on glassy carbon has been reported to be appropriate resulting in the higher peak current values for Pb<sup>2+</sup> and Cd<sup>2+</sup>, respectively. When the suspension volume is > 5  $\mu$ L it results in the formation of an irregular distribution of GO layers that hinder the electron transfer, which in turn reduces the conductivity as well as electron exchange becomes difficult, resulting in a decrease of the stripping current.

# 2.4. Ternary composite as sensing material

2.4.1. PPY-based Ternary Composites: Rehman, A.U., et al., (2018) employed a ternary electrode material PPY/rGO/SnO<sub>2</sub> prepared in the ratio of 4:1 (PPY/rGO/SnO<sub>2</sub>) for electrochemical determination of heavy metal ions. The synergetic effect between these individual materials enhances the electrochemical response of the PPY/rGO/SnO<sub>2</sub> ternary composite, making it a potent material for the sensing of HMs ions (Cd<sup>2+</sup>, Cu<sup>2+</sup>, Hg<sup>2+</sup>, and Pb<sup>2+</sup>). The electrochemical response of the individual (GCE, GO, SnO<sub>2</sub>) binary (rGO/SnO<sub>2</sub>), and the ternary (PPY/rGO/SnO<sub>2</sub>) was studied using cyclic voltammetry. The redox peak current response of 5.1×10<sup>-5</sup> A for GCE and SnO<sub>2</sub> electrodes is higher compared to that of the GO electrode. Different oxygen functionalities on the surface of GO slow the rate of electron transport on its surface. The binary composite (rGO/SnO<sub>2</sub>) shows a higher current response of 9.3×10<sup>-5</sup> A. Compared to the individual electrode material. compared to the individual as well as binary electrodes the ternary composite 5.1×10<sup>-5</sup> A shows higher electrochemical performance with the current response of 1.14×10<sup>-4</sup> A. This is due to the synergetic effect of PPY and GO/SnO<sub>2</sub> that provide the best electrocatalytic conduct and the essential conduction gallery for electron transfer on the electrode surface, assisting the fast electron transfer process at the electrode surface. The stripping peak analysis for the sensing of Cd<sup>2+</sup>, Cu<sup>2+</sup>, Hg<sup>2+</sup>, and Pb<sup>2+</sup> metal ions was studied using SWASV measurements. The (PPY/rGO/SnO<sub>2</sub>) electrode shows higher sensitivity, selectivity, and long-term stability compared to that of individual and the binary composite for the sensing of these metal ions. They reported a LOD of  $7.5 \times 10^{-13}$ ,  $8.3 \times 10^{-13}$ ,  $8.1 \times 10^{-13}$ , and  $8.8 \times 10^{-13}$  M for the Cd<sup>2+</sup>, Cu<sup>2+</sup>, Hg<sup>2+</sup>, and Pb<sup>2+</sup> metal ions within 0.5 to 3 μM concentration range on the surface of the ternary electrode material.

**Zhuang, Y., et al. (2018)** reported a high electrochemical response for Hg<sup>2+</sup> using ZnO/rGO/PPY composite with an interference barrier. The physical barrier acts as a shield for the electroactive material and as a driving force for electrochemical detection with outstanding anti-interference capacity because of the Schottky barrier. DPV was employed for detecting the electrochemical behavior of Hg<sup>2+</sup> with varying concentrations and a sensitive and high response was obtained with a change in the concentration of Hg<sup>2+</sup> using

ZnO/rGO/PPY composite in comparison to the rGO/PPY and ZnO/PPY composites under the same conditions. The developed sensors show a LOD of 1.9 nM within the concentration range of 2 to 10 nM of Hg<sup>2+</sup> ion in actual seawater.

**2.4.2. PANI-based electrode material:** A novel PANI/Gr/polystyrene nanoporous fiber-modified on screen-printed carbon electrode (SPCE) was developed by **Promphet, N., et al. (2014).** The electrochemical characterization was achieved by CV measurements by employing a conventional ferro/ferricyanide [Fe(CN)6]<sup>4-/3-</sup> redox pair. The results show a threefold increase in sensitivity of (Gr/PANI/PS) over unmodified SPCE due to the increased surface area of the Gr/PANI/PS nanoporous fibers. Pb<sup>2+</sup> and Cd<sup>2+</sup> were measured simultaneously in the presence of Bi<sup>3+</sup> using SWASV. The results showed a linear relationship between peak current and concentration of metal ion over the working range of 10 – 500 μgL<sup>-1</sup>, with LOD of 4.43 and 3.30 μgL<sup>-1</sup> for Cd<sup>2+</sup> and Pb<sup>2+</sup>, respectively.

Ruecha, N., et al. (2015) developed an electrochemical sensor for the simultaneous detection of Pb<sup>2+</sup>, Cd<sup>2+</sup>, and Zn<sup>2+</sup> ions using a PANI /Gr nanocomposite electrode. The material was deposited on filter paper and plastic films using drop-casting and electrospraying deposition methods. The PANI/Gr nanocomposites exhibit high electrochemical performance with an increase in anodic peak current value compared to the unmodified electrode using the SWASV technique. The modified electrode is also used to select target metals in the presence of common metal interferences. A LOD of 0.1 μgL<sup>-1</sup> for Cd<sup>2+</sup>, Pb<sup>2+</sup> and 1.0 μgL<sup>-1</sup> for Zn<sup>2+</sup> was reported. **Muralikrishna, S., et al., (2017)** prepared a PANI and GO hydrogel (PANI/GO) composite for Pb<sup>+2</sup> ions detection. The composites were prepared in different ratios, % w/w as PANI/GO (80:20, 50:50, and 20:80), and correspondingly, their electrochemical behavior was studied. They reported that the composite with less GO content shows well-defined redox peak current values as compared to the other composites. The different oxygen functionalities on the surface of GO hinder the electron transfer process when present in large amounts. They reported a LOD of 0.04 nM for Pb<sup>2+</sup> ions.

Akhtar, M., et al., (2020) synthesized rGO decorated with alanine and PANI (PANI /rGO/Ala/GCE) through an in-situ oxidative polymerization approach. The electrochemical response of the electrodes was studied using the CV technique, the results of which show that the PANI/rGO/Ala/GCE electrode shows a better response compared to that of other prepared electrodes (Bare GCE, PANI/GCE, rGO/GCE, and Ala/GCE). The higher peak current in the case of PANI /rGO/Ala/GCE is mainly due to the improved conductivity, fast electron transfer kinetics, and strong binding affinity. SWASV technique was used for the sensing of the Cd<sup>2+</sup>, Pb<sup>2+</sup>, and Cu<sup>2+</sup>. The oxidation peak current corresponding to these metal ions at different electrodes follows the order as PANI/GCE< Ala/GCE < rGO/GCE < rGO/Ala/PANI/GCE. A LOD of 0.045, 0.063, and 0.03 nM for Pb<sup>2+</sup>, Cu<sup>2+</sup>, and Cd<sup>2+</sup> was reported.

#### **CHAPTER 3**

\_\_\_\_\_

- **3. Materials and Methods:** Polypyrrole (PPY) has been synthesized by the chemical oxidative polymerization method using the oxidant ferric chloride. Graphene oxide has been synthesized using a modified hammer's method. Binary composites of PPY and GO (i.e., PGs) at different ratios (wt %) have been synthesized using the ex-situ method. Similarly, the ternary composites of PPY and GO i.e., (PGXs) with transition metal oxides (ZnO and MnO<sub>2</sub>) at various ratios (wt %) have also been prepared using the ex-situ method. Individual material as well as the prepared binary and ternary composites were then subjected to various characterizations and are employed for the sensing of detection and removal of the heavy metals.
- **3.1. Materials:** Monomer Pyrrole (PY, > 99%) was procured from Spectrochem, Dimethyl formamide (DMF), Graphite powder, Sulphuric acid (H<sub>2</sub>SO<sub>4</sub>), Hydrogen Peroxide (H<sub>2</sub>O<sub>2</sub>), Hydrochloric acid (HCl), Potassium permanganate (KMnO<sub>4</sub>), Cupric chloride (CuCl<sub>2</sub>), and Cadmium nitrate [Cd(NO<sub>3</sub>)<sub>2</sub>] were acquired from Loba Chemie. Lead nitrate [Pb(NO<sub>3</sub>)<sub>2</sub>], Ferric chloride (FeCl<sub>3</sub>), from Alpha Chemika, Potassium ferricyanide K<sub>3</sub>[Fe(CN)<sub>6</sub>] from CDH fine chem, Potassium Chloride (KCl) from Rankem, and ascorbic acid from SD fine chem. Ltd were obtained. Sodium acetate (CH<sub>3</sub>COONa) was acquired from Loba Chemie. Ethanol was used as a medium (for sonication) to prepare both binary and ternary composites. All the chemicals used were of analytical quality and therefore were not purified further.

#### 3.2. Preparation of Electroactive Materials

**3.2.1. Preparation of Polypyrrole (PPY):** The preparation of PPY has been carried out by the chemical oxidative polymerization method. 0.072 M Pyrrole monomer was added dropwise into the freshly prepared surfactant solution of N- cetyl -N, N, N-Trimethylammonium Bromide (CTAB, 4.6 g) in 100 ml distilled water with continuous stirring (**Fig. 3**). The process of polymerization starts with the addition of freshly prepared

oxidant solution of FeCl<sub>3</sub> (50ml, 0.074 mol/dL) at the rate of 1ml/min to the above solution content. Polymerization was then allowed to be carried out for 6 hours with continuous mechanical stirring at 500 rpm and room temperature. The resultant solution was then filtered, further washed with distilled water, and then dried. (Mudila, H., et al., 2013)

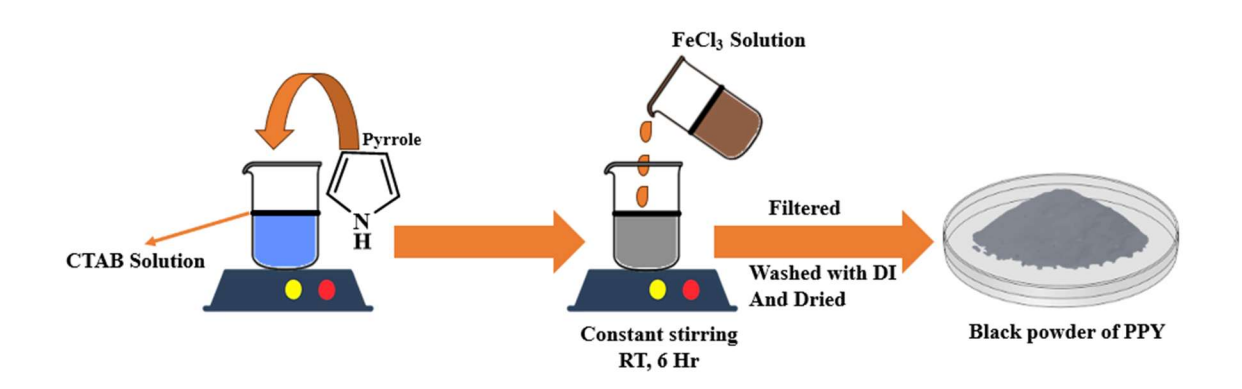


Figure 3. Scheme showing the synthesis process of polypyrrole

**3.2.2. Preparation of Graphene Oxide (GO):** The preparation of GO from pure Graphite powder was done by the modified Hummers method (**Fig. 4**). Graphite powder (2g) was added to the conc. H<sub>2</sub>SO<sub>4</sub> (46 ml) was taken in a beaker, and the above composition was allowed in an ice-containing bath at 0-5°C for 30 minutes with constant stirring. 46 g of KMnO<sub>4</sub> was then added slowly to the graphite solution while maintaining the temperature of 0-5°C with continuous stirring for the next 4 hours. The above reaction solution was then removed from the ice bath and allowed to stir for 1 hour at a temperature of 30-35°C. 100 ml of Deionized water (DI) was then added to the solution mixture to obtain the homogeneous suspension, and the temperature of the suspension was allowed to rise to 95-98°C with constant stirring for 1 hour. 20 ml H<sub>2</sub>O<sub>2</sub> and 100 ml DI was then added to the solution mixture to remove the excess of KMnO<sub>4</sub> left in the solution, which was followed by 2 hours of further stirring. The resultant suspension was centrifuged, washed multiple times with 5% HCl solution and deionized water until a clear filtrate was obtained. The brownish-black solid residue obtained was then allowed to dry at 60°C. (**Guerrero-Contreras, J., and Caballero-Briones, F., 2015**).

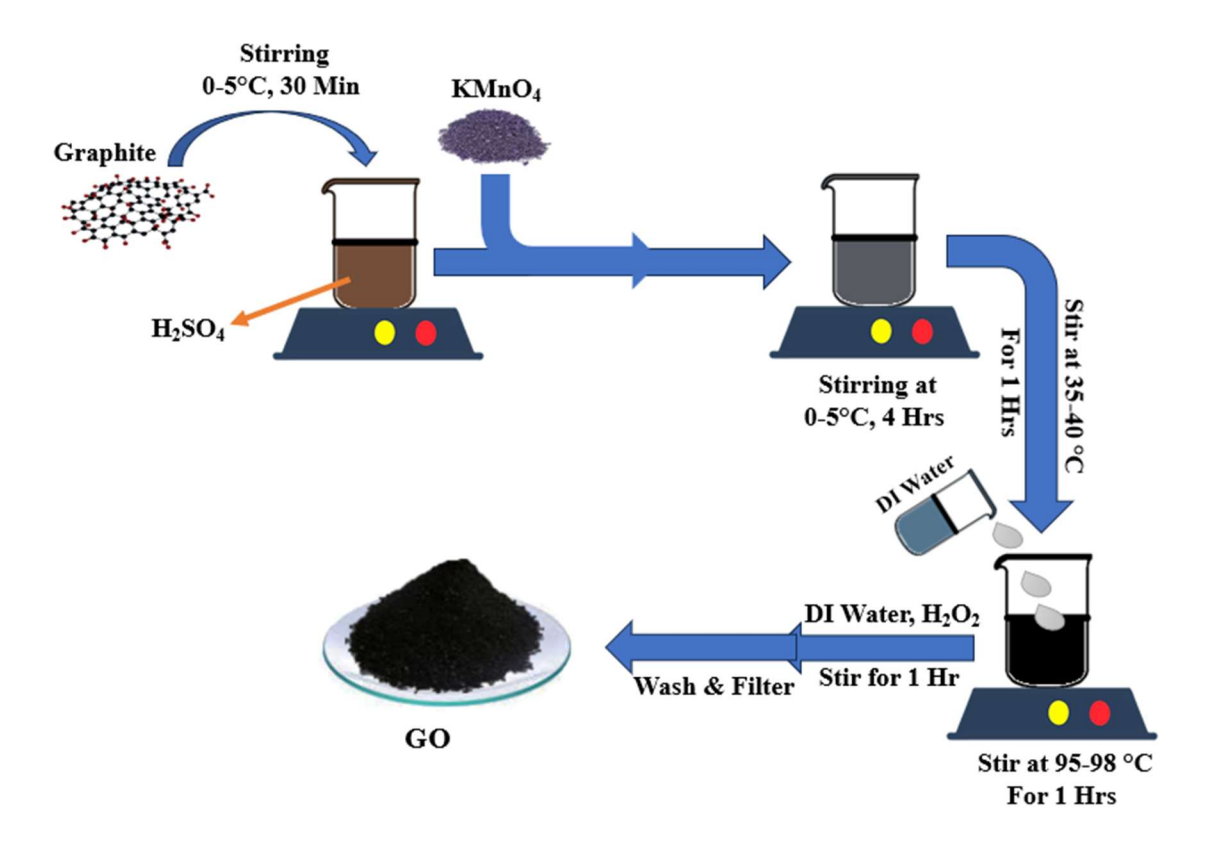


Figure 4. Scheme depicting the synthesis process of GO.

**3.2.3. Preparation of Polypyrrole/Graphene Oxide (PPY/GO, PGs) binary Composites:** The preparation of PGs composite in different ratios was carried out by the ex-situ method. In this method required amount of PPY and GO was taken in ethanol (as a medium), followed by mechanical mixing through sonication for 30 minutes to acquire homogeneity. The resulting mixture was then allowed to dry at 60°C to remove the ethanol, followed by grinding.

Table 2. Amount of PPY and GO, corresponding to the ratio for preparation of PPY/GO composites (PGs)

Materials _	Ratio and corresponding amount			
	4: 1	2: 1	1:1	1: 2
PPY (mg)	100	100	100	100
GO (mg)	25	50	100	200

PGs are prepared in different wt % ratios (mg) as 100:25, 100:50, 100:100, and 100:200 and are named PG 1, PG 2, PG 3, and PG 4, respectively.

# **3.2.4.** Preparation of Polypyrrole/Graphene Oxide/ZnO (PPY/GO/ZnO, PGZs) Ternary Composites: The preparation of PGZs composite in different ratios was carried out by the ex-situ method. Binary composite (PG 1 of a fixed amount) and ZnO were taken in ethanol (as a medium) followed by mechanical mixing through sonication for 30 minutes to acquire homogeneity. The resultant mixture was then dried in at 60°C to remove the ethanol followed by grinding.

Table 3. Amount of PG 1 and ZnO, corresponding to the ratio for preparation of PPY/GO/ZnO composites (PGZs)

Materials	Ratio and the corresponding amount			
	2: 1	1:1	1: 2	
PG (mg)	100	100	100	
ZnO (mg)	50	100	200	

PGZs prepared in different wt % ratios (mg) as 100:50, 100:100, and 100:200 are named PGZ 1, PGZ 2, and PGZ 3, respectively.

#### 3.2.5. Preparation of Polypyrrole/Graphene Oxide/ MnO<sub>2</sub> (PPY/GO/MnO<sub>2</sub>, PGMs)

**Ternary Composites:** Preparation of PGMs composites in different ratios was carried out by the ex-situ method. Binary composite (PG of a fixed amount) and MnO<sub>2</sub> were taken in ethanol (as a medium), followed by mechanical mixing through sonication for 30 minutes to acquire homogeneity. The resultant mixture was then dried at 60°C to remove the ethanol, followed by grinding.

Table 4. Amount of PG and MnO<sub>2</sub>, corresponding to the ratio for preparation of PPY/GO/MnO<sub>2</sub> composites (PGMs)

Materials	Ratio and the corresponding amount			
	2: 1	1:1	1: 2	
PG (mg)	100	100	100	
MnO <sub>2</sub> (mg)	50	100	200	

PPY/GO/MnO<sub>2</sub> composites prepared in different wt % ratios (mg) as 100:50, 100:100, and 100:200 are named **PGM 1, PGM 2,** and **PGM 3,** respectively.

3.3. Preparation of working electrodes: The preparation of carbon paste electrodes (CPE) was carried out by mixing the graphite powder (1 gram) in paraffin oil (1.8 ml) in a mortar pestle to obtain a homogeneous paste. This paste was filled into the electrode cavity, and its surface was smoothed by polishing it on clean paper. The electrical contact was made using the copper wire. The suspension of the electroactive material was prepared by dissolving 2 mg of the material in 1 ml DMF, followed by its ultrasonication for 30 minutes. The suspension of the electroactive material was then drop-cast ( $10\mu L$ ) on the surface of CPE and then dried. The obtained modified electrode then functions as our working electrode. (Oularbi, L., et al., 2017)

# 3.4. Characterization of PPY, GO and prepared Composites (PGs and PGXs)

Various techniques were employed to characterize the individual as well as the composite materials. Below paragraphs will explain the techniques used to analyze the respective materials.

**3.4.1. FT-IR** (Fourier Transform Infrared Spectroscopy): A Perkin Elmer FT-IR Spectrometer using KBr pellets was used to record the FT-IR spectrum of the samples within 400-4000 cm<sup>-1</sup> range. The existence of different functionalities and the type of bond interactions present in the molecules are confirmed by the FT-IR studies of the material. The vibrational excitations of the bonds take place on the absorption of radiation of

wavelength falling in the infrared region of electromagnetic radiation. The vibrational frequency is calculated by equations (1 and 2).

$$v = \frac{1}{2\pi c} \sqrt{\frac{k}{\mu}} \qquad ----- (1)$$

where  $\nu$  is the vibrational frequency, k represents the force constant, and  $\mu$  signifies reduced mass, calculated as

$$\mu = \frac{m_1 m_2}{m_1 + m_2} \qquad ---- (2)$$

**3.4.2. XRD (X-ray Diffractometry):** The XRD studies of the powdered sample at room temperature were analyzed on a Bruker D8 advanced X-ray diffractometer using Cu-K $\alpha$  radiation. The diffraction patterns of the finely powdered prepared samples were recorded at a scanning rate of 2° per minute over a 2 $\theta$  range of 10° to 80° with a high-resolution step size of 0.02 degrees.

**3.4.3.** X-ray Photoelectron Spectroscopy (XPS): XPS is an important technique used to study surface analysis, like elemental, chemical, and electronic composition of materials. The sample was placed on a holder and inserted into the ultra-high vacuum (UHV) chamber with having pressure of  $\sim 10^{-9}$  mbar. This vacuum condition prevents surface contamination and ensures accurate electron detection. A X-ray beam (Al K $\alpha$ , 1486.4 eV) is incident onto the sample surface, which ejects the electrons from the atom. The binding energy of emitted electrons is used to determine the elemental states of the material.

**3.4.4. SEM** (Scanning Electron Microscopy): The surface characterization of the prepared samples was analyzed using FE-SEM on a Joel model-based instrument. A gold coating was employed on the sample before its analysis which reduces the charging effects and improves the image quality of the material under investigation. The FE-SEM image of the individual, binary, and ternary composite materials was studied at different magnifications (5000x, 10000x, 20000x).

- **3.4.5. Thermogravimetric Analysis (TGA):** Thermogravimetric analysis (TGA) was used to study the thermal stability of the prepared samples. The experiment was carried out using a thermogravimetric analyzer (TGA)-50H of Perkin Elmer. A sample of the weight (10 mg) was heated under an N<sub>2</sub> atmosphere at a rate of 10 °C/min in the temperature range of 25-600 °C to record the corresponding TGA data.
- **3.4.6.** UV-Vis Spectroscopy: This spectroscopic technique is based on the absorbance of wavelength in the UV-Vis region (200-800 nm). UV-1900i Plus, a Shimadzu-made UV-Spectrophotometer, was used for studying the adsorption and removal of heavy metal (Pb<sup>2+</sup>) from the aqueous solution.

#### 3.5. Electrochemical measurements

The interfacial properties, including chemical, physical, and electrochemical, of the material under investigation were studied using electron impedance spectroscopy (EIS). The resulting impedance graphs were obtained in 5 mM K<sub>3</sub>[Fe(CN)<sub>6</sub>] along with 0.1 M KCl aqueous solution as an electrolyte within the frequency range of 0.1 Hz to 10<sup>6</sup> Hz. In the EIS spectra, Nyquist plots are used to study the different processes taking place within the material. The electron transfer kinetics takes place either through redox behavior or through diffusion, depending on the diameter of the semicircle in different frequency regions of the Nyquist plots in the EIS spectra. A Metrohm NOVA 2.1.8 potentiostat-galvanostat three-electrode system was used to carry out EIS characterizations.

**3.5.1.** Cyclic Voltammetry (CV) studies: The electrochemical properties as well as the redox behavior of the different materials were studied using CV. The electrochemical response of the material was analyzed using a Metrohm NOVA 2.1.8 potentiostat-galvanostat three-electrode system comprising Ag/AgCl as a Reference electrode, Pt foil of 1 cm<sup>2</sup> area as a Counter electrode, and CPE as a Working electrode. The cyclic voltammograms having current versus potential relationship (CVs) were recorded in 5 mM K<sub>3</sub>[Fe(CN)<sub>6</sub>] and 0.1 M KCl aqueous solution as an electrolyte within the potential window of -0.5 to 1.2 V at 0.05 V/s scan rate. The CV curves of the different samples were

analyzed, and the material having higher redox peak current values shows a better electrochemical performance compared to the other.

**3.5.2.** Differential Pulse Anodic Stripping Voltammetry (DPASV) measurements: The sensing of heavy metal was analyzed electrochemically using the DPASV performed on a Metrohm NOVA 2.1.8 potentiostat-galvanostat using a three-electrode system. The working electrode modified with the electroactive material along with a reference (Ag/AgCl) and counter (Pt foil) electrode, was placed in a cell having an acetate buffer (pH 4.6) solution and Pb<sup>2+</sup> metal ion. The DPASV measurements were then performed by applying the voltage in the range of -1.2 to 0.2 V for different electrodes, resulting in the stripping peak current value at different concentrations of Pb<sup>2+</sup> ions. The limit of detection (LOD) for the detection of Pb<sup>2+</sup> ion for the electrode was determined using the formula (4).

$$LOD = \frac{3 \times SD}{S} \qquad ----- (4)$$

Where SD represents the standard deviation of the blank solution, and S denotes the slope of the resulting calibration curve.

**3.6. Probable Mechanism for Heavy Metal Sensing:** Various phenomena taking place in the reaction medium are responsible for detecting metal ions on the surface of the electrode material. According to previous literature studies, the detection of HM ions largely depends on the adsorptive properties of the active material relative to the metal ion under investigation (Pb<sup>2+</sup>). out of the proposed phenomena, one involves the accumulation of Pb<sup>2+</sup> ions on the surface of the electrode by electrostatic attraction and surface complexation. The presence of the heteroatom functionalities (O, N, S) on the composite surface (PGZ 2 and PGM 1) can coordinate to the valencies of the Pb<sup>2+</sup> ion through coordinate bonds that lead to the accumulation of Pb<sup>2+</sup> ions on the surface of the ternary composite material. The greater the quantity of accumulated Pb<sup>2+</sup> ions on the electrode surface higher the stripping peak current value during the DPASV measurements. PPY

shows high electrical conductivity and also binds the Pb<sup>2+</sup> ion through the presence of the Nitrogen functionalities (-NH-, =NH-) on its surface. The enlarged area and different oxygen functionalities in GO act as binding sites for the Pb<sup>2+</sup> ion. TMOs (ZnO and MnO<sub>2</sub>) have high catalytic properties and provide several anchoring sites to adsorb metal ions on their surface. These synergetic effects arising from PPY, GO, and ZnO/MnO<sub>2</sub> in the ternary composite (PGZ 2/PGM 1) improve the surface area, conductivity, and more number of anchoring sites for the adsorption of Pb<sup>2+</sup> ion thus facilitating fast electron transfer processes in ternary composites resulting in stripping peak current of metal ion during their electrochemical measurements. (Dai, H., et al., 2016; Muralikrishna, S., et al., 2017)

The systematic representation (**Fig. 5**) of the binding mechanism and the reaction involved in the sensing of the Pb<sup>2+</sup> ions on the working electrode surface during DPASV measurements is shown below.

Figure 5: Chemical representation of the detection of Pb<sup>2+</sup> ion on PGXs

Where WS represents the working surface Sol represents a solution of Pb<sup>2+</sup> metal ion, and PGX represents the working electrode (PGZ 2 and PGM 1).

Firstly, the adsorption of  $Pb^{2+}$  ions on the surface of the working electrode in open circuit takes place. During the pre-concentration step at a deposition potential of -1.2 V, which leads to the reduction of  $Pb^{2+}$  metal ions to the corresponding metal atom ( $Pb^{0}$ ). The voltametric analysis was then performed, resulting in the oxidation of the metal ( $Pb^{0}$ ) to its ion ( $Pb^{2+}$ ), which are stripped back into the solution, resulting in the corresponding anodic stripping peak current value (Muralikrishna, S., et al., 2017).

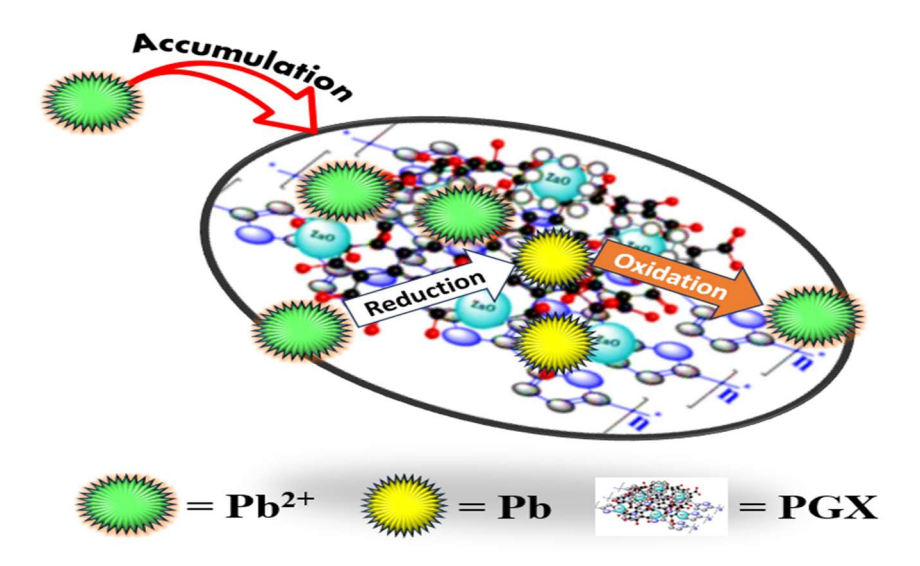


Figure 6: Graphical representation of the detection of Pb<sup>2+</sup> ion on PGX

\_\_\_\_\_\_

#### 4. Characterization:

4.1. FT-IR of PPY, GO, PG, ZnO. and PGZ Ternary Composite: The process of polymerization of the monomer unit and the presence of the different functional groups in the synthesized PPY, GO, ZnO, and the composites (binary, ternary) were examined using FT-IR studies Fig. 7. In the FTIR spectra of PPY a broad band in between 3100-2800 cm<sup>-1</sup> <sup>1</sup> is due to stretching vibrations of N-H bond. The vibrational bands at 1631, 1543, and 1415 cm<sup>-1</sup> are due to symmetric stretching of the ring's C=N, C=C, and C-N bonds. The wavenumbers associated with 1039 cm<sup>-1</sup> and 1300 cm<sup>-1</sup> are due to the in-plane deformations of the C-H and C-N bonds, whereas out-of-plane C-H deformation is centered at 884 cm<sup>-1</sup>. The absorption band at 1140 cm<sup>-1</sup> is assigned to the C-C stretching vibrations. (Chougule, M. A., et al., 2011; Yussuf, A., et al., 2018). In the FT-IR studies of GO, a broad band occurring at 3272 cm<sup>-1</sup> corresponds to the O-H stretching of the H<sub>2</sub>O molecule absorbed in GO. The occurrence of absorption bands at 1714 and 1585 cm<sup>-1</sup> is due to the stretching vibrations of carbonyl (C=O) and aromatic C=C bonds. The absorption bands arising at 1045 and 1225 cm<sup>-1</sup> are due to alkoxy (C-O) and epoxy (C-O-C) stretching vibrations. The occurrence of oxygen functionalities (C=O, C-O, etc.) confirms the oxidation of graphite to GO. After the oxidation of graphite, its layered structure is still retained in the GO, which is supported by the existence of C=C bonds in it. (Song, J., et al., 2014; Yussuf, A., et al., 2018). In the FT-IR spectrum of PPY/GO (PG), the characteristic peak due to C=O stretching appears at 1705 cm<sup>-1</sup>. The absorption bands at 2979 and 1038 cm<sup>-1</sup> are due to stretching vibrations of the 0-H and C-O-C bonds of GO in the composite material. The interactions among PPY and GO in the composite materials affect the electron densities and bond strengths, resulting in the shifting of peak positions compared to those of PPY and GO. (Konwer, S., et al., 2011; Ningaraju, S., et al., 2019). The absorption bands at 1558 and 1210 cm<sup>-1</sup> are ascribed to the C=C and C-N stretching of the PPY ring which further confirms the presence of PPY in the PG binary composite. (Konwer, S., et al., 2011; Kulandaivalu, S., et al., 2019)

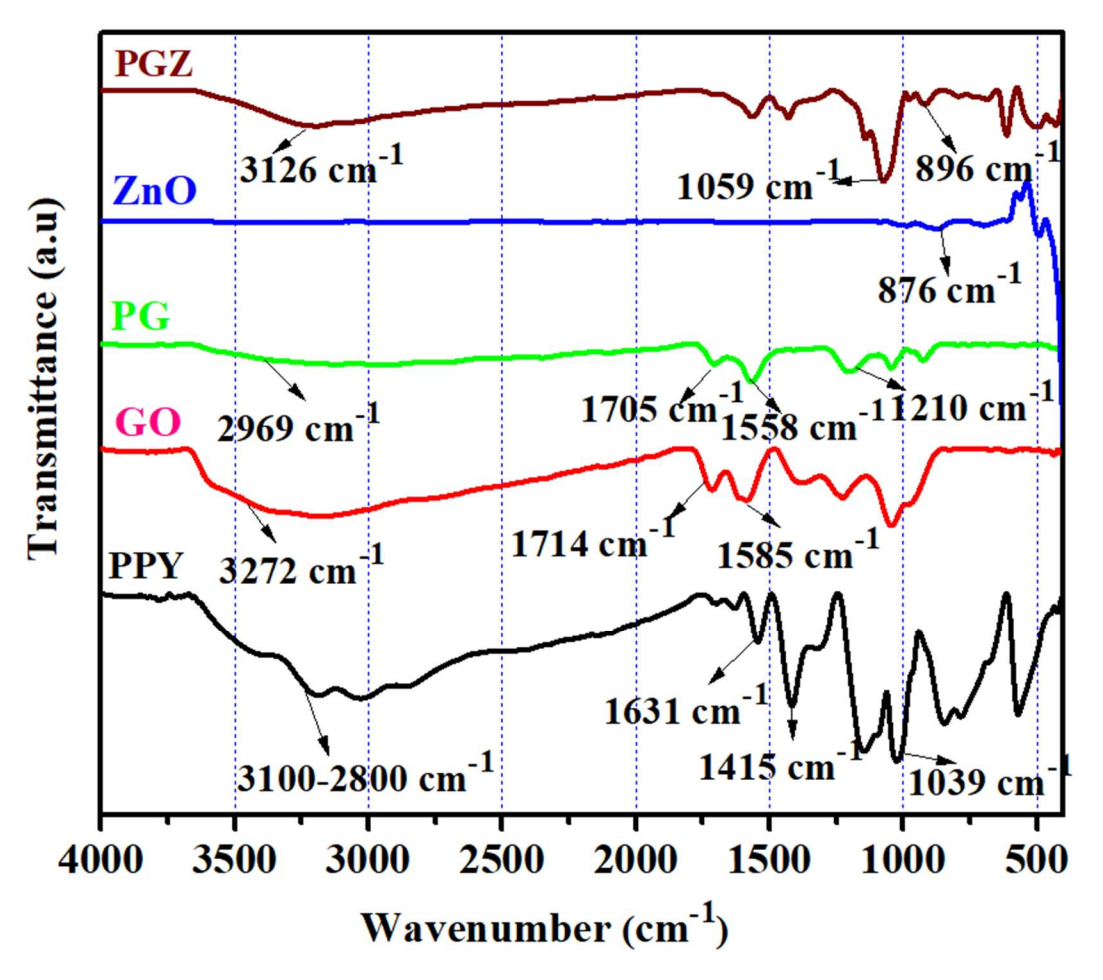


Figure 7. FTIR spectra of PPY, GO, PG, ZnO, and PGZ

The FT-IR spectra of ZnO show a characteristic absorption band at 876 cm<sup>-1</sup> ascribed to the ZnO vibrational mode. The FT-IR studies of the PGZ ternary composite reflect the characteristic bands of its individual components with some shifting in peak positions and peak intensities. This shifting in peak positions is due to the interactions among the PPY, GO, and ZnO affecting bond strengths and electron densities in the composite material. The characteristic peak at 1708 cm<sup>-1</sup> is due to C=O stretching. (**Pruna**, **A.**, et al., 2015: Sing, G., et al 2023.) The absorption bands at 3126 and 1059cm<sup>-1</sup> are due to vibrations of 0-H and epoxy C-O-C bonds of GO present in the ternary composite. The absorption bands at 1562 and 1130 cm<sup>-1</sup> are ascribed to the C=C and C-N stretching of the PPY ring, which further confirms the presence of PPY in PGZ composites. The absorption

band at 896 cm<sup>-1</sup> due to the metal oxide bond in the spectra of PGZ suggests the presence of ZnO in the composite material. (Batool, A., et al., 2012; Pruna, A., et al., 2015). The FT-IR analysis of the binary PG and the ternary composite (PGZ) reflects all the characteristic peaks of its individual components with some shifting in peak positions and intensities, as shown in Table 5. This shifting of the absorption bands is ascribed to the interaction among the individual components in the composite material, which results in the displacement of electron densities as well as the bond strength, thus affecting the vibrational frequencies.

Table 5. Important FT-IR peaks of PPY, GO, ZnO, PG, and PGZ

Materials _	Wavenumber (v, cm <sup>-1</sup> )							
	О-Н	N-H	C=C	C=O	С-О-С	C-N	C=N	Zn-O
PPY	-	3100- 2800	1543	-	-	1415	1631	-
GO	3272	-	1585	1714	1225	-	-	-
ZnO	-	-	-	-	-	-	-	876
PG	2969	-	1558	1705	1038	1210	-	-
PGZ	3126	-	1562	1708	1059	1130	-	896

**4.2. XRD spectra of PPY, GO, PG, ZnO, and PGZ:** - The XRD spectra of PPY, GO, PG, ZnO, and PGZ is shown in **Fig. 8.** The XRD spectra of PPY show a broad peak at  $2\theta = 27.52^{\circ}$  corresponding to the (100) plane. The broader peak signifies the non-crystalline nature of the PPY with a stacked structure due to the short-range arrangements of the polymer layers. **(Chitte, H. K., et al.,2011; Yussuf, A., et al., 2018).** In the XRD spectra of GO, the presence of an intense and sharp diffraction peak at  $2\theta = 10.91^{\circ}$  (001) plane, with an increase in the gallery spacing (d-spacing), signifies the oxidation of graphite to GO. This increase in gallery spacing in the case of GO indicates that the compact and periodic structure of graphite is oxidized by the encapsulation of oxygen moieties between its carbon layers. The appearance of the additional peaks, one at  $2\theta = 42.44^{\circ}$  of the (100)

plane, is due to the short order of the stacked graphitic layers. (Bose, S., et al., 2010; Konwer, S., et al., 2011).

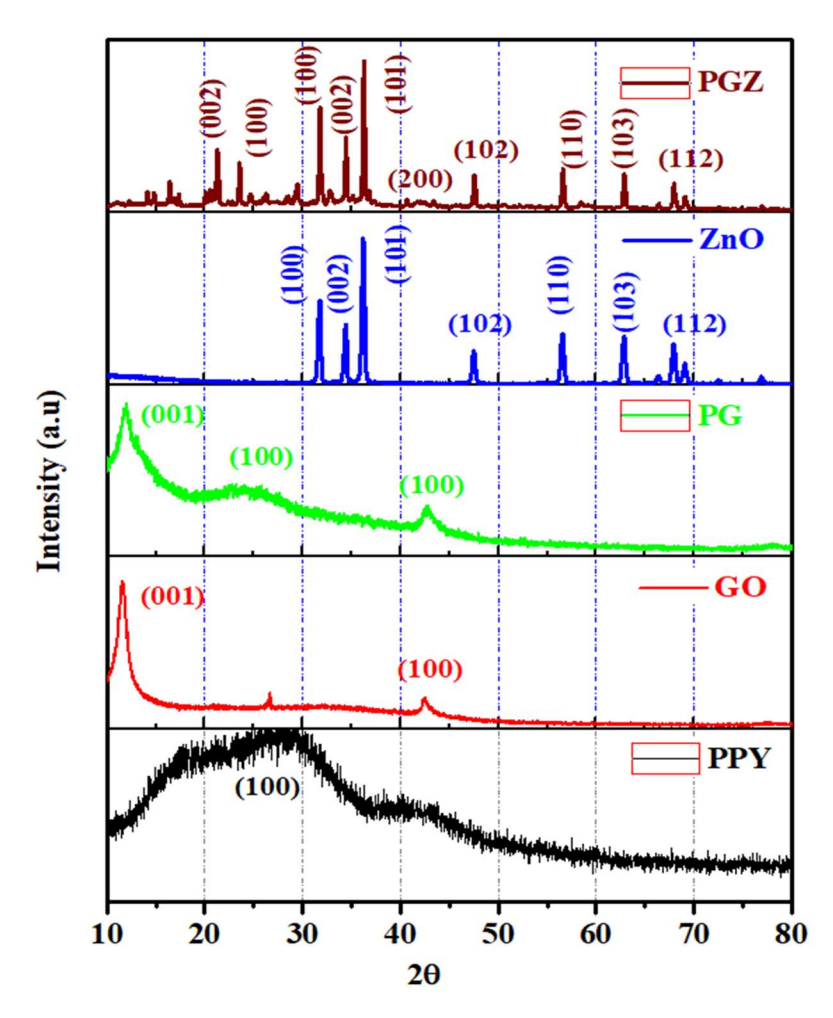


Figure 8. XRD of PPY, GO, PG, ZnO, and PGZ

The appearance of the diffraction peaks at  $2\theta = 11.89^{\circ}$  (001) due to GO and broad diffraction peak at  $2\theta = 23.53^{\circ}$  (100) due to PPY in the XRD spectra of PG binary composite supports its successful development. The peak of the GO has been shifted from  $2\theta = 10.91^{\circ}$  to  $2\theta = 11.89^{\circ}$  in PG with a decrease in the intensity. This reduction in the intensity of the GO peak in the PG may be due to the surface modification of GO sheets during sonication. The broadening of the PPY peak in the PG composite is due to the encapsulation of the GO sheets over the PPY chains, signifying the non-crystalline nature

of the composite. (Konwer, S., et al., 2011; Oularbi, L., et al., 2017; Zhou, X. 2024). The XRD spectra of ZnO show intense and sharp diffraction peaks at 2θ values of 31°, 34°,36°, 47°, 56°, 63° and 72°, suggesting its crystal behavior with hexagonal wurtzite mode. (Sharif, M., et al., 2021). In the XRD spectra of PGZ the peaks of PPY and GO are suppressed and slightly shifted towards higher 2θ values whereas intensive diffraction peaks are due to the presence of ZnO in the composite material corresponding to different planes as (100), (002), (101), (200), (102), (110), (103), and (112). The weakening of the diffraction peaks of PPY and GO in ternary composite could be due to the presence of ZnO on their surfaces, which do not allow them to aggregate during the preparation of ternary composite by ex-situ method. (Ghanbari, K., and Bonyadi, S. 2018; Arumugama, C., et al., 2022).

#### 4.3. Morphological analysis:

The morphological study of the PPY, GO, ZnO, and the prepared ternary composite (PGZ) was analyzed using scanning electron microscopy (SEM) as represented in Fig. 9 (A-D). The SEM micrographs show the spherical granular like morphology of the PPY polymer matrix. These grain-like structures are tightly stacked over one another with a phase variance in the case of PPY. (Konwer, S. et al., 2011) The dense stacking layers-like structures, are seen in the SEM morphology of GO, probably due to the structural deformations caused by the exfoliation of the well-ordered arrangements of the graphitic sheets during the oxidation process. (Mudila, H., et al., 2013). ZnO shows the tiny granular-like structures that are largely agglomerated, producing bunches of grains-like spherical shapes. (Chougule, M. A., 2011).

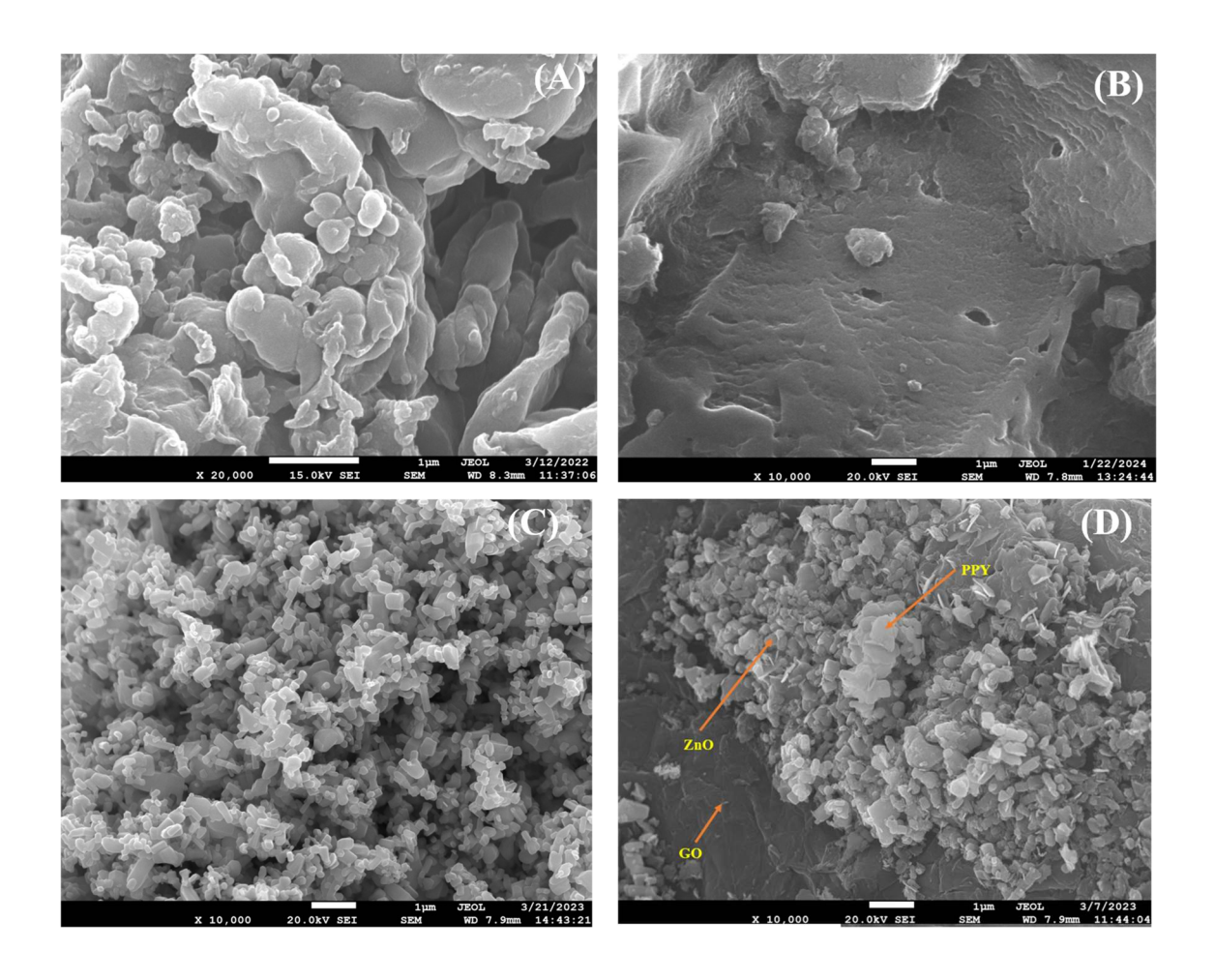


Figure 9: SEM micrograph of (A) PPY, (B) GO, (C), ZnO, and (D), PGZ.

SEM micrographs of PGZ reveal the presence of rolled and folded sheets generated by the fibrous morphology of GO sheets in the composite material. The presence of different oxygen functionalities results in folding and accumulation of the sheets in GO. PPY gets accumulated on the surface of the GO sheets through electrostatic and π-π stacking resulting in non-granular morphology with pores on its surface thus representing flakes-like structures. The presence of ZnO as granules covers the whole surface of the PPY and GO in the composite, resulting in different shapes in repeated manners, thus, providing the enlarged surface area and porous structure to the ternary composite. (Ding, C., et al., 2010; Ali, Z. R., et al., 2022; Arumugam, C., et al., 2023)

The successful development of the ternary composite PGZ was further confirmed by examining the elemental composition of the PGZ composite material, which shows the presence of C, N, O, and Zn as shown in Fig. 10 (A-B) The nano size (56.56 nm) of the PGZ particles is also suggested by the SEM images and is also conveyed by the histogram (Fig. 11). (Sebastian, N., et al., 2022: Arumugam, C., et al., 2023).

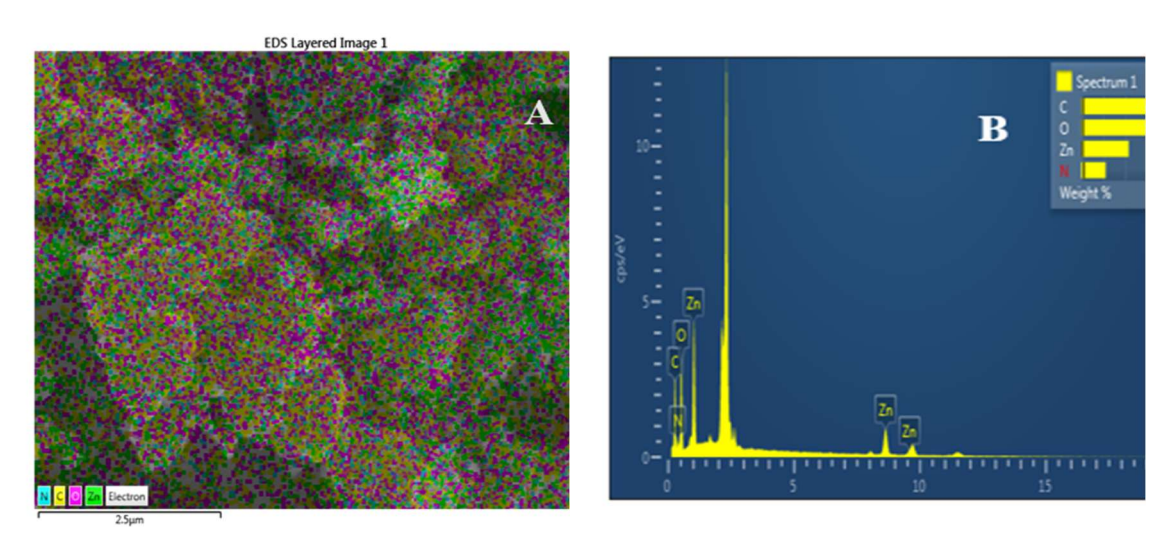


Figure 10. (A-B): Mixed elemental mapping of PGZ

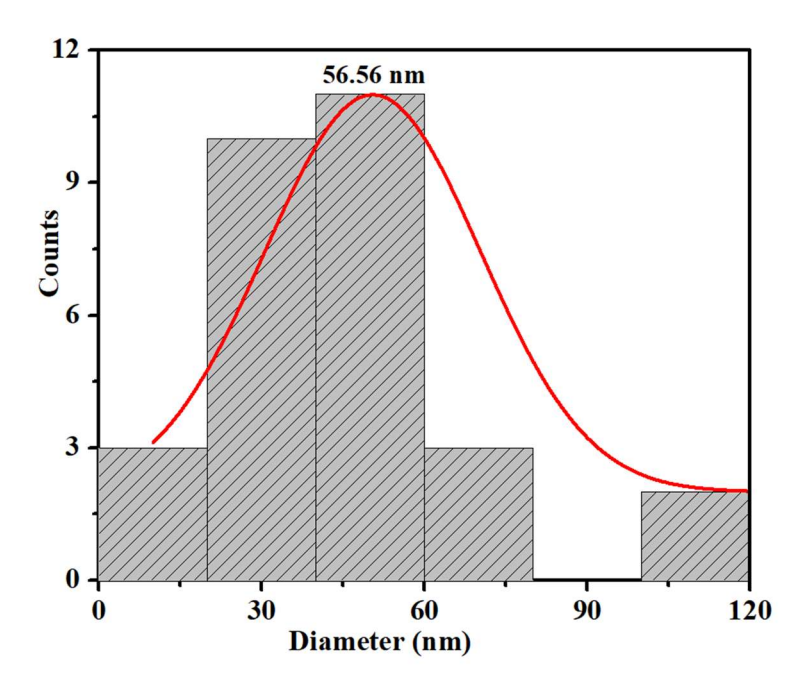


Figure 11. Average particle size of PGZ ternary composite.

**4.3.1 XPS Studies of PGZ composite:** The elemental state of components in bulk material was analyzed using XPS studies **Fig. 12.** All the characteristic peaks in the XPS spectrum of PGZ are due to the presence elements C, N, O, and Zn, further confirming the successful synthesis of PGZ ternary composite.

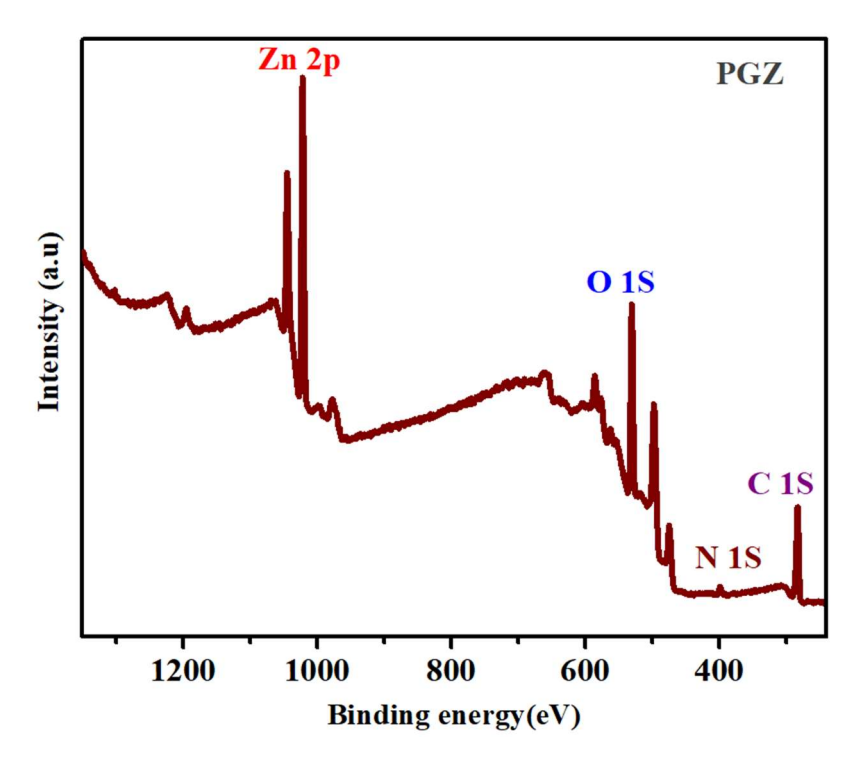


Figure 12. XPS spectral analysis of PGZ Ternary composite

**Fig. 13 (A-D)** shows the deconvolution curves of the C 1s, N 1s, O 1s, and Zn 2p of the PGZ composite. The deconvolved C 1S spectrum gives rise to the three peaks corresponding to C-C (282.58 eV), C-O (283.64 eV), and C=O (286.02 eV), **Fig. 13 A.** The N 1s spectrum shows the two characteristic peaks, with binding energies of 398.09 and 400.39 eV corresponding to the C-N / N-H and N-C=O bond, confirming the presence of the PPY in the ternary composite **Fig. 13 B**. The deconvolved spectrum of O 1s gives rise to two characteristic peaks at 529.15 eV due to Zn-O / C-O / C=O bonds, while at 530.88 eV due to O-C=O and H<sub>2</sub>O, **Fig. 13 C**. The deconvolved spectra of Zn 2p, which give two peaks with the orbital splitting of ( $\Delta$ = 23.05 eV), **Fig. 13 D**. The peak at 1021.73

eV corresponds to the Zn 2p3/2 while the peak at 1044.78 eV is due to the Zn 2p1/2 which is in good agreement with the previous literature. (Ghanbari, K., and Bonyadi, S., 2018; Sebastian, N., et al., 2022).

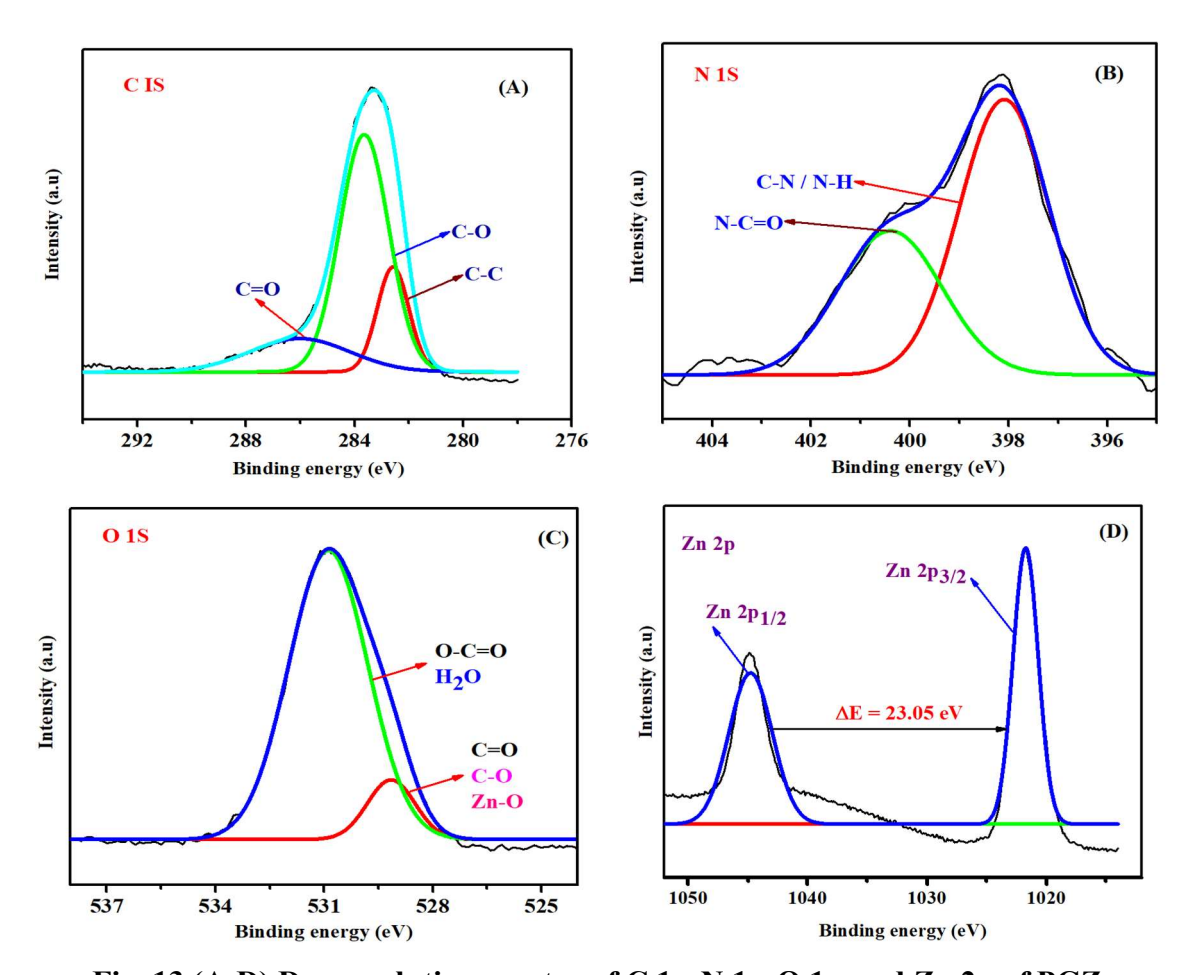


Fig. 13 (A-D) Deconvolution spectra of C 1s, N 1s, O 1s, and Zn 2p of PGZ

#### 4.4 Thermal Studies:

Thermogravimetric Analysis (TGA) curves of PPY, GO, ZnO, PG, and PGZ are shown in **Fig. 14 A**. Initially, the loss in weight at temperatures < 100 °C is due to the amputation of moisture content from the prepared samples. The percentage of weight loss (wt%) at this temperature range depends on the composition of the prepared material; the more hygroscopic the nature, the greater is the weight loss percentage. The major weight loss for

the PPY starts at a Tonsset of 248.28 °C with residual weight (Wr %) of 79.22. The weight loss of PPY continuously increases as the temperature rises, and it ends at a T<sub>offset</sub> of 575 °C, indicating the volatilization of PPY. In the case of GO, the main mass loss takes place at T<sub>onset</sub> 208.71 °C with W<sub>r</sub> % of 76.26. This loss is due to the loss of different oxygen functionalities from the GO surface. After this major weight loss, the material behaves as a graphene and expanded graphite sheet-like structure. (Konwer, S., et al., 2011; Mudila, **H.**, et al., 2013). In PG initially, the weight loss at the temperature of  $\sim 100$  °C is due to the removal of moisture content from the composite surface. The weight loss in the temperature range of 150-170 °C is probably due to the loss of different oxygen moieties introduced by the presence of GO in the composite material. The major weight loss in binary composite T<sub>onset</sub> 243.28 °C arises due to the degradation of PPY from the composite. (Bose, S., et al., 2010: Sing, G., et al, 2025). The higher thermal stability of the PG compared to that of PPY and GO, may be due to the presence of PPY over the GO sheets, which provides stability to the structure as well as blocks the accumulation of heat between the GO sheets in the composite material. After removing moisture content from PPY GO and PG, the W<sub>r</sub>% left up to the T<sub>onset</sub> of the respective material may be due to the loss of impurities and unreacted dopants. (Bose, S., et al., 2010; Li, L., et al., 2012) In the TGA curve of ZnO, a small weight loss at Tonset 300.32 °C due to the removal of moisture content was observed, suggesting the thermal stability of ZnO. (Batool, A., et al., 2012). In case of PGZ, the weight loss at T<sub>onset</sub>, 211 °C, and 348 °C is due to the removal of oxygencontaining functional groups and the degradation of the polymer chain from the surface of composite material. The weight loss in ternary composite occurs at higher temperatures than that of PPY, GO, and PG. Additional stability of the PGZ compared to PPY, GO, and PG is due to the lower mobility of polymer due to the synergetic effect of PPY and GO functionalities along with the barrier effects of ZnO in the composite material. A comparative representation of T<sub>onset</sub>, decomposition temperature (T<sub>d</sub>), and % char has been represented in Fig. 14 B. (Batool, A., et al., 2012; Ates, M., et al., 2018).

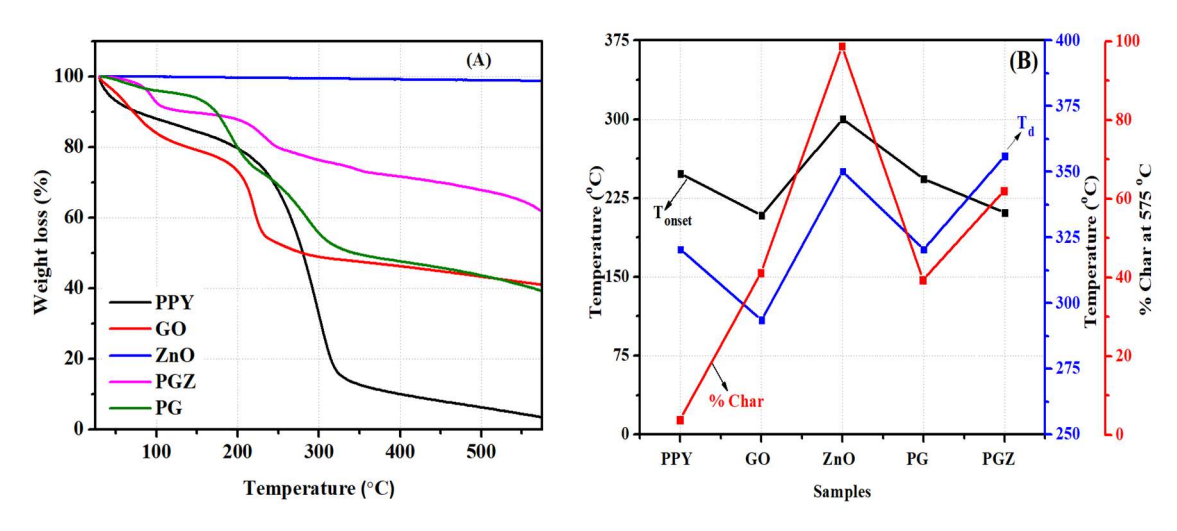


Figure 14. TGA of PPY, GO, ZnO, PG, and PGZ (A), Graphical representation TGA parameter (Tonset, Td, and Char%) of all the samples (B).

### 4.5. Electrochemical measurements using Cyclic Voltammetry:

The electrochemical behavior of PPY, GO, ZnO, binary PGs, and ternary PGZs composites prepared at different weight ratios was studied using Cyclic voltammetry. Cyclic voltammograms (CV curves), which have a current versus potential relationship, were used to study the electrochemical activity of the above-prepared materials. CV studies of the respective electrodes were carried out at 0.05 V/s scan rate within the -0.5 to 1.2 V of window in 5 mM potassium ferrocyanide K<sub>3</sub>[Fe(CN)<sub>6</sub>] and 0.1M KCl as supporting electrolyte. The resulting CV graphs of CPE, PPY, GO, PGs, and PGZs showing distinct peaks of [Fe (CN)<sub>6</sub>]<sup>3-/4-</sup> are shown in Fig. 15 (Lee, S., et al., 2016). The current response of PPY, as seen from the CV curves, is higher than that of the CPE and GO-modified electrode, signifying the better electron transfer properties and fast redox mechanism on the surface of PPY. A lower peak current value in the case of the CPE electrode is due to the non-conductive nature of paraffin oil used during its preparation. In the case of GO, the oxygen functionalities (C=O, C-O, COOH, etc.) on its surface act as a barrier for the smooth transfer of electrons, resulting in a decrease of current values. (Seenivasan, R., et al., 2015: Sing, G., et al 2025). However, in the case of binary composites PGs (at different

w/w ratios) the peak current values are higher compared to CPE, PPY, and GO-based electrodes.

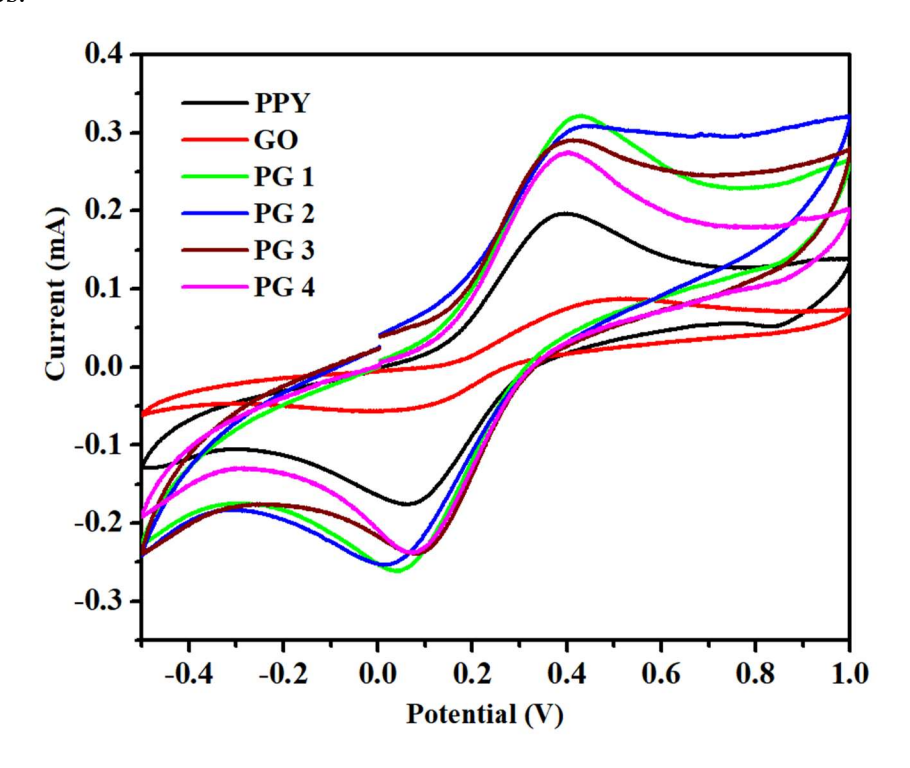


Figure 15. CV curves of PPY, GO, and PGs in 5 mM K<sub>3</sub>[Fe(CN)<sub>6</sub>] and 0.1M KCl

The increase in the current values in PGs is due to the synergetic effect between PPY and GO that increases its porous structure and surface area which promotes the fast electron transfer kinetics on its surface and hence enhances its electrochemical behavior. (Seenivasan, R., et al., 2015; Rong, R., et al., 2017). For the optimization of the best binary composite in terms of its better electrochemical performance, the prepared PGs were studied by their CV studies. The low peak current of PG 4 compared to other composites may be because at this amount of GO, the agglomeration takes place in the composite (PG 4), which leads to the formation of a small amount of nanocomposite on the surface of CPE, slowing down the process of electron transfer. (Seenivasan, R., et al., 2015; Zhang, H., et al., 2023). The PG 1 composite shows better electrochemical response and hence has a high peak current value compared to other binary composites and is therefore considered for the preparation of a ternary composite with ZnO.

The CV curves of ternary composites PGZs (at different w/w ratios) are shown in Fig. 16. The peak current values first increase and then decrease with an increase in the amount of ZnO. This suggests that ZnO up to a certain amount, improves the electrochemical activity by behaving both as a filler and as a pseudo-capacitor, providing a smooth surface for the fast electron transport within the electrode material. With further increase in the amount of ZnO in the composite material results in negative charge agglomeration at the interface of electrode/electrolyte, as well as stacking of the GO sheets, which hinders the transfer of electrons, lowering the current values. (Chee, W. K., et al., 2015; Palsaniya, S., et al., 2021). The composite PGZ 2 has a high peak current value as compared to other composite materials, suggesting a better electrochemical performance and fast electron transfer kinetics at its surface, and hence it has been opted for further studies. (Seenivasan, R., et al., 2015; Zhou, X. 2024).

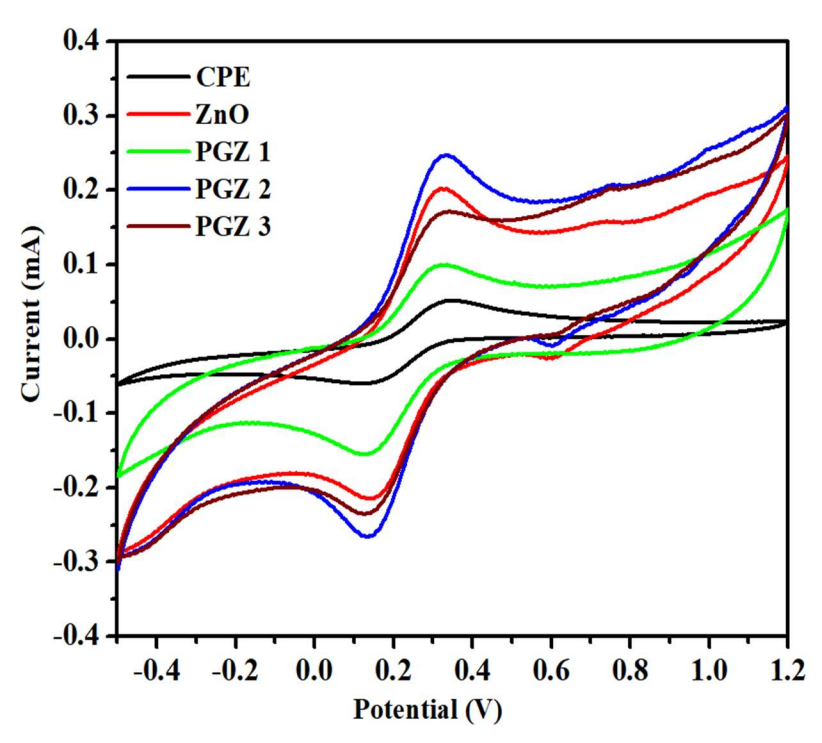


Figure 16. CV curves of CPE, ZnO, and PGZs in 5 mM K<sub>3</sub>[Fe(CN)<sub>6</sub>] and 0.1M KCl

A comparative study of the electrochemical response of PPY, GO, PG 1, and PGZ 2 at 0.05 V/s scan rate is shown in **Fig. 17**. The redox peak of PGZ 2 composite is higher

than that of individual components (CPE, PPY, GO, and ZnO) and the binary composite material PG 1. The increase in the peak current value of PGZ 2 may be due to the synergistic interaction among PPY, GO, and ZnO, thus improving both the redox behavior and surface area of the ternary composite that promotes efficient electron transfer process between the electrolyte K<sub>3</sub>[Fe(CN)<sub>6</sub>] and the electrode surface. (Pruna, A., et al., 2015; Muralikrishna, S., et al., 2017; Palsaniya, S., et al., 2021)

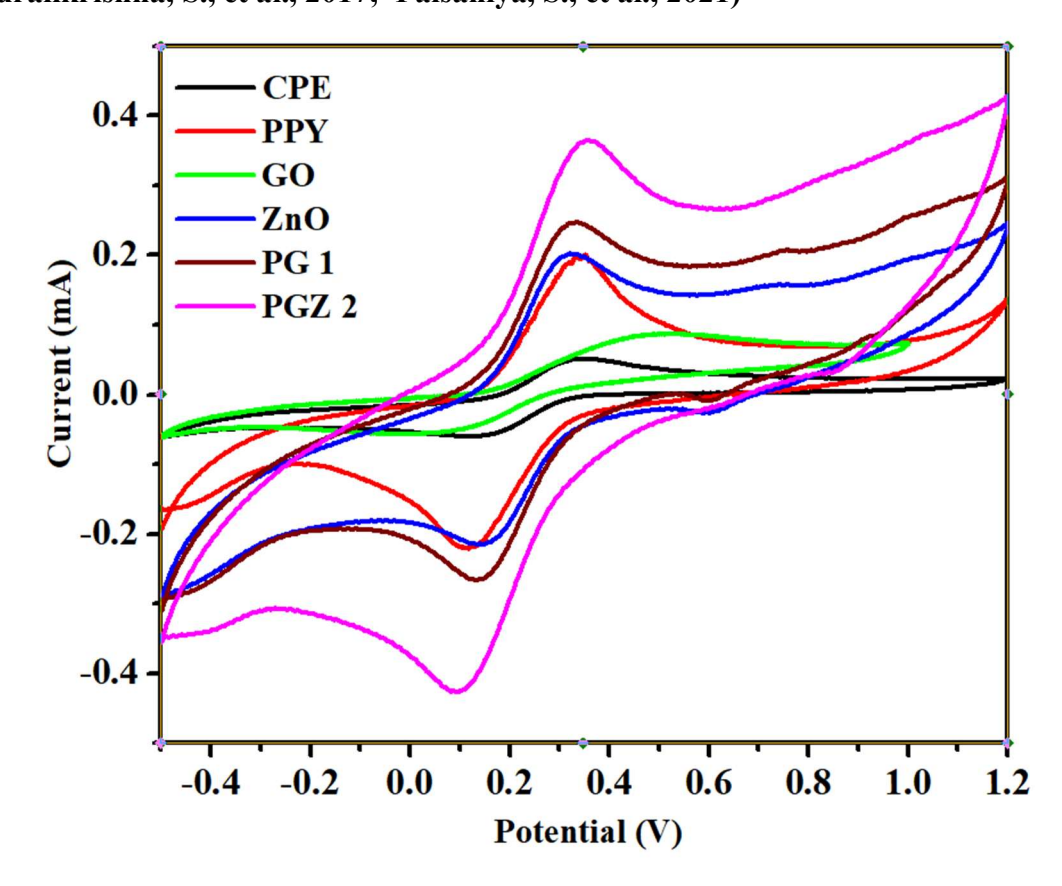


Figure 17. Comparative CV graphs of different electrodes at 0.05 V/s scan in 5 mM K<sub>3</sub>[Fe(CN)<sub>6</sub>] and 0.1M KCl

#### 4.6. Electrochemical impedance spectroscopy (EIS) studies:

The features of surface-modified electrodes were analyzed by EIS studies. The electron transfer process taking place at CPE, PPY, GO, PG 1, and PGZ 2 based electrode materials was examined in 5 mM  $K_3$ [Fe(CN)<sub>6</sub>] and 0.1 M KCl aqueous solution within the range of 0.1 Hz to  $10^6$  Hz. (Oularbi, L., et al., 2017).

The Nyquist plots in the EIS analysis consist of the linear and semicircle portions each signifies a different process. The diameter of the semicircle in high-frequency region reflects the electron transfer resistance (R<sub>ct</sub>) process taking place on the electrode surface. The diffusion-limited processes taking place on the electrolyte-electrode interface are studied from the linear portion in the lower frequency regions of the Nyquist plots. The smaller the diameter of the semicircle lower will be the impedance and charge transfer resistance (R<sub>ct</sub>), signifying a fast charge transfer process. (Seenivasan, R., et al., 2015) The total electrode impedance depends on electron transfer resistance (R<sub>ct</sub>) in series with the parallel connection of the double-layer capacitance (C<sub>dl</sub>) and Warburg impedance (Z<sub>w</sub>). The EIS spectra of bare CPE, PPY, GO, PG 1, and PGZ 2 is shown in Fig. 18

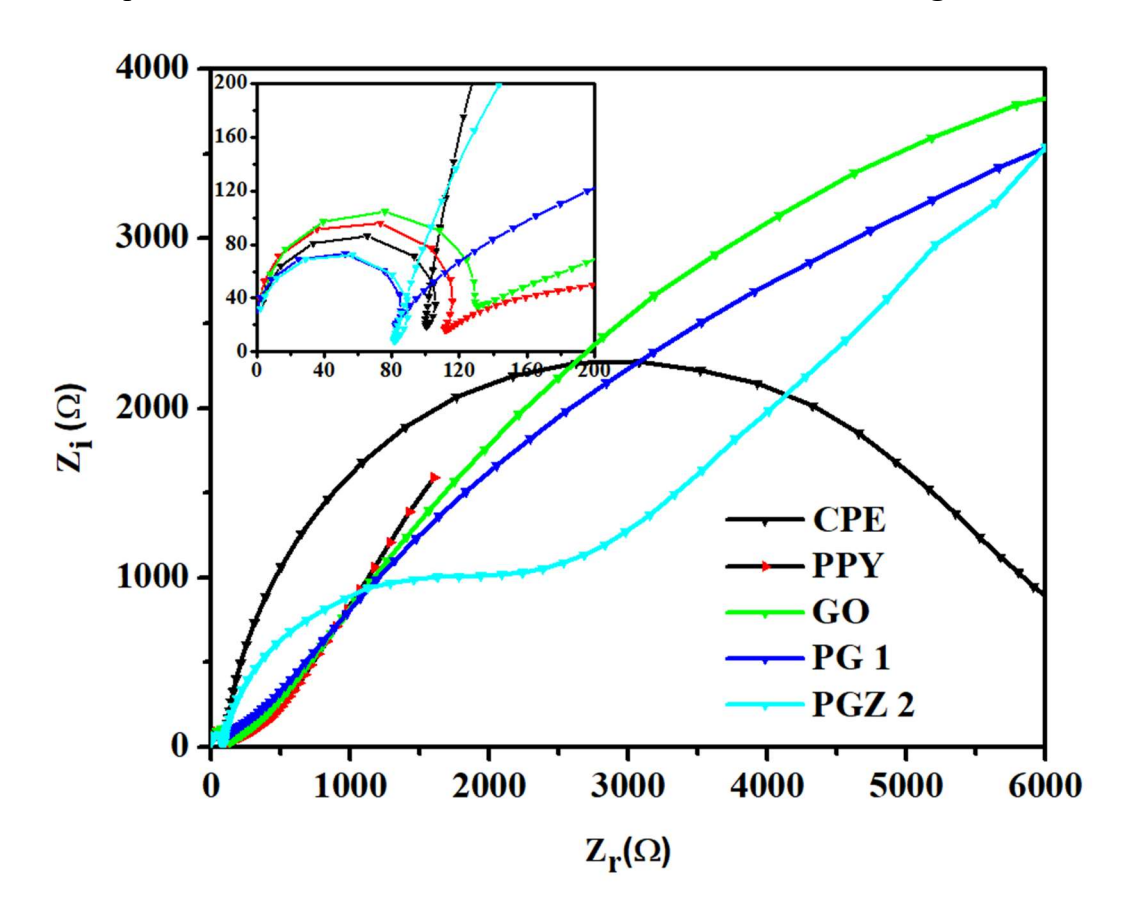


Figure 18. The electrochemical impedance spectroscopy (EIS) of CPE, PPY, GO, PG1, and PGZ 2 in 5 mM K<sub>3</sub>[Fe(CN)<sub>6</sub>] and 0.1 M KCl electrolytic solution

A small semicircle at higher frequency region, and an inclined line in the low frequency region in the EIS spectra of PGZ 2 compared to CPE, PPY, GO, and PG 1, signifying the fast electron transfer processes on its surface. This could be due to better conductivity and improved surface area of PGZ 2 ternary composite, speeding the electron transfer kinetics on its surface, thus speeds the electron transfer rate and the detection of Pb<sup>2+</sup> ions in water samples. These results are in agreement with those reported by the CV studies. (Krasovska, M., et al., 2018; Zhou, H., et al., (2016).

# 4.7. Electrochemical detection of Pb<sup>2+</sup> using DPASV technique:

#### 4.7.1. DPASV measurements of different electrodes:

The electrochemical studies using DPASV for the detection of Pb<sup>2+</sup> ions were performed at different electrodes, CPE, PPY, GO, PG 1, and PGZ 2, in a buffer acetate having pH 4.6 . (Oularbi, L. et al., 2017).

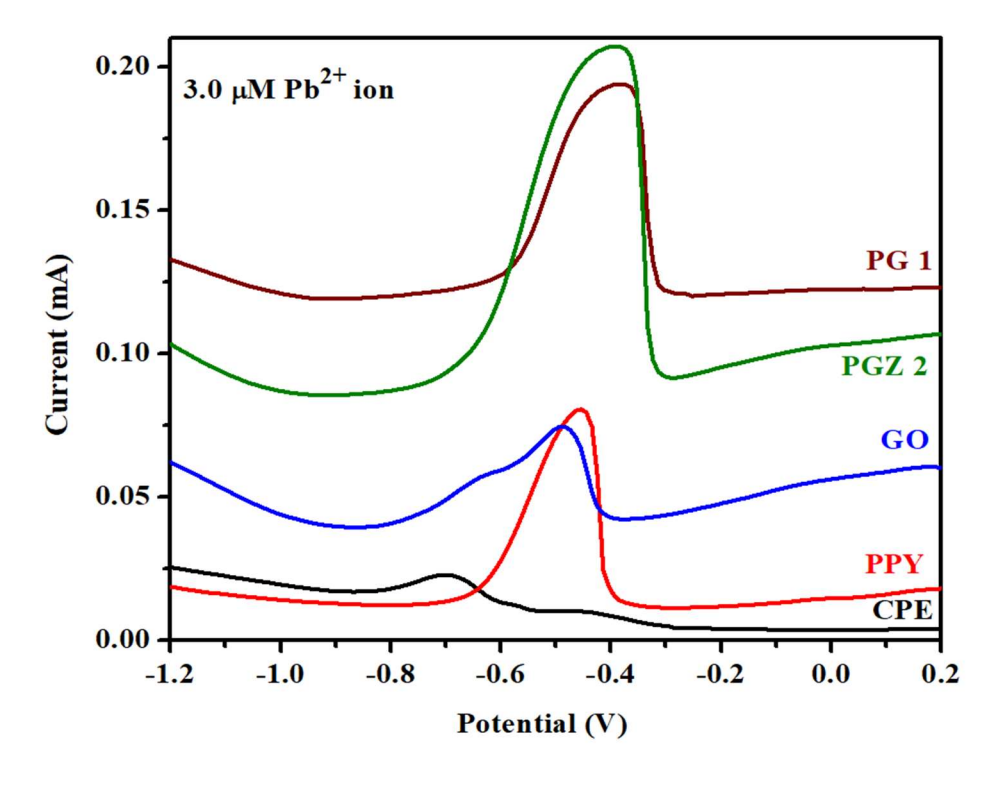


Figure 19: Comparative DPASV of CPE, PPY, GO, PG 1, and PGZ 2 at 3.0  $\mu$ M Pb<sup>2+</sup> ion

Pb<sup>2+</sup> ions are accumulated on the surface of PGZ 2 composite through electrostatic attractions and surface complexations, followed by the reduction of Pb<sup>2+</sup> to Pb<sup>0</sup> with the deposition potential of -1.2 V for 5 minutes. After the deposition step, the DPASV was carried out by applying the potential from -1.2 to 0.2 V for different electrodes. (**Karthik, R., and Thambidurai, S., 2017**). The stripping behavior of the CPE, PPY, GO, PG 1, and PGZ 2 electrodes was analyzed in the presence of 3.0 μM Pb<sup>2+</sup> ions. The stripping peak current value at a potential of -0.45 V for the PGZ 2 composite is higher compared to CPE, GO, PPY, and PG 1 electrodes (**Fig. 19**).

The enhancement in the peak current of PGZ 2 ternary composite compared to the other electrodes may be due to improved surface area by the presence of GO and pseudocapacitive behavior of PPY and ZnO, making the electron transfer process more feasible on its surface. Secondly, negatively charged functional groups in PPY, GO, and ZnO act as binding sites for the Pb<sup>2+</sup> ions, thus improving the deposition ability of Pb<sup>2+</sup> ions on the surface of the ternary composite through surface complexation and coordinate bonds. This results in increasing the number of selective sites for the accumulation of Pb<sup>2+</sup> ions in the case of PGZ 2 and enhances the sensitivity for the detection/determination of Pb<sup>2+</sup> ions. The stripping peak current for the other electrodes follows the trends as CPE < GO < PPY < PG 1. (Dai, H., et al., 2016); Luyen, N.D., et al., 2023)

## 4.7.2. Electrochemical performance of the electrode material:

DPASV studies were performed on PG 1 binary and PGZ 2 ternary composites for different concentrations (0.3 to 3.0 μM) of Pb<sup>2+</sup> metal ion. Well-defined redox peaks that are proportional to the concentration of metal ions were observed for both composites. **Fig.** (20 and 22). A slight shift and broadening of the peak potential with an increase in the concentration of metal ions (Pb<sup>2+</sup>) was observed. This may be attributed to the multilayer metal ions formation on the already formed monolayer on the electrode surface. (**Dong., Y.P. et al., 2014**)

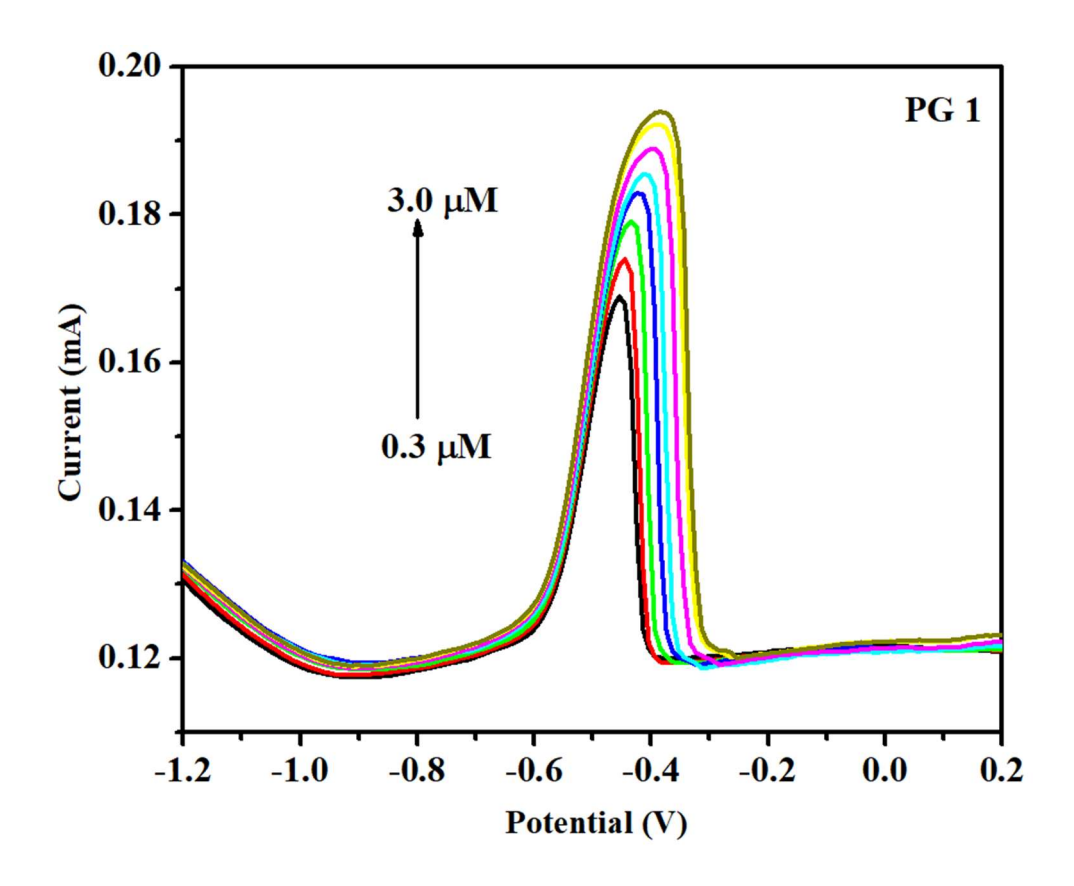


Figure 20. DPASV curves of PG at various concentrations of Pb<sup>2+</sup> (0.3 to 3.0 μM)

The peak current values for the sensing of  $Pb^{2+}$  ion in the working range of 0.3 to 3.0  $\mu$ M on binary composite (PG 1) is shown in **Fig. 20** The corresponding calibration curve of PG 1 within the concentration range of 0.3 to 3.0  $\mu$ M of  $Pb^{2+}$  ions is determined as  $y = 0.0106 \ Pb^{2+} + 0.1707 \ with (R^2 = 0.95)$  as regression coefficient (**Fig. 20**) (**Ghanbari**, **K.**, and Bonyadi, S., 2018).

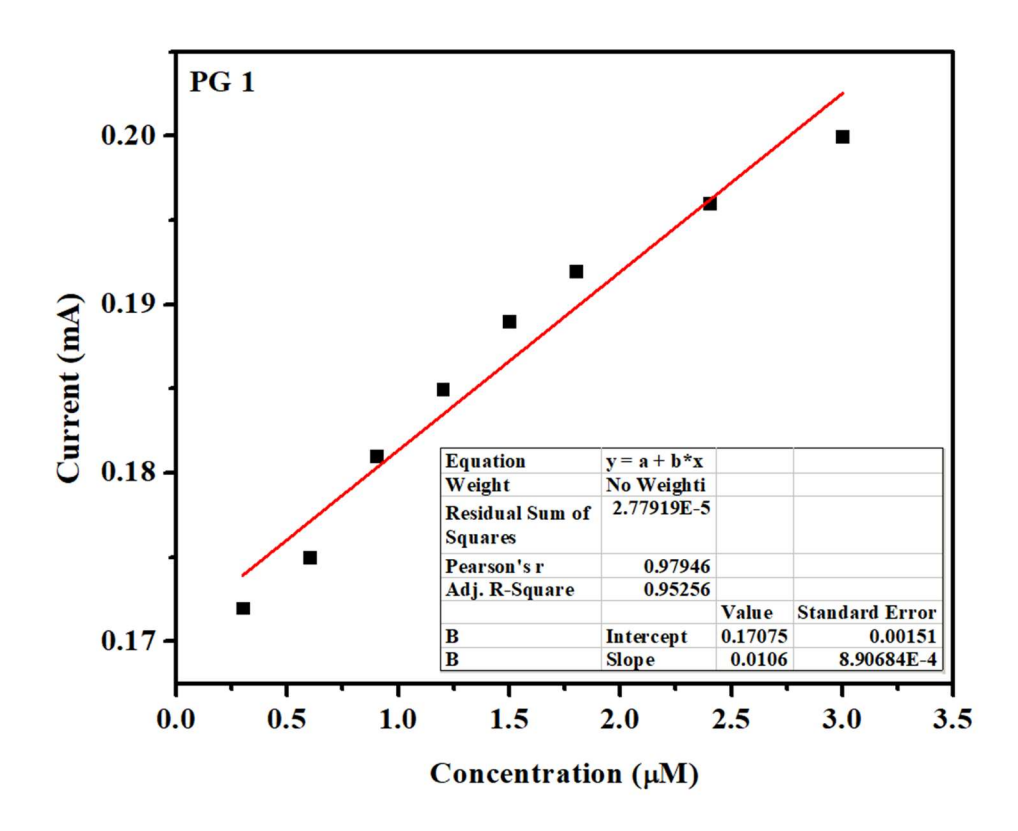


Fig. 21. Calibration curve of PG 1 at various concentrations of Pb<sup>2+</sup> (0.3 - 3.0 μM)

The electrochemical behavior for the sensing of  $Pb^{2+}$  ion at different concentration (0.3 to 3.0  $\mu$ M) on PGZ 2 ternary composite results in the well-defined stripping peaks as shown in **Fig. 22** The calibration curve of PGZ 2 composite for sensing of  $Pb^{2+}$  at different concentrations (0.3 to 3.0  $\mu$ M) represented as  $y = 0.0127 \ Pb^{2+} + 0.1759 \ (R^2 = 0.97)$  (**Fig. 23).** The regression coefficient ( $R^2 = 0.97$ ) in the case of PGZ 2 ternary composite shows linear relationship of the anodic stripping peak current values on the  $Pb^{2+}$  ion concentrations.

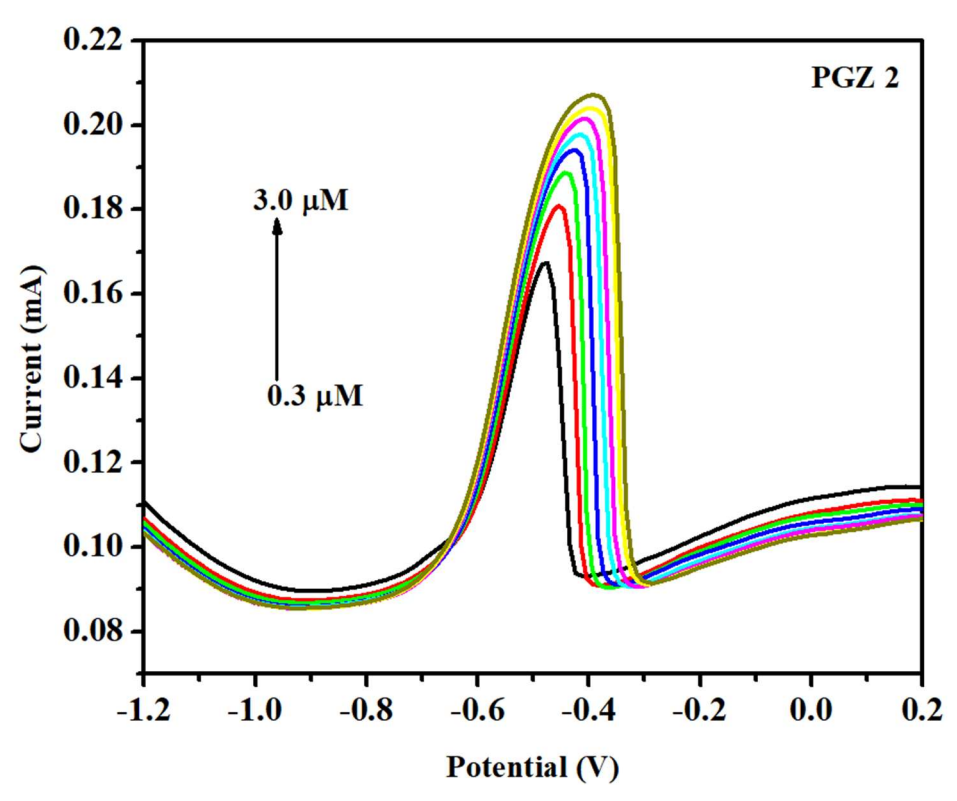


Figure 22. DPASV curves of PGZ 2 at various concentrations of Pb $^{2+}$  (0.3 to 3.0  $\mu$ M)

The limit of detection (LOD) was calculated using the formula "3×SD/S" where "SD" denotes the standard deviation of the blank solution and "S" determines the slope of the resultant calibration curve. The ternary composite (PGZ 2) shows a LOD of 0.05 μM for the detection/determination of Pb<sup>2+</sup> ions. (**Ghanbari, K., and Bonyadi, S., 2018; Luyen, N.D., et al., 2023).** The sensitivity of 0.0127 mA/μM for ternary PGZ 2 composite is higher than the binary PG 1 (0.0106 mA/μM), which further signifies that ternary composite is better than binary composite as a sensor for the sensing of Pb<sup>2+</sup> ion (**Muralikrishna, S., et al., 2017; Oularbi, L., et al., 2017**)

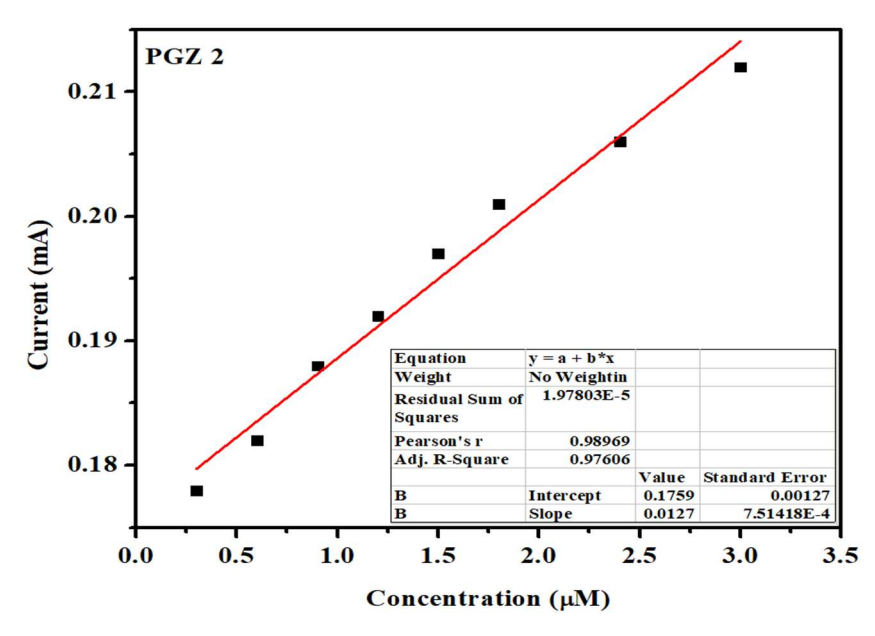


Fig. 23. Calibration curve of PGZ 2 composites at various concentrations of Pb<sup>2+</sup> (0.3 - 3.0 μM)

# 4.7.3. Selectivity of PGZ electrode for sensing Pb<sup>2+</sup> ions:

The selectivity of the PGZ 2 electrode material was analyzed by adding different concentrations of the substance (Cd<sup>2+</sup>, Cu<sup>2+</sup>) to the electrochemical cell containing 3.0 μM Pb<sup>2+</sup> ions in 0.1 M acetate buffer. The existence of these foreign metal ions (Cu<sup>2+</sup>, Cd<sup>2+</sup>) might be co-deposited on the electrode surface containing Pb<sup>2+</sup> ions during the preconcentration process in DPASV studies. (**Dai, H., et al., 2016**). **Fig. 24** below shows the stripping peak current values of Pb<sup>2+</sup> ions in the absence and in the presence of interfering metal ions. The results show minimal changes in the stripping peak current and potential values of the Pb<sup>2+</sup> ion in the presence of high and low concentrations of interfering ions. The peak responses changed from 0.212 mA without interference to 0.214 mA and 0.221 mA at low and high concentrations of interfering ions, whereas a negligible shift in the peak potential was observed. This slight shifting in values and broadening of the Pb<sup>2+</sup> ion peak may be due to the creation of new intermetallic compounds like Pb-Cu and Pb-Cd during the accumulation step. The intensity of the Pb<sup>2+</sup> metal ion signal remains unaffected by the introduction of such interference, which shows the selective detection of Pb<sup>2+</sup> ions.

This may be due to the inactive response of the added metal ions within the oxidation potential range of the Pb<sup>2+</sup> metal ion on the PGZ 2 electrode surface. (Seenivasan, R., et al., 2015; Blaise, N. et al., 2022)

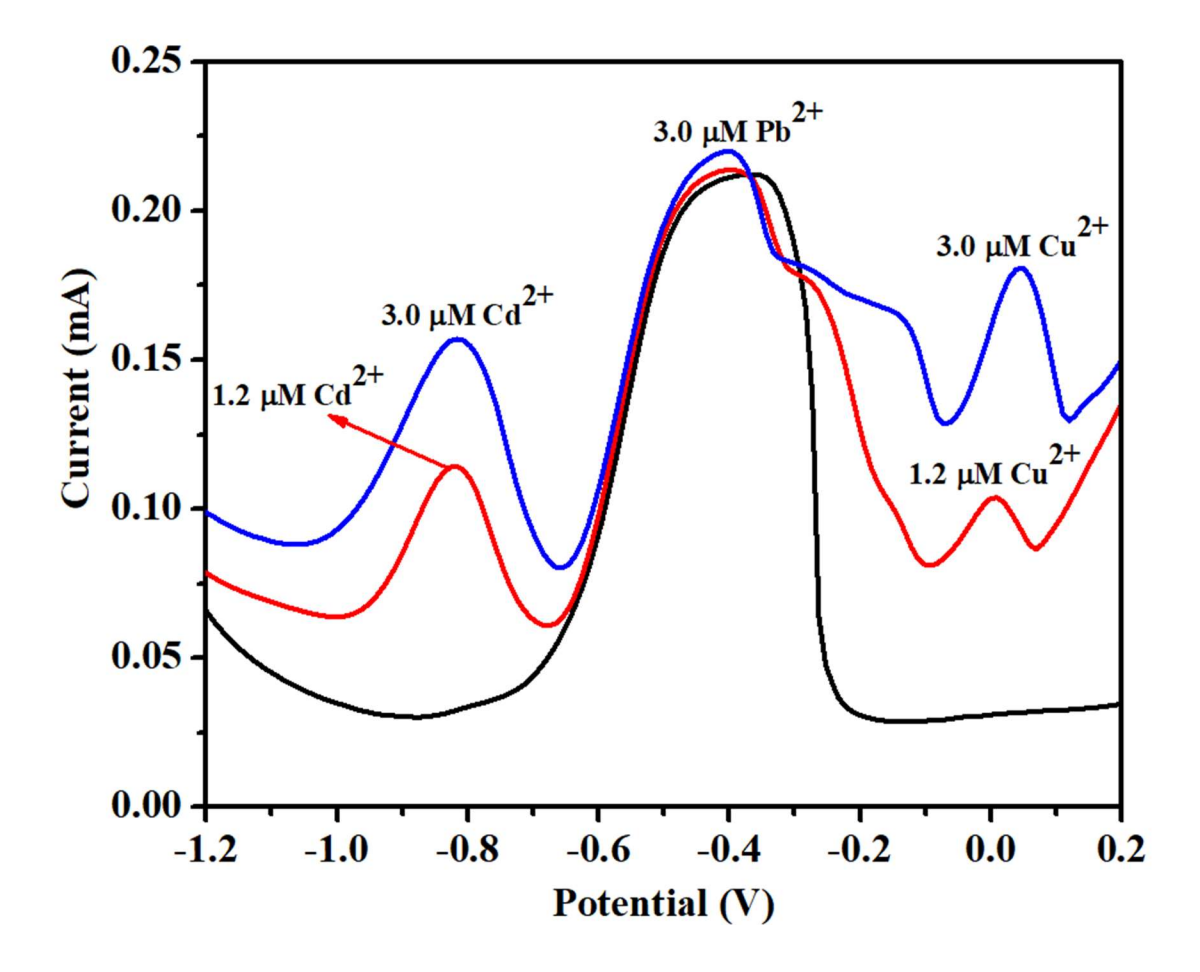


Figure 24. DPASV results of PGZ 2 composite in the presence of 3.0  $\mu$ M Pb<sup>2+</sup> ions and in the presence of interference 1.2 and 3.0  $\mu$ M Cd<sup>2+</sup> and Cu<sup>2+</sup> ions

4.7.4. Reproducibility and stability of PGZ electrode for sensing  $Pb^{2+}$  ions: - Five different electrodes modified equally with the electroactive material were prepared to study the reproducibility of the PGZ 2 electrode. The DPASV measurements were performed in 3.0  $\mu$ M concentration of  $Pb^{2+}$  in an acetate buffer of pH 4.6 as an electrolyte. The corresponding stripping current values for each electrode were recorded (**Fig. 25**). A

stripping peak current at -0.45 V was observed irrespective of the electrode material with a Relative Standard Deviation (RSD) of 1.089% and minimum peak current variation showing the reproducibility of the electrode material. (Seenivasan, R., et al., 2015; Karthik, R., and Thambidurai, S., 2017).

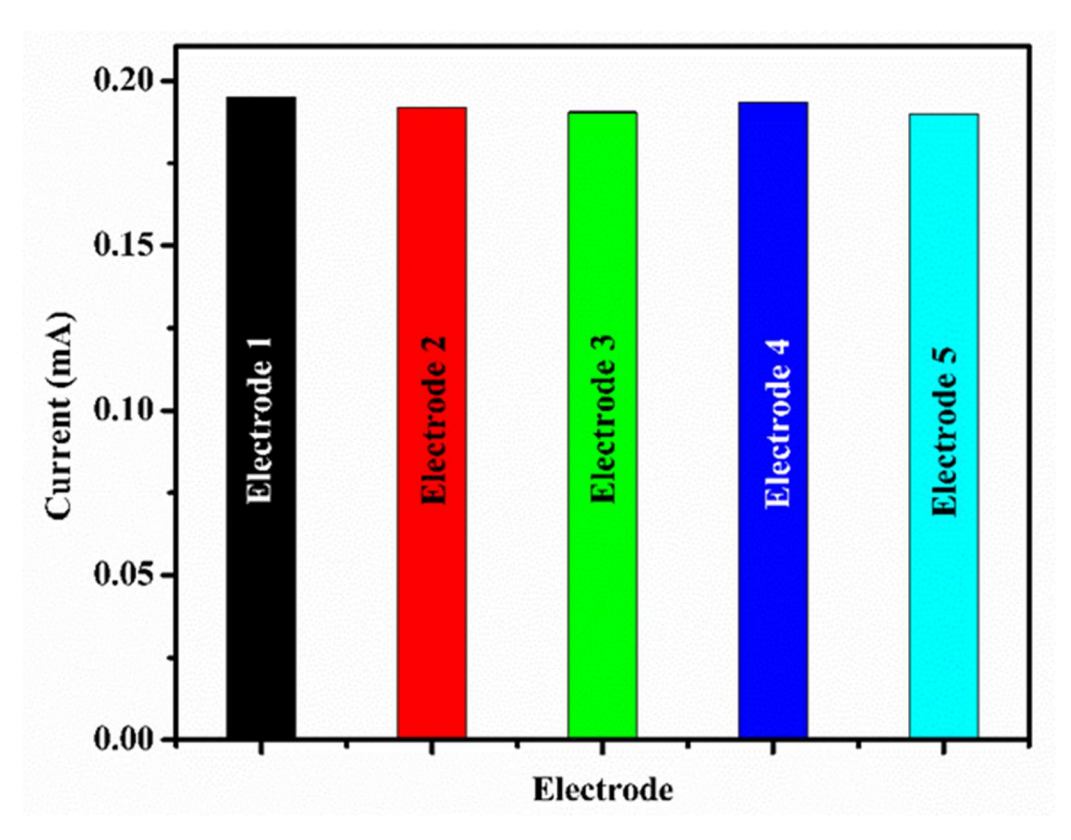


Figure 25. Representation of the reproducibility of PGZ 2 electrodes in 3.0μM Pb<sup>2+</sup> ion solution.

The stability of the PGZ 2 composite was analyzed by performing the DPASV measurements in the same concentration of Pb<sup>2+</sup> ion (3.0 µM). The electrode, after each measurement, was washed with distilled water and acetate buffer solution pH 4.6 kept safe for further measurement. Each measurement was performed after 7 days for the next 4 weeks and the corresponding current response was recorded (Fig. 26). The electrode material shows long-term stability with loss of initial current response RSD 3.67% and retention of 96.33% current response, thus representing the stability of the electrode material (Chen, L., et al., 2014).

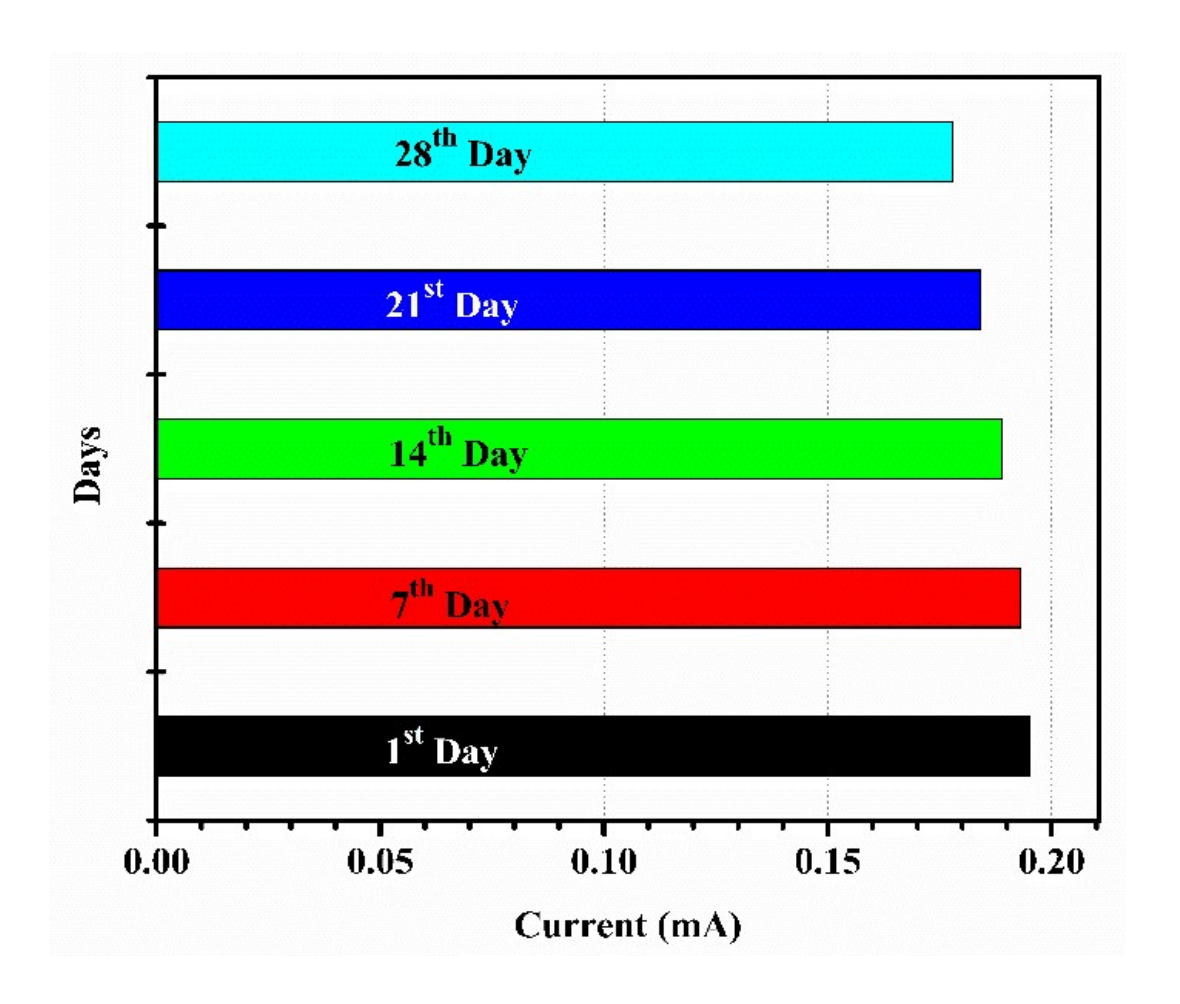


Figure 26. Representation of the stability of PGZ 2 electrodes in 3.0 $\mu$ M Pb $^{2+}$  ion concentration

**4.8. Removal of the Pb**<sup>2+</sup> **metal ion using PGZ 2 composite:** UV-visible spectroscopy technique was employed to analyze the percentage removal of Pb<sup>2+</sup> ion from the aqueous solution. A known amount (2 mg) of the PGZ 2 ternary composite as adsorbent was added to 30 ml of a 100ppm concentration of the lead solution. The resultant solution was allowed to sonicate for 10 minutes and then allowed to stand for the next 15 minutes to form a stable suspension. The effect of the contact time of the adsorbent to the Pb<sup>2+</sup> ion solution at different time intervals (1, 4, 24 hours) was then studied using UV-Visible spectroscopy (**Fig. 27**). The percentage removal efficiency of the Pb<sup>2+</sup> ion on the surface of PGZ 2

composite was calculated, as shown in the table using the equation (Li, S., et al., 2012: Birniwa, A. H., et al., 2022)

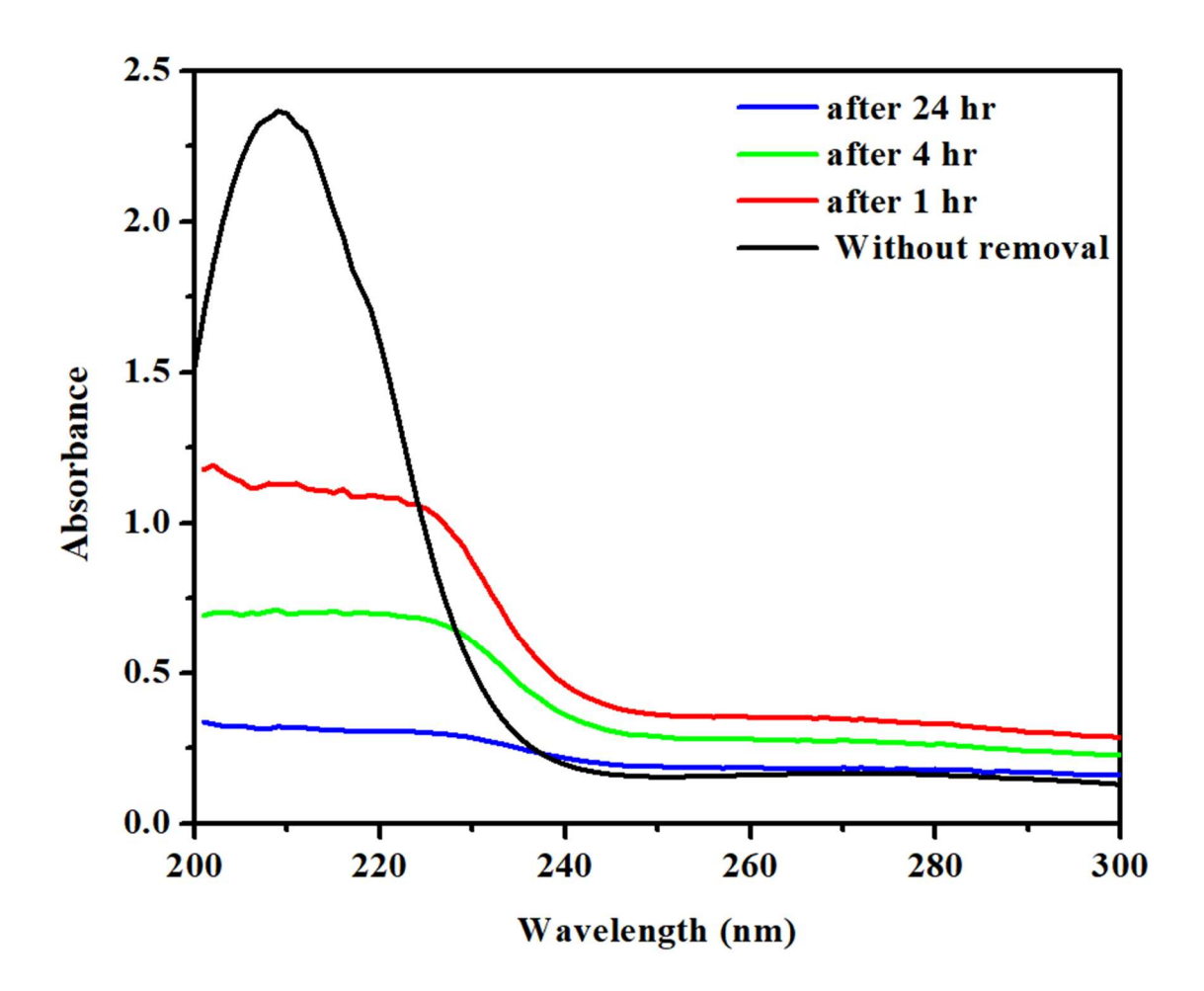


Figure 27. UV-Visible spectra representing the detection and removal of Pb<sup>2+</sup> ions in aqueous solution

% removal efficiency = 
$$\frac{C_o - C}{C_o} \times 100$$
 -----(6)

Where Co is the initial concentration and C is the final concentration

From the graph, it can be seen that with an increase in the duration of the contact time of the adsorbent with the Pb<sup>2+</sup> ion solution, more of these ions get adsorbed on the

surface of the composite material, resulting in a decrease in the concentration of the Pb<sup>2+</sup> ion in the solution.

Table 6. The removal efficiency of Pb2+ ions by PGZ 2 composite with time

S. No	Contact time	% Removal		
1	1 hr	51.48		
2	4 hr	70.47		
3	24 hr	86.92		

## 4.9. FT-IR of PPY, GO, PG, MnO<sub>2</sub>, and PGM Ternary Composite:

The presence of different functionalities and the types of bonds present in the material under investigation were analyzed by FT-IR studies. Fig. 28 below shows the FT-IR analysis of the synthesized PPY, GO, MnO<sub>2</sub>, PG, and PGM recorded in the range of 500-4000 cm<sup>-1</sup>. In the FTIR spectra of PPY, the vibrational bands at 1631, 1543, and 1415 cm<sup>-1</sup> <sup>1</sup> are associated with the symmetric stretching vibrations of the ring's C=N, C=C, and C-N bonds. A broad band in the range 3100-2800 cm<sup>-1</sup> is due to the presence of the N-H bond. The wave numbers associated with 1039 cm<sup>-1</sup> and 1300 cm<sup>-1</sup> are due to the in-plane deformations of the C-H and C-N bonds, and the C-H out-of-plane deformation is centered at 884 cm<sup>-1</sup>. The band at wavenumbers 1140 and 910 cm<sup>-1</sup> corresponds to the doped state of PPY with Fe<sup>3+</sup>. (Chougule, M. A., et al., 2011; Song, J., et al., 2014). The FT-IR spectra of GO a broad absorption band of O-H stretching vibrations at 3272 cm<sup>-1</sup>. The bands at 1714 and 1585 cm<sup>-1</sup> are due to the vibrations of carbonyl (C=O) and aromatic C=C bonds. The absorption bands arising from epoxy (C-O-C) and alkoxy (C-O) stretching occur at 1225 and 1045 cm<sup>-1</sup>. (Song, J., et al., 2014). FT-IR spectra of MnO<sub>2</sub> show the vibrational mode of Mn-O and O-Mn-O at 990 cm<sup>-1</sup> and 507 cm<sup>-1</sup>. (Ramachandran, T., and Dhayabaran, V. V., 2019). In the FT-IR spectrum of PG, the characteristic peak due to C=O stretching appears at 1705 cm<sup>-1</sup>, which has been shifted towards the lower

wavenumber compared to the same peak that appeared in the FT-IR of GO. This fluctuation of the C=O peak towards the lower wavenumber may be due to the interaction between the carbonyl (C=O) group of GO and the N-H group of PPY. These interactions among PPY and GO in the composite materials affect the electron densities and bond strengths, resulting in the shift of the vibrational frequencies of the bonds in the composite. The bands at 2979 and 1038 cm<sup>-1</sup> are due to vibrations of O-H and epoxy (C-O-C) bonds of GO. The presence of PPY in binary composites is confirmed by the presence of absorption bands C=C and C-N stretching vibrations of PPY rings at 1558 and 1210 cm<sup>-1</sup>. (**Konwer, S., et al., 2011**; **Kulandaivalu, S., et al., 2019**) The FT-IR spectra of the PGM composite reflect all the characteristic peaks of its components with some shifting in peak positions and intensities. The characteristic peak due to C=O stretching at 1714 cm<sup>-1</sup> in the case of GO is shifted towards the lower wavenumber and appears at 1708 cm<sup>-1</sup> in the FT-IR spectrum of the ternary composite. (**Pruna, A., et al., 2015**)

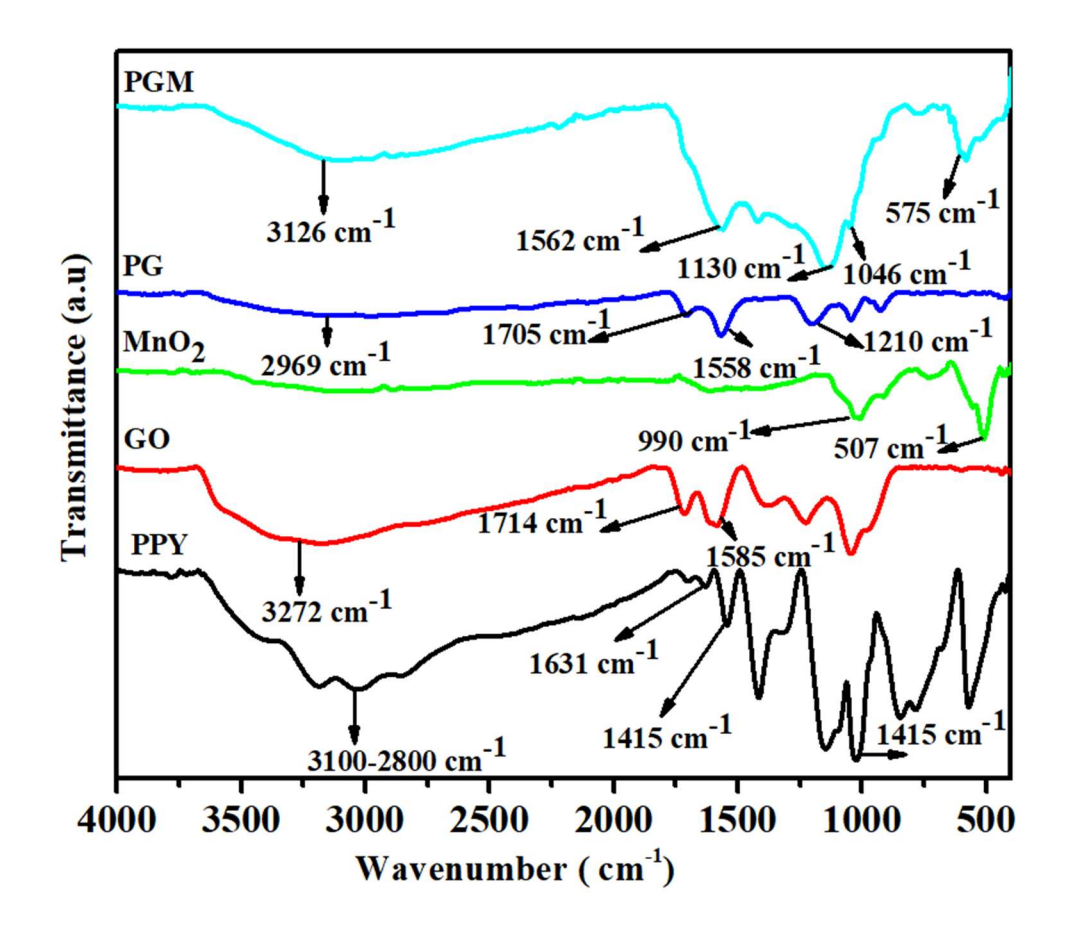


Figure 28. FTIR spectra PPY, GO, MnO<sub>2</sub>, PG, and PGM.

This shifting of the C=O peak in the case of ternary composites towards lower wavenumber may be due to interaction between the carbonyl (C=O) group of GO and the N-H group of PPY. The bands at 3126 and 1046 cm<sup>-1</sup> are due to vibrations of 0-H and epoxy (C-O-C) bonds of GO. The vibrational bands at 1562, and 1130 cm<sup>-1</sup> are ascribed to the C=C and C-N stretching of the PPY ring which further confirms the presence of PPY in ternary composites. (Liang, F., et al., 2017). The absorption band at 575 cm<sup>-1</sup> due to the metal oxide bond in spectra of PGM suggests the presence of MnO<sub>2</sub> in composite material. The FT-IR spectra of the binary PG and the ternary composite (PGM) reflect all the characteristic peaks of its individual components with some shifting in peak positions and intensities as shown in Table 6. (Konwer, S., et al., (2011; Kulandaivalu, S., et al., 2019)

Table 7. Important FT-IR peaks of PPY, GO, MnO2, PG, and PGM

Material _		Wavenumber (v, cm <sup>-1</sup> )						
	О-Н	N-H	С=С	C=O	С-О-С	C-N	N C=N	Mn-O
PPY	-	3100-2800	1543	-	-	415	1631	-
GO	3272	-	1585	1714	1225	-	-	-
MnO <sub>2</sub>	-	-	-	-	-	-	-	990, 507
PG	2969	-	1558	1705	1038	210	-	-
PGM	3126	-	1562	1715	1046	.130	-	575

#### 4.10. XRD spectra of PPY, GO, PG, MnO<sub>2</sub>, and PGM:

The XRD spectra of PPY, GO, PG, MnO<sub>2</sub>, and PGM are shown in Fig. 29. The XRD spectra of PPY show a broad peak at  $2\theta = 27.52^{\circ}$  corresponding to the (100) plane. The broader peak signifies the amorphous nature of the polymer powder with an intermolecular stacking structure due to the short-range arrangements of the polymer layers. (Chitte., H. K. et al., 2011; Yussuf., et al., 2018). The XRD spectra of GO show a sharp and intense diffraction peak at  $2\theta = 10.91^{\circ}$  (001) plane with an increase in the gallery spacing compared to that of graphite. This increase in gallery spacing in the case of GO signifies that the compact and periodic structure of graphite is oxidized by the encapsulation of oxygen moieties between its carbon layers. The appearance of the additional peaks, one at  $2\theta =$ 42.44° of the (100) plane, is due to the short order of the stacked graphitic layers (Bose, S., et al., 2010; Konwer, S., et al., 2011). The appearance of the diffraction peaks at  $2\theta =$  $11.89^{\circ}$  (001) due to GO and broad peak at  $2\theta = 23.53^{\circ}$  (100) due to PPY in the XRD spectra of PG composite material supports its successful development. The diffraction peak of the GO has been shifted from  $2\theta = 10.91^{\circ}$  to  $2\theta = 11.89^{\circ}$  in PG with a decrease in the intensity. This reduction in the intensity of the GO peak in the PG may be due to the surface modification of GO sheets during sonication. The broadening of the PPY peak in the composite is due to encapsulation of the GO sheets over the PPY chains suggesting the amorphous nature of the composite. (Konwer, S., et al., 2011; Oularbi, L., et al., 2017). The XRD spectra of MnO<sub>2</sub> show diffraction peaks at 2θ values of 22.48°, 28.50°,37.54°, 42.25°, and 56.54°, corresponding to the planes (002), (100), (101), (102) and (110) signifying its crystalline behavior (Liang, F., et al., 2017). In the XRD spectra of PGM, the peaks of GO are suppressed and the broad diffraction peaks with a decrease in the intensity of PPY and MnO<sub>2</sub> are observed in the composite material. The weakening of the diffraction peaks of MnO<sub>2</sub> in the PGM may be due to the change in the crystal structure of MnO<sub>2</sub> towards amorphous in the composite material. (Liang, F., et al., 2017). (Ramachandran, T., and Dhayabaran, V. V., 2019).

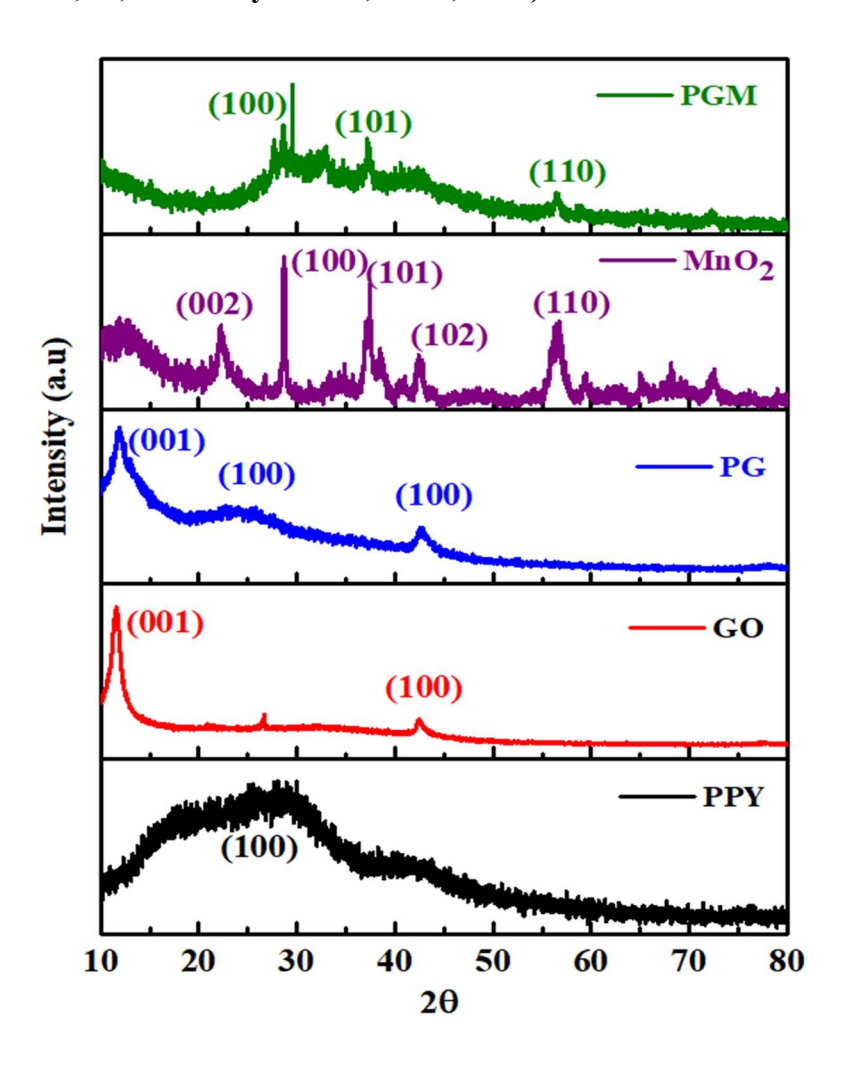


Figure 29. XRD of PPY, GO, PG, MnO<sub>2</sub>, and PGM

### 4.11. Morphological studies:

The morphological study of the PPY, GO, MnO<sub>2</sub>, and the prepared ternary composite (PGM) was studied using scanning electron microscopy (SEM) as represented in **Fig. 30** (A-D). The SEM micrographs of the PPY show the spherical granular morphology of the polymer matrix. These grain-like structures are tightly stacked over one another with a phase variance in the case of PPY. (Konwer, S., et al., 2011) The SEM image of GO shows the dense stacking layers-like structures, probably due to the structural deformations caused by the exfoliation of the well-ordered arrangements of the graphitic sheets during the oxidation process. (Mudila, H., et al., 2013). SEM image of MnO<sub>2</sub> shows the spherical shapes that are largely that are uniformly distributed. (Ramachandran, T., and Dhayabaran, V. V., 2019).

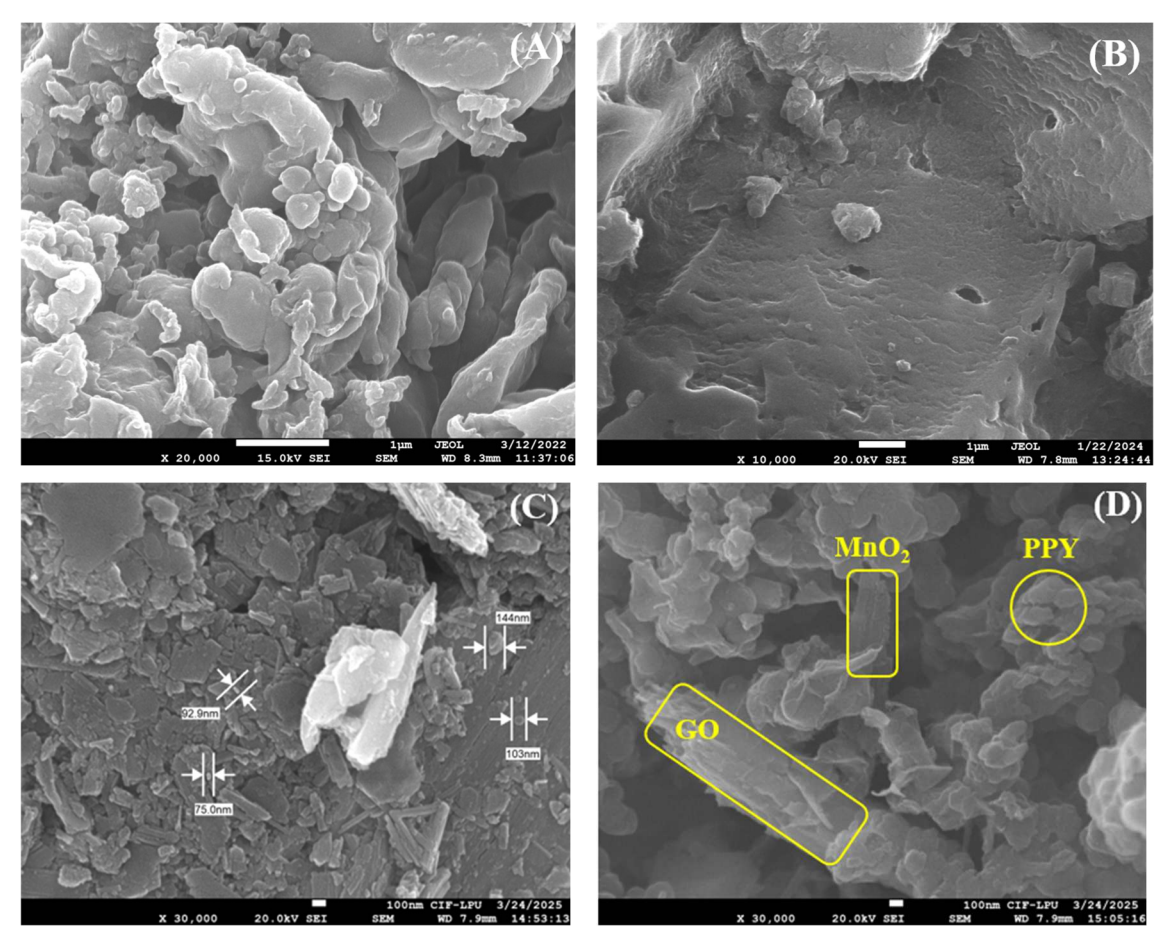


Fig. 30. SEM micrograph of PPY (A), GO (B), MnO<sub>2</sub> (C), and PGM (D)

SEM micrographs of PGM reveal the presence of rolled and folded sheets generated by the fibrous morphology of GO sheets in the composite material. PPY gets adsorbed on the surface of the GO sheets through electrostatic and π-π stacking, resulting in non-granular morphology with pores on its surface, thus representing flake-like structures. The presence of MnO<sub>2</sub> as spherical structures covers the whole surface of the PPY and GO in the composite, resulting in different shapes in repeated manners, thus providing the porous structure and increased surface area of the ternary composite material. The successful development of the ternary composite PGM was further confirmed by examining the elemental composition of the PGM composite material, which shows the presence of C, N, O, and Mn as shown in Fig. 31 (A-B) The nano size (73.97 nm) of the PGM particles is also suggested by the SEM images and is also conveyed by the histogram (Fig. 32). (Ramachandran, T., and Dhayabaran, V. V., 2019: Ates, M., et al., 2020).

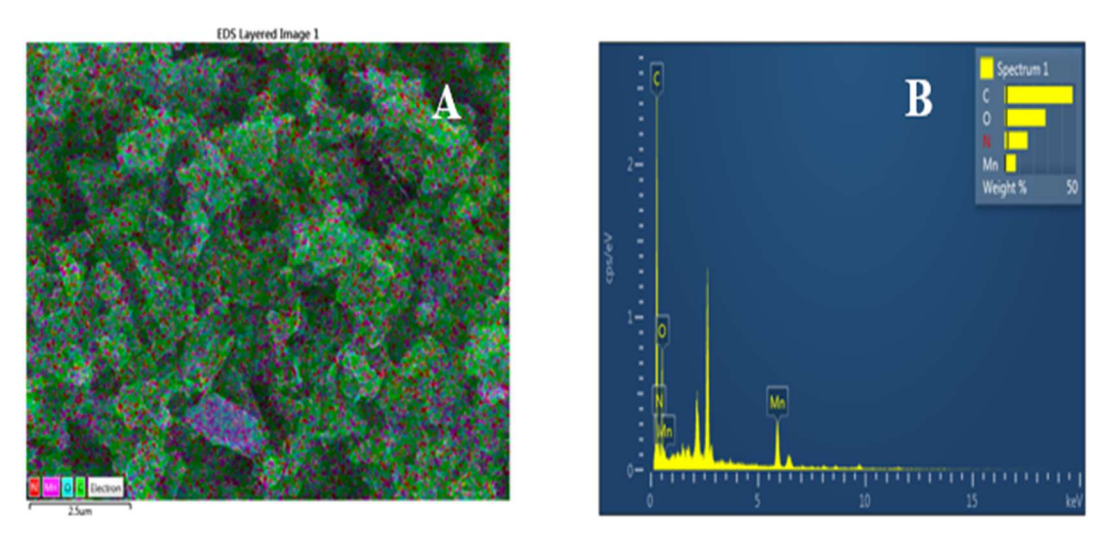


Figure 31. (A-B): Mixed elemental mapping of PGM

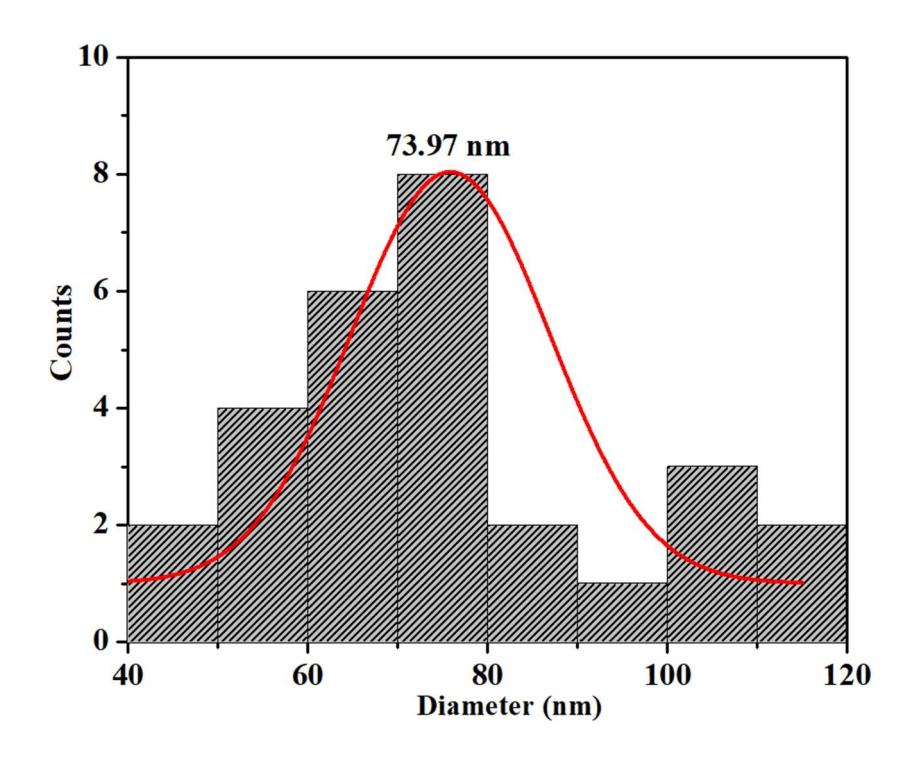


Figure 32. Average particle size of PGM ternary composite.

# 4.11.1. XPS Studies of PGM composite:

The elemental composition was analyzed using XPS studies. **Fig. 33**. The characteristic peaks in the XPS spectrum of PGM centered at 640.9, 528.4, 397.7, and 276.2 eV are due to the presence of Mn, O, N, and C, confirming the presence of these elements in PGM.

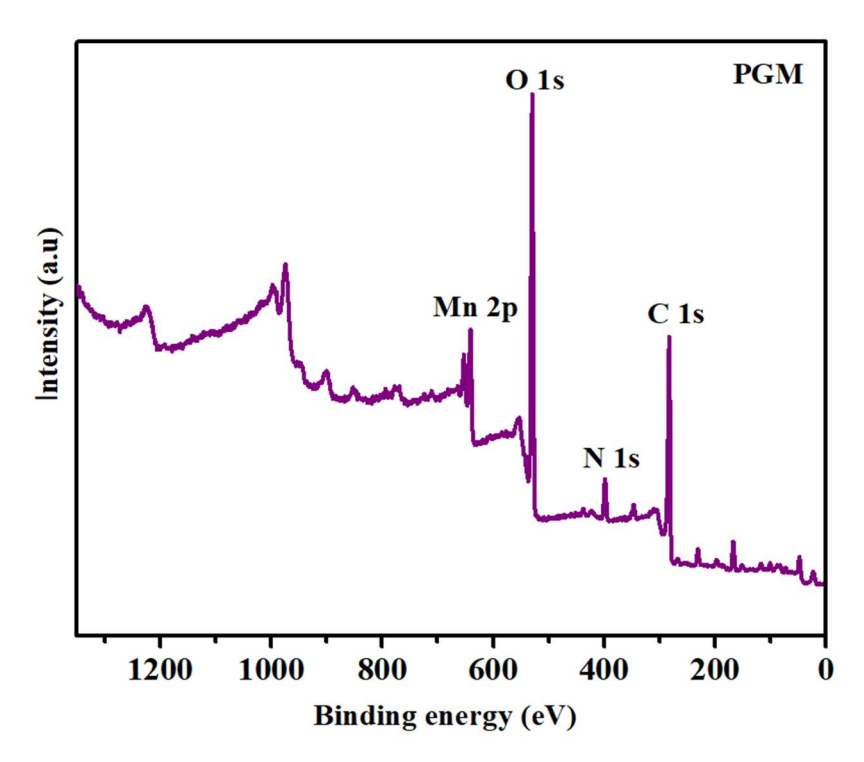


Figure 33. XPS spectral analysis of PGM Ternary composite

The deconvolution curves of the C 1s, N 1s, O 1s and Mn 2p of PGM composite are shown in Fig. 34 (A-D). The deconvolved C 1s spectrum of PGM gives rise to the two peaks corresponding to C-C (282.5 eV), and C=N (284.7 eV), (Fig. 34 A). The N 1s spectrum shows the three peaks, at binding energy of 397.7, 402.3, and 399.9 eV, corresponding to the imine (=N-H) positively charged (-NH<sup>+</sup>-) and neutral amine (-NH) like structures, (Fig. 34 B). The deconvolved spectrum of O 1s, (Fig. 34 C), gives rise to two characteristic peaks at 528.7 eV due to Mn-O-Mn bonds, while at 530.88 eV and H-O-H bond. Fig. 34 D shows the deconvolved spectra of Mn 2p which give two peaks with the orbital splitting of ( $\Delta$ = 11.08 eV). The peak at 641.5 eV corresponds to the Mn 2p<sub>3/2</sub> while the peak at 652.6 eV is due to the Mn 2p<sub>1/2</sub> which is in agreement with the literature. The C 1s, N 1s, O 1s and Mn 2p characteristic peaks in the XPS spectrum show the existence of PPY, GO, and MnO<sub>2</sub> in the ternary nanocomposite PGM. (Han, G., et al., 2014; Niu, T., et al., 2021).

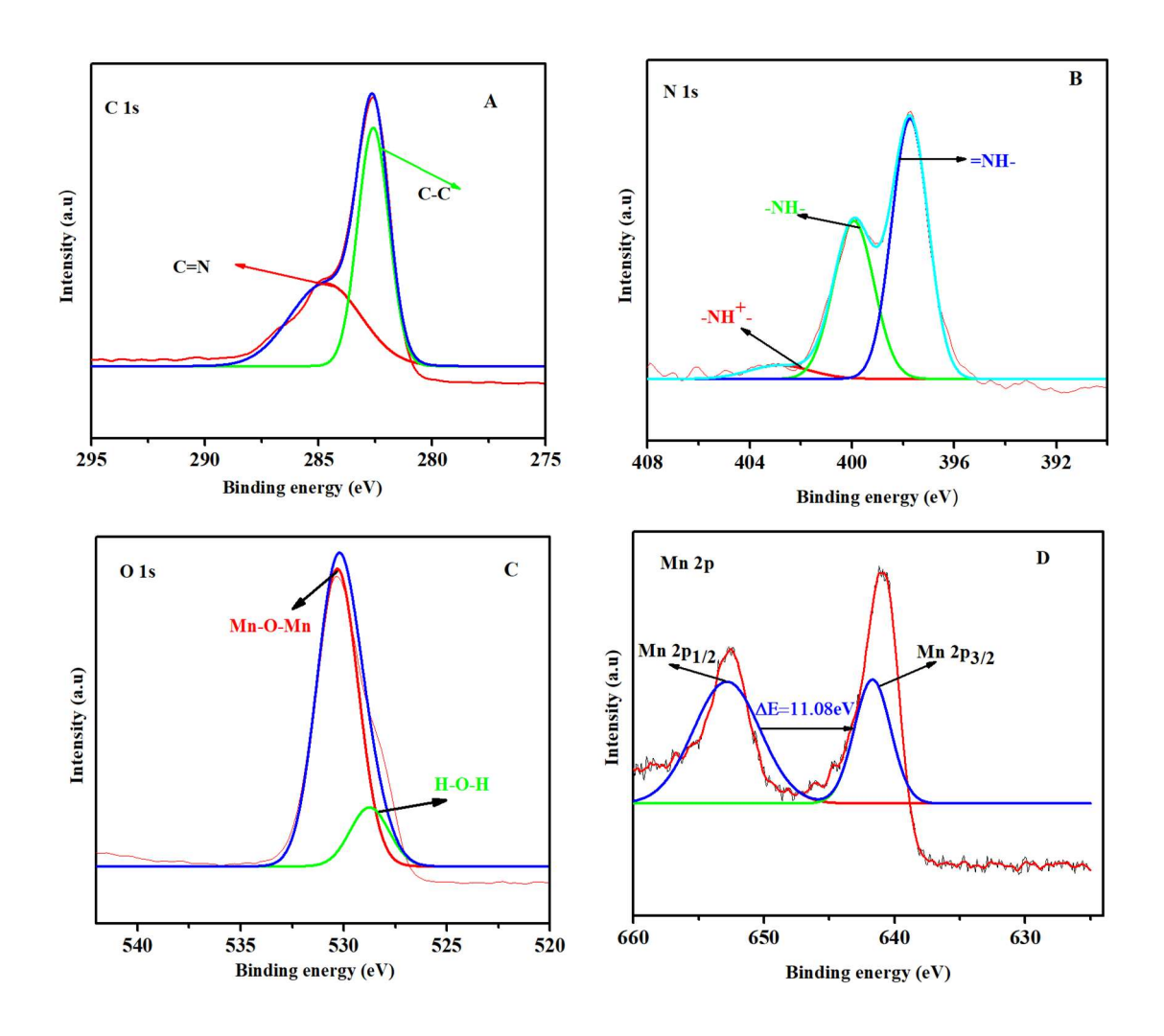


Fig. 34 (A-D) Deconvolution spectra of C 1s, N 1s, O 1s, and Mn 2p of PGM

#### 4. 12. Thermal Studies:

Thermogravimetric Analysis (TGA) curves of PPY, GO, MnO<sub>2</sub>, PG, and PGM are shown in **Fig. 35 A.** Initially, the weight loss at temperature < 100 °C is due to the removal of moisture content in the prepared samples. The percentage of weight loss in this temperature range depends on the composition of the prepared material, more the hygroscopic nature, the greater the percentage of weight loss. The major weight loss for the PPY starts at a T<sub>onset</sub> of 248.28 °C with residual weight (W<sub>r</sub> %) of 79.22. The weight loss of PPY

continuously increases as the temperature rises and it ends at a Toffset of 575 °C indicating the volatilization of PPY (Mudila, H., et al., 2013). In the case of GO, the main mass loss takes place at T<sub>onset</sub> 208.71 °C with W<sub>r</sub> % of 76.26. The loss in this temperature range is mainly due to the removal of oxygen functionalities from the surface of GO. After this major weight loss, the material behaves as a graphene and expanded graphite sheet-like structure. (Konwer, S., et al., 2011; Mudila, H., et al., 2013). In PG initially, the weight loss at the temperature of 100 °C is due to the removal of moisture content from the composite surface. The weight loss in the temperature range of 150-170 °C is probably due to the removal of oxygen-containing moieties introduced by the presence of GO in composite material. The major weight loss in binary composite Tonset 243.28 °C arises due to the degradation of PPY from the composite. (Bose, S., et al., 2010). The thermal stability of the PG is higher compared to that of PPY and GO, which may be due to the presence of PPY over the GO sheets, which provide stability to the structure by blocking the accumulation of heat between the GO sheets in the composite material. After removing moisture content from PPY GO and PG, the W<sub>r</sub> % left up to the T<sub>onset</sub> of the respective material may be by eliminating impurities and unreacted dopants (Bose, S., et al, 2010; Li, L., et al., 2012). In the TGA curve of MnO<sub>2</sub>, a small weight loss at the T<sub>onset</sub>, 294.57 °C, was observed, which could be due to the phase transition (MnO<sub>2</sub> to Mn<sub>2</sub>O<sub>3</sub>) resulting in the elimination of oxygen from the MnO<sub>2</sub> lattice, (Naderi, H. R., et al., 2016). A comparative representation of T<sub>onset</sub>, decomposition temperature (T<sub>d</sub>) and % char had been represented in Fig. 35 B. In the case of PGM, the weight loss at T<sub>onset</sub>, 248.02 °C, due to the degradation of the polymer chain and removal of the dopant ions from the surface of the composite material. The decomposition temperature in ternary composite (498.33 °C) is higher compared to that of PPY, GO, and PG. Additional stability of the PGM compared to PPY, GO, and PG is due to its thermal stability arising from the synergetic effect of PPY and GO functionalities and the presence of stable MnO<sub>2</sub> in the composite material. (Liang, F., et al., 2017; Ates, M., et al., 2018).

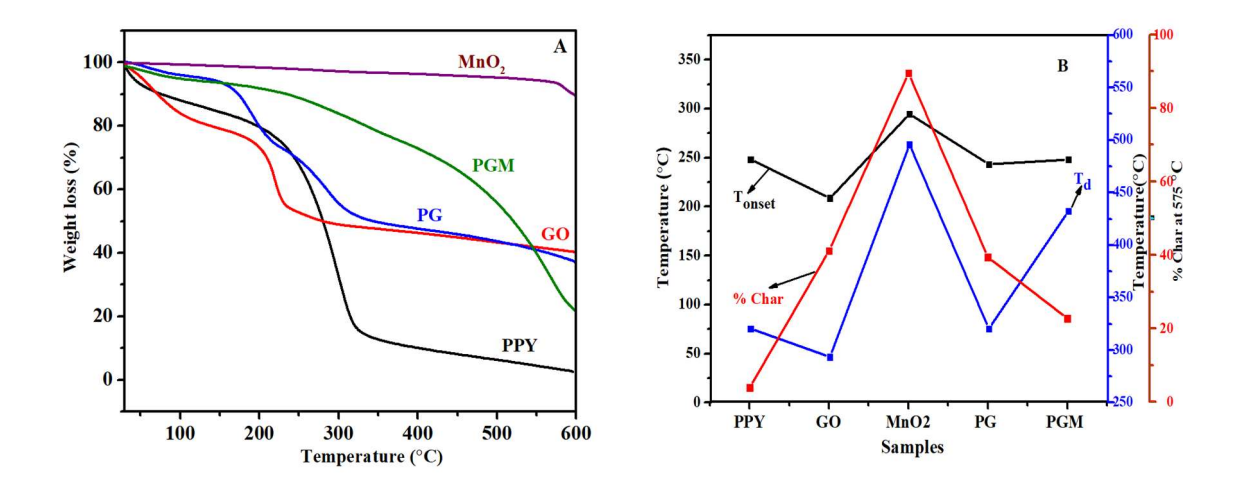


Figure 35. TGA of PPY, GO, ZnO, PG, and PGM (A), Graphical representation of TGA parameter (Tonset, Td, and Char%) of all the samples (B).

#### 4.13. Electrochemical measurements using Cyclic Voltammetry:

The electrochemical behavior of the individual (PPY, GO, MnO<sub>2</sub>,) and the composite binary and ternary materials (PGs, and PGMs) prepared at different weight ratios were studied using the cyclic voltammetry (CV) technique. The CV curves which have a current versus potential (I vs V) relationship were used to analyze the electrochemical activity of the electrode material under investigation. CV studies of the respective electrodes were carried out at a scan rate of 0.05 V/s within the potential window of -0.5 to 1.2 V in 5 mM potassium ferrocyanide K<sub>3</sub>[Fe (CN)<sub>6</sub>] and 0.1 M KCl as an electrolyte. The resulting CV graphs of CPE, PPY, GO, PGs, and PGMs showing distinct peaks of [Fe (CN)<sub>6</sub>]<sup>3-/4-</sup> are shown in Fig. 36. (Lee, S., et al., 2016). The electrochemical activity of PPY as seen from the CV is higher than that of the CPE and GO-modified electrode signifying the better electron transfer properties and fast redox mechanism on PPY electrode. The lower current response in the case of the CPE electrode is due to the non-conductive nature of paraffin oil used during its preparation. The current response in GO drops because the smooth movement of electrons on its surface is impeded by the presence of oxygen moieties (C=O, C-O, COOH, etc.) thus, hindering the smooth transfer of electrons on its surface resulting in the decrease of current values. (Seenivasan, R., et al., 2015). Compared to CPE, PPY,

and GO-based electrodes the peak current values are higher in the case of binary composites PGs prepared at different w/w ratios. This improved electrochemical response in the case of PGs compared to individual electrode material may be due to the synergetic effect (π-π stacking and hydrogen bonding) that arises due to the interaction between PPY and GO increasing the porosity and surface area of PGs that promotes the fast electron transfer process on its surface and hence enhances its electrochemical behavior (Seenivasan, R., et al., 2015; Rong, R., et al., 2017). For the optimization of the best binary composite in terms of its better electrochemical performance, the prepared PGs were studied by their CV studies. The low peak current of PG 4 compared to other composites may be due to the reason that at this amount of GO the agglomeration of PPY and GO in composite results in the formation of a small amount of nanocomposite material on the surface of CPE that slows the rate of electron transfer during the process. (Zhang, H., et al., 2023). The PG 1 composite shows better electrochemical response and hence has a high peak current value compared to other binary composites and is therefore considered for preparation of ternary composite with MnO<sub>2</sub>.

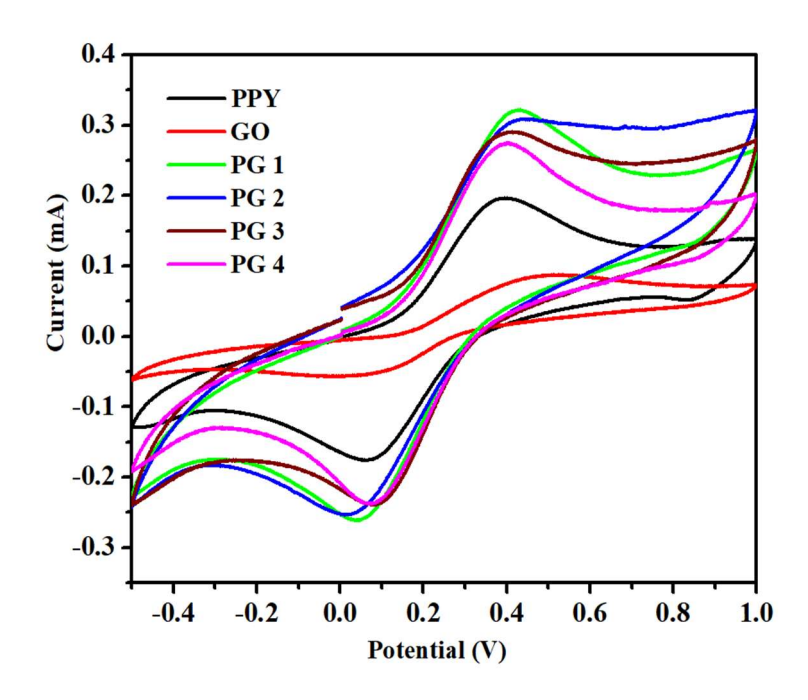


Figure 36. CV curves of PPY, GO, and PGs in 5 mM K<sub>3</sub>[Fe(CN)<sub>6</sub>] and 0.1M KCl

The CV curves of CPE, MnO<sub>2</sub>, and the ternary nanocomposites (PGMs) prepared at different weight ratios with MnO<sub>2</sub> are shown in Fig. 37. From the CV curves of the ternary composites, the composite PGM 1 having the optimal ratio of 2:1 (PG/MnO<sub>2</sub>) shows a higher peak current response compared to other composites. (Sun, H., et al.,2019). The higher electrochemical performance of PGM 1 at this amount of MnO<sub>2</sub> may be due to the synergetic effect operating between PPY, GO, and MnO<sub>2</sub>, which improves its current response compared to other ternary composites. A further increase in the amount of MnO<sub>2</sub> in the composite may lead to the breakdown of the synergetic effect due to the accumulation of PPY, GO, and MnO<sub>2</sub> that hindered the transport of electrons on its surface thus decreasing the electrochemical response. Therefore, the PGM 1 composite because of its better electrochemical activity than the other ternary composite material is considered ideal for the detailed studies. (Zhou, H., et al., 2016; Palsaniya, S., et al., 2021).

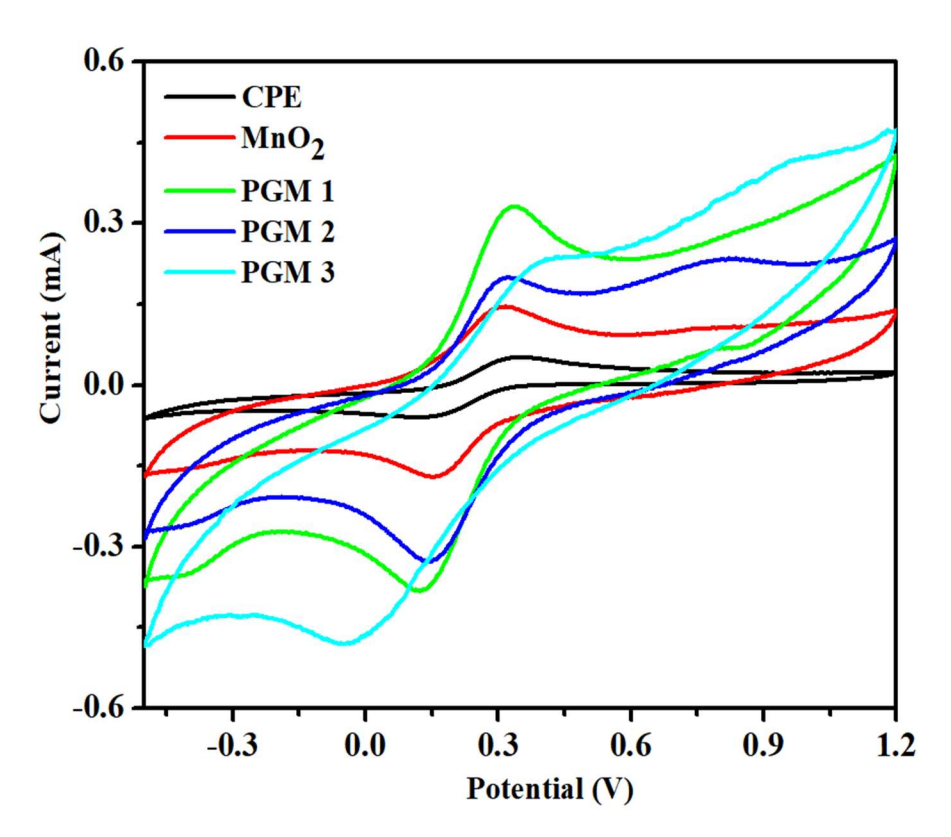


Figure 37. CV curves of CPE, MnO<sub>2</sub>, and PGMs in 5 mM K<sub>3</sub>[Fe(CN)<sub>6</sub>] and 0.1M KCl

A comparative study of PPY, GO, PG 1, and PGM 1 at a scan of 0.05 V/s is shown in Fig. 38. The peak current of PGM 1 is increased than that of individual components (CPE, PPY, GO, and MnO<sub>2</sub>) and the binary composite material PG 1. This enhancement in the case of the PGM 1 may be due to the combined synergetic effect of PPY, GO, and MnO<sub>2</sub> resulting in improving the surface area as well as the catalytic properties of the ternary composite material compared to that of the individual as well as binary composite facilitating the fast transport of the electron between the electrolyte K<sub>3</sub>[Fe(CN)<sub>6</sub>] and electrode surface. (Zhou, H., et al., 2016; Liang, F., et al., 2017)

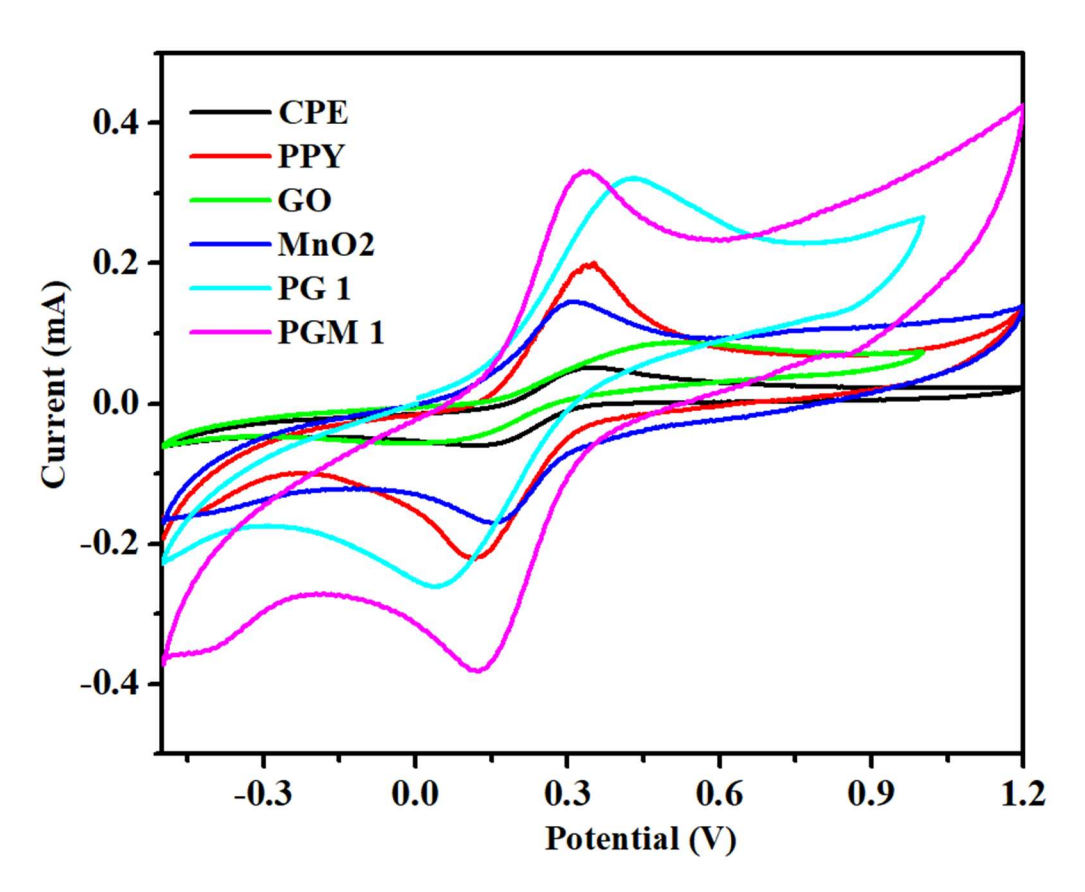


Figure 38. Comparative CV graphs of different electrodes at the scan of 0.05 V/s 5 mM  $K_3[Fe(CN)_6]$  and 0.1M KCl

### 4.14. Electrochemical impedance spectroscopy (EIS) studies:

The features of surface-modified electrodes was analyzed by Electrochemical impedance spectroscopy (EIS). The electron transfer of CPE, PPY, GO, PG 1, and PGM 1 electrode material was examined in 5mM  $K_3[Fe(CN)_6]$  aqueous solution containing 0.1 M KCl within the frequency range of 0.1 Hz to  $10^6$  Hz. (Oularbi, L., et al., 2017).

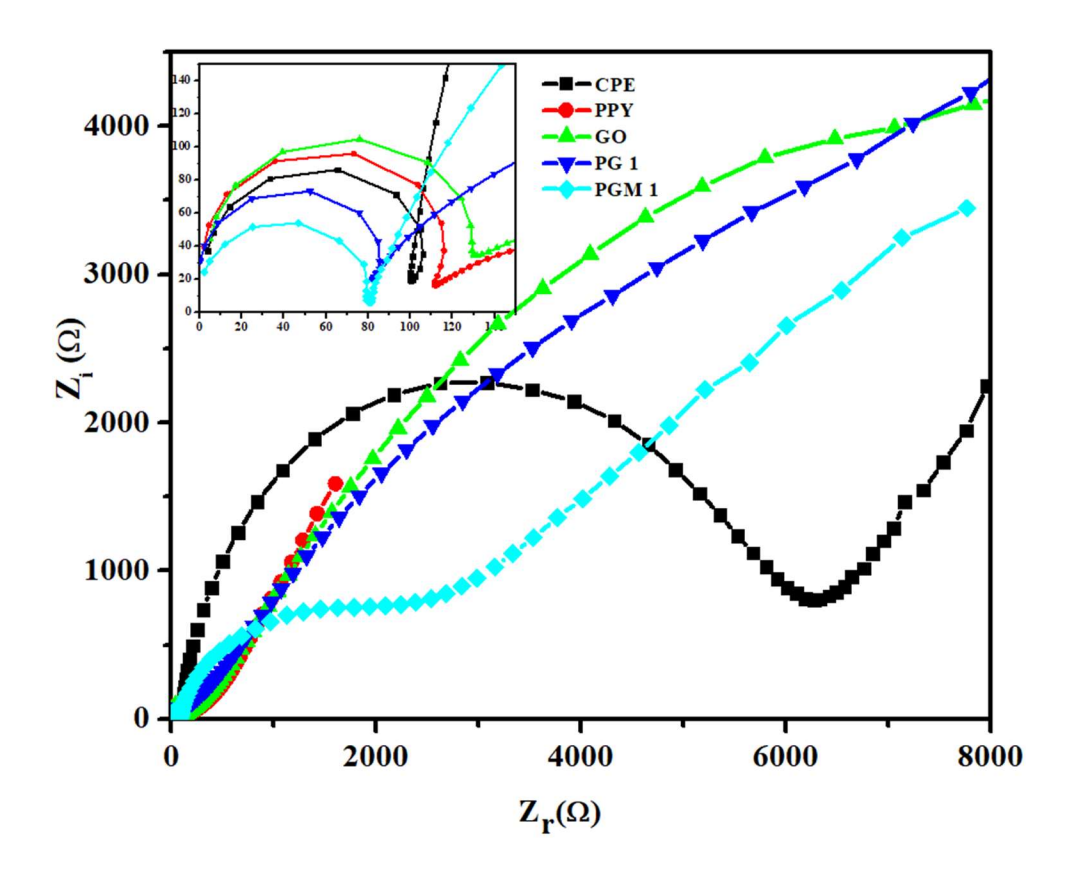


Figure 39: EIS spectra of CPE, PPY, GO, PG 1, and PGM 1 in 5 mM k<sub>3</sub>[Fe(CN)<sub>6</sub>] an electrolytic solution containing 0.1 M KCl

The Nyquist plots in the EIS analysis consist of the linear, and semicircle portion each signifies different process. The diameter of the semicircle in high-frequency region reflects the electron transfer resistance ( $R_{ct}$ ) process taking place on the electrode surface. The diffusion-limited processes taking place on the electrolyte- electrode interface are studied from the linear portion in the lower frequency regions of the Nyquist plots. Smaller

the diameter of the semicircle lower will be the impedance and charge transfer resistance (R<sub>ct)</sub> signifying fast charge transfer process. (Seenivasan, R., et al., 2015) The total electrode impedance depends on electron transfer resistance (R<sub>ct</sub>) in series with the parallel connection of the double-layer capacitance (C<sub>dl</sub>) and Warburg impedance (Z<sub>w</sub>). The EIS spectra of bare CPE, PPY, GO, PG 1, and PGM 1 is shown in Fig. 39.

A small semicircle in the higher frequency region, and an inclined line in the low frequency region in the EIS spectra of PGM 1 compared to CPE, PPY, GO, and PG 1 signifying the fast electron transfer processes on its surface. This could be due to better conductivity and improved surface area of PGM 1 ternary composite, speeding the electron transfer kinetic on its surface thus improving the electron transfer rate and the detection of Pb<sup>2+</sup> ions in water samples. These results are in agreement as reported by the CV studies. (Liang, F., et al., 2017; Ramachandran, T., and Dhayabaran, V. V., 2019).

### 4.15. Electrochemical detection of Pb<sup>2+</sup> using DPASV technique:

#### 4.15.1. DPASV measurements of different electrodes:

The electrochemical performance of the different electrodes CPE, PPY, GO, PG 1, and PGM 1 was carried out using DPASV studies to determine the Pb<sup>2+</sup> ion in buffer of acetate solution with pH 4.6. (**Oularbi, L., et al., 2017**).

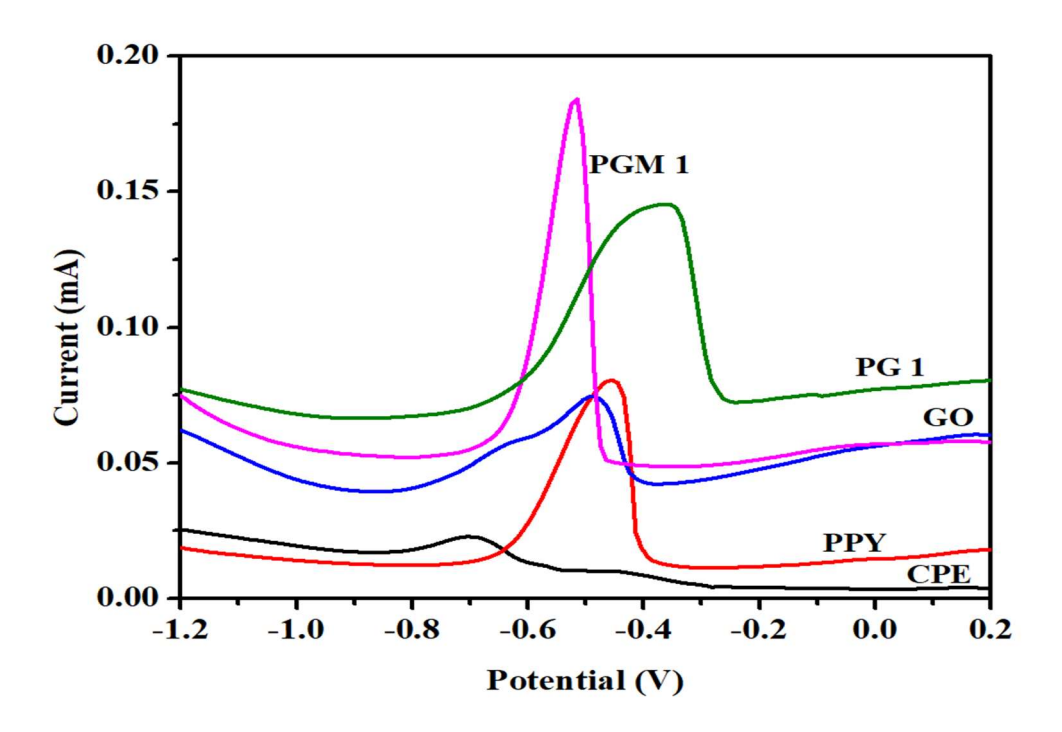


Figure 40: Comparative DPASV of CPE, PPY, GO, PG 1, and PGM 1 at 3.0  $\mu M$  Pb<sup>2+</sup> ion

 $Pb^{2+}$  ions are accumulated on PGM 1 electrode surface through electrostatic attractions and surface complexations followed by the reduction of  $Pb^{2+}$  to  $Pb^0$  with the deposition potential of -1.2 V for 5 minutes. The DPASV measurements were then performed by sweeping the potential in the range of -1.2 to 0.2 V for different electrodes. The stripping behavior of the CPE, PPY, GO, PG 1, and PGM 1 electrodes in the presence of 3.0  $\mu$ M  $Pb^{2+}$  ion was shown in **Fig. 40**.

The stripping peak current value at -0.51 V for the PGM 1 composite is higher as compared to other electrodes (CPE, GO, PPY, and PG 1). This may be due to the synergetic effect of all the individual components in the ternary composite thus increasing surface area, conductivity, and the number of anchoring sites for Pb<sup>2+</sup> ions adsorption, further enhancing the sensor's performance (Wanekaya, A., and Sadik, O. A., 2002; Karthik, R., and Thambidurai, S., 2017; El Sikaily, et al., 2025)

## 4.15.2. Electrochemical performance of electrode material:

DPASV measurements were performed on PG 1 binary and PGM 1 ternary composites at different concentrations (0.3 to 3.0 μM) of Pb<sup>2+</sup> metal ion. strong and intense redox peaks that increase with the concentration of metal ions were observed for both composites. **Fig** (41 and 43). The peak potential slightly shifts towards the positive potential and is somewhat broad with increase in the concentration of metal ions. This may due to the formation of multilayer metal ions on the surface of the already formed monolayer on the electrode surface. (**Dong.**, **Y.P.** et al., 2014).

The peak current values for the sensing of  $Pb^{2+}$  ion in the concentration range of 0.3 to 3.0  $\mu$ M on PG binary composite is shown in **Fig. 41**. The corresponding calibration curve of PG 1 for 0.3 to 3.0  $\mu$ M of  $Pb^{2+}$  ions was determined as  $y = 0.0106 \ Pb^{2+} + 0.1707$  with ( $R^2 = 0.95$ ) as regression coefficient (**Fig. 42**) (**Ghanbari, K., and Bonyadi, S., 2018**).

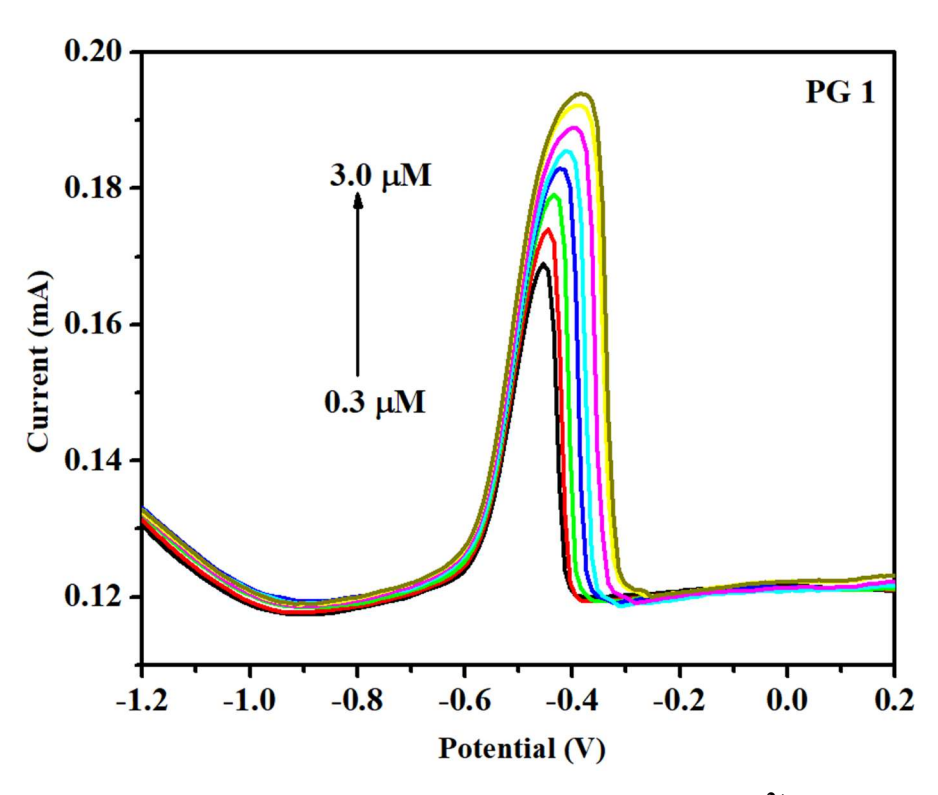


Figure 41. DPASV curves of PG at various concentrations of Pb<sup>2+</sup> (0.3 to 3.0 μM)

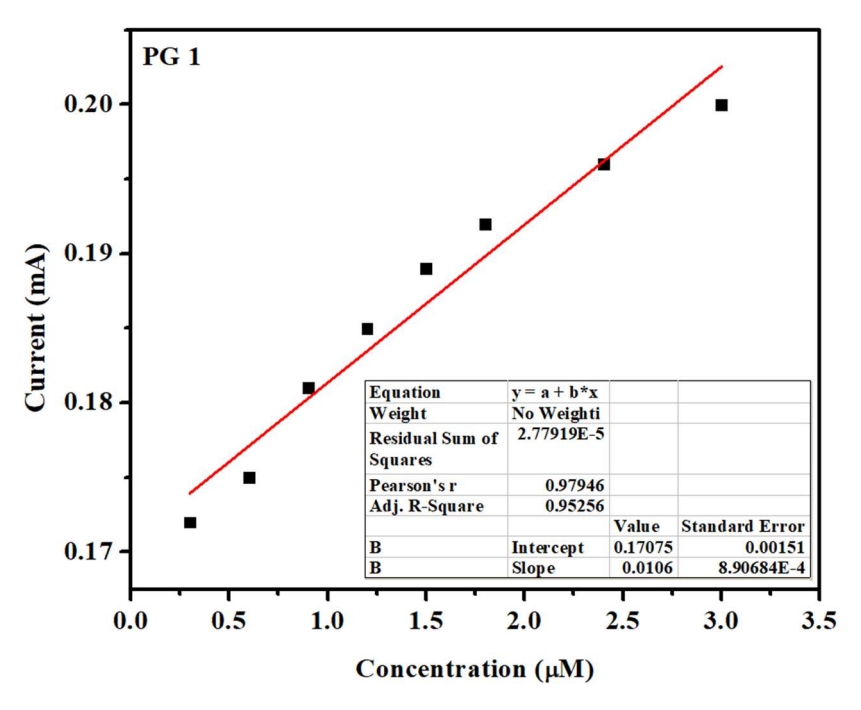


Fig. 42. Calibration curve of PG 1 at various concentrations of Pb<sup>2+</sup> (0.3 - 3.0 μM)

The electrochemical behavior for the determination of  $Pb^{2+}$  ion within the concentration range (0.3 to 3.0  $\mu$ M on PGM 1 ternary nanocomposite results in the well-defined stripping peaks as shown in **Fig. 43**. The calibration curve of PGM 1 composite for sensing of  $Pb^{2+}$  at different concentrations (0.3 to 3.0  $\mu$ M) represented as y=0.0373  $Pb^{2+}+0.0672$  ( $R^2=0.99$ ) (**Fig. 44**). The regression coefficient ( $R^2=0.99$ ) in the PGM 1 ternary composite case shows linear variation of the anodic stripping peak current values on the  $Pb^{2+}$  ion concentrations. The limit of detection (LOD) was calculated using the formulae "3×SD/S" where "SD" is the standard deviation of the blank solution and "S" is the slope of the calibration curve and it comes out to be 0.03  $\mu$ M for  $Pb^{2+}$  ion by the PGM 1 ternary composite. (**Ghanbari, K., and Bonyadi, S., 2018; Luyen, N.D., et al., 2023).** The sensitivity for ternary (PGM 1) is 0.0373 mA/ $\mu$ M, which is higher than the binary composite (0.0106 mA/ $\mu$ M), which further signifies that the ternary nanocomposite shows better electrochemical response for the sensing of  $Pb^{2+}$  metal ion (**Muralikrishna, S., et al., 2017**; **Oularbi, L., et al., 2017**)

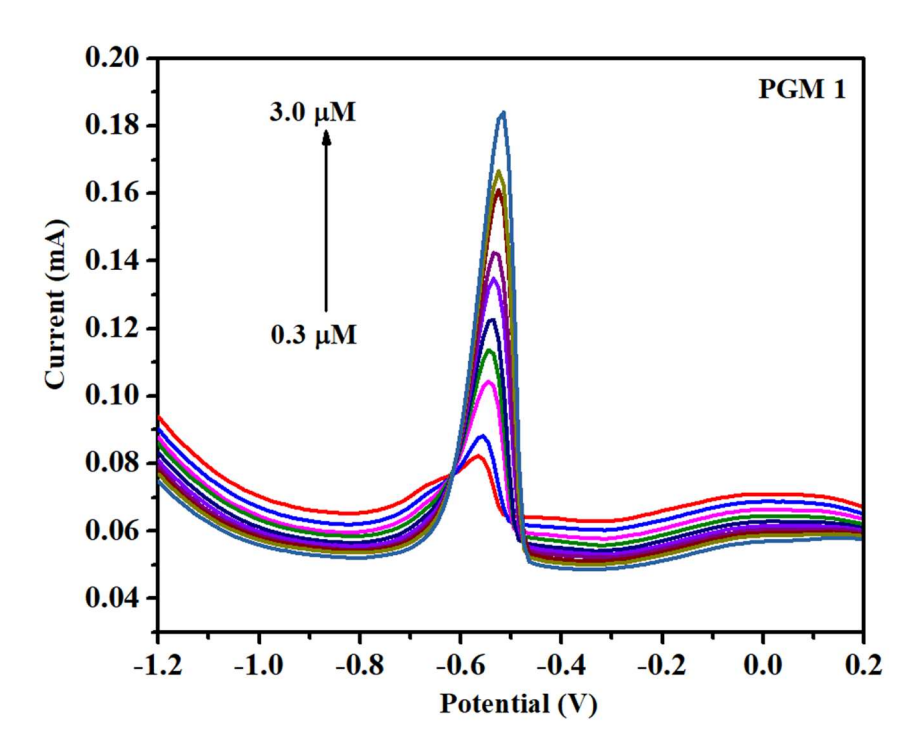


Figure 43. DPASV curves of PGM 1 at various concentrations of Pb $^{2+}$  (0.3 to 3.0  $\mu M$ )

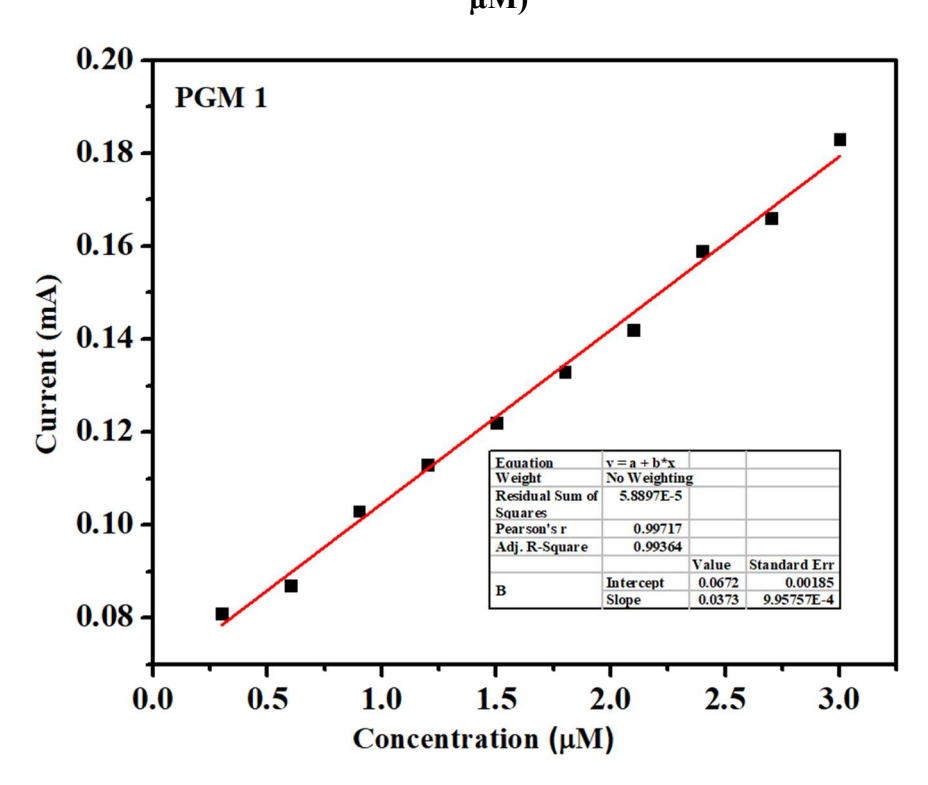


Fig. 44. Calibration curve of PGM 1 at various concentrations of Pb<sup>2+</sup> (0.3 - 3.0 μM)

# 4.15.3 Selectivity of PGM 1 electrode for sensing Pb<sup>2+</sup>ions:

The selectivity of the PGM 1 electrode material was examined by introducing varying amounts of the foreign material (Cd<sup>2+</sup> and Cu<sup>2+</sup>) as an interfering metal ion to the 0.1 M acetate buffer containing 3.0 µM Pb<sup>2+</sup> ion in the cell. During the pre-concentration phase of DPASV investigations, the surface of electrode material containing Pb<sup>2+</sup> ions may codeposit these interfering ions. (Dai, H et al., 2016). The peak current values of Pb<sup>2+</sup> ions both with and without interfering metal ions are displayed in Fig. 45. The results show minimal changes in the stripping peak current and peak potential values of the Pb<sup>2+</sup> ion in the presence of low and high concentrations of interfering ions. The peak current values changed from 0.075 mA without interference to 0.077 mA and 0.065 mA at low and high concentrations of interfering ions. In contrast, a negligible shift in the peak potential was observed.

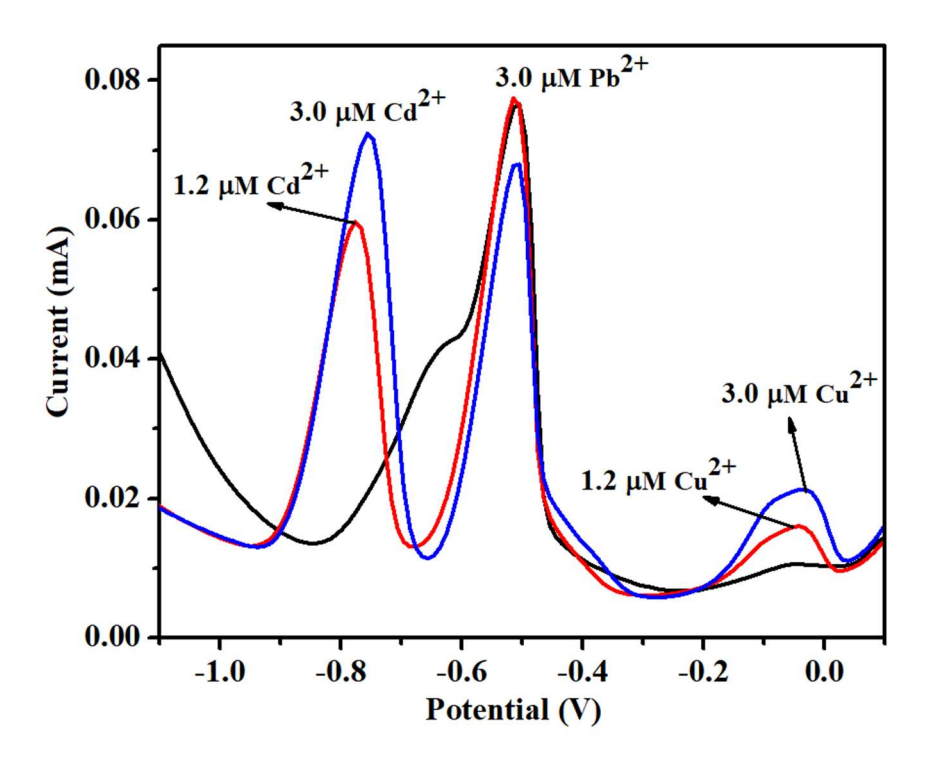


Figure 45. DPASV results of PGM 1 in the presence of 3.0  $\mu$ M Pb<sup>2+</sup> and in the presence of interference, 1.2 and 3.0  $\mu$ M Cd<sup>2+</sup> and Cu<sup>2+</sup> ions.

An increased in the stripping peak current value at 1.2  $\mu$ M concentration of the interfering (Cd<sup>2+</sup>, Cu<sup>2+</sup>) ions is due to the formation of the favorable intermetallic compounds on the surface of the PGM 1 composite during the deposition step that enhances the stripping current of the existing Pb<sup>2+</sup> ion. like Pb-Cu, and Pb-Cd compounds during the deposition step. The decline in the stripping peak current of Pb<sup>2+</sup> metal ion at 3.0  $\mu$ M may be ascribed to the competition of deposition (reduction) between these metal ions on the surface of the PGM 1. However, the intensity of the Pb<sup>2+</sup> metal ion signal remains unaffected by the introduction of such interference that shows the selective detection of Pb<sup>2+</sup> ions. This may be due to the inactive behavior of the added interfering ions within the oxidation potential range of the Pb<sup>2+</sup> metal ion. (**Zhang, Q. X., et al., 2015; Blaise, N. et al., 2022**)

## 4.15.4. Reproducibility and stability of PGM 1 electrode for sensing Pb<sup>2+</sup>ions: -

Reproducibility of the sensor (PGM 1) refers to the reliability of the electrode material under the same conditions repeated multiple times. The DPASV studies were carried out at a fixed concentration (3.0 µM) of Pb<sup>2+</sup> in an acetate buffer having pH 4.6 over five electrodes modified equally with the electroactive material **Fig 46.** The corresponding stripping current values for each electrode were recorded. A stripping peak current at -0.51 V was observed irrespective of the electrode material with a Relative Standard Deviation (RSD) of 4.12% and minimum peak current variation showing the reproducibility of the electrode material (PGM 1). (Seenivasan, R., et al., 2015; Luyen, N.D., et al., 2023)

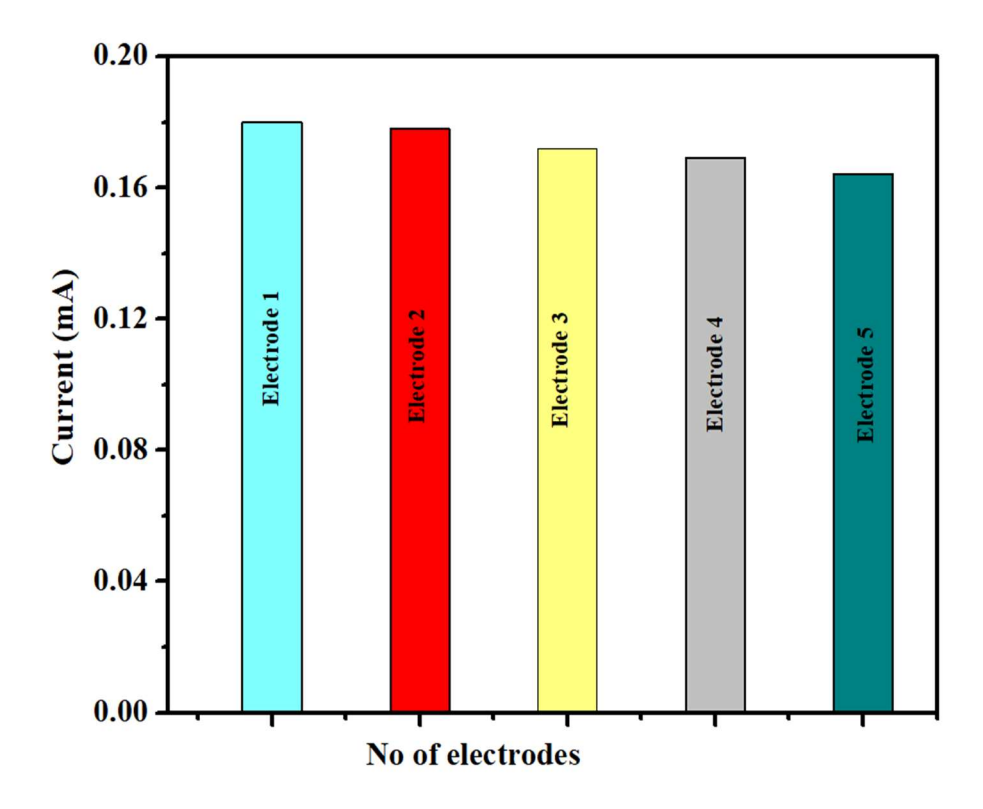


Figure 46. Representation of the reproducibility of PGM 1 in 3.0  $\mu M$  Pb<sup>2+</sup> ion solution

The stability of the electrode refers to its ability to show the minimum degradation from the initial current values when repeated over a period of time. The stability of the PGM 1 electrode was analyzed by performing the DPASV measurements in the same concentration of Pb<sup>2+</sup> ion (3.0 µM). The electrode, after each measurement, was washed with distilled water and kept in an acetate buffer solution (pH 4.6). Each measurement was performed after 7 days for the next 4 weeks and the corresponding current response was recorded in Fig. 47. The electrode material shows long-term stability with a minimum drift of initial current response with RSD 6.99 % and retention of 93.01 % current response, thus representing the stability of the electrode material (Zhou, H., et al., 2016; Karthik, R., and Thambidurai, S., 2017).

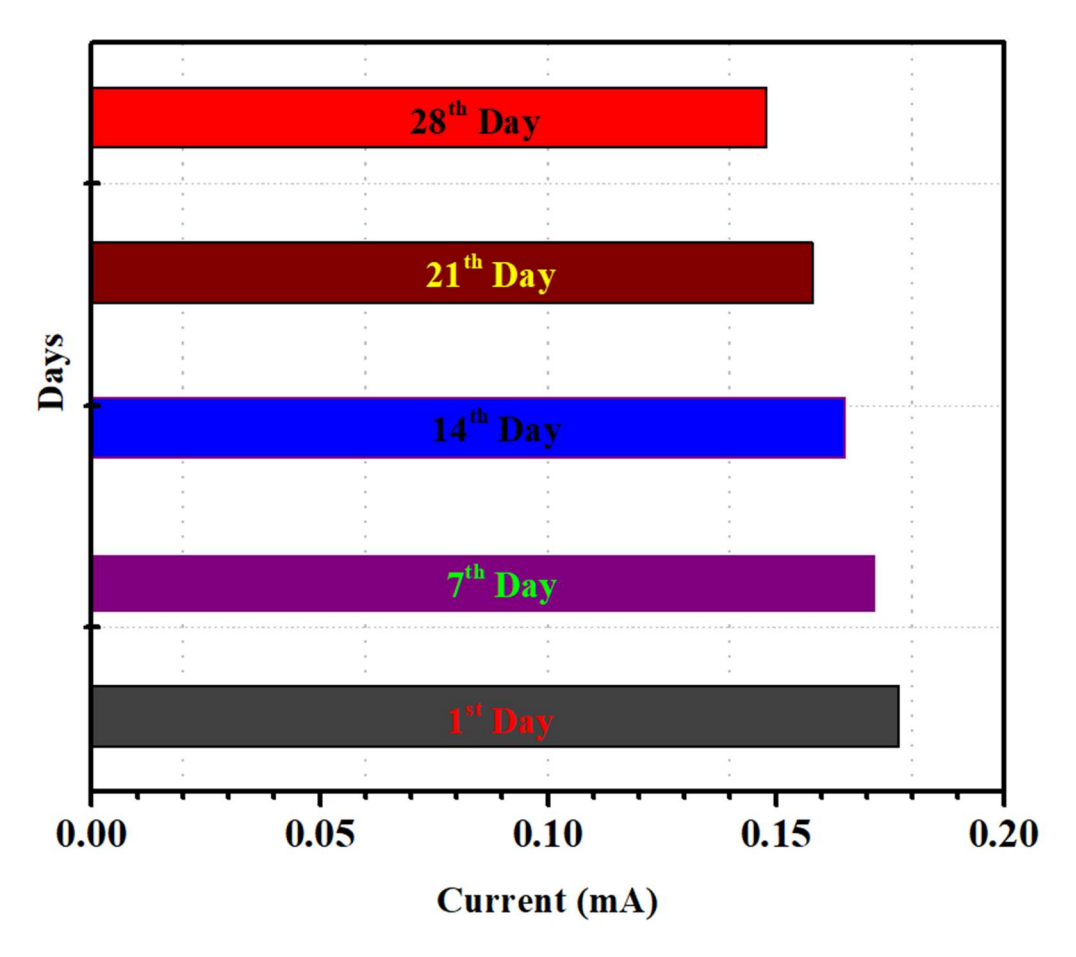


Figure 47. Representation of the stability of PGM 1 in 3.0 μM Pb<sup>2+</sup> ion solution

**4.16.** Removal of the Pb<sup>2+</sup> metal ion using PGM 1 composite: UV-visible spectroscopy technique was employed to study the percentage removal of Pb<sup>2+</sup> ion from the aqueous solution. A known amount (2 mg) of the PGM 1 ternary composite as adsorbent was added to the 30 ml of 100 ppm concentration of the lead solution. The resultant solution was allowed to sonicate for 10 minutes and then allowed to stand for the next 15 minutes to form a stable suspension. The effect of contact time of the adsorbent to the Pb<sup>2+</sup> ion solution at different time intervals (1, 4, 24 hours) was then studied using UV-visible spectrometry (**Fig. 48**). The percentage removal efficiency of the Pb<sup>2+</sup> ion on the surface of PGM 1 composite was calculated, shown in the table using the equation. (**Yadav, V. B., et al., 2019: Birniwa, A. H., et al., 2022).** 

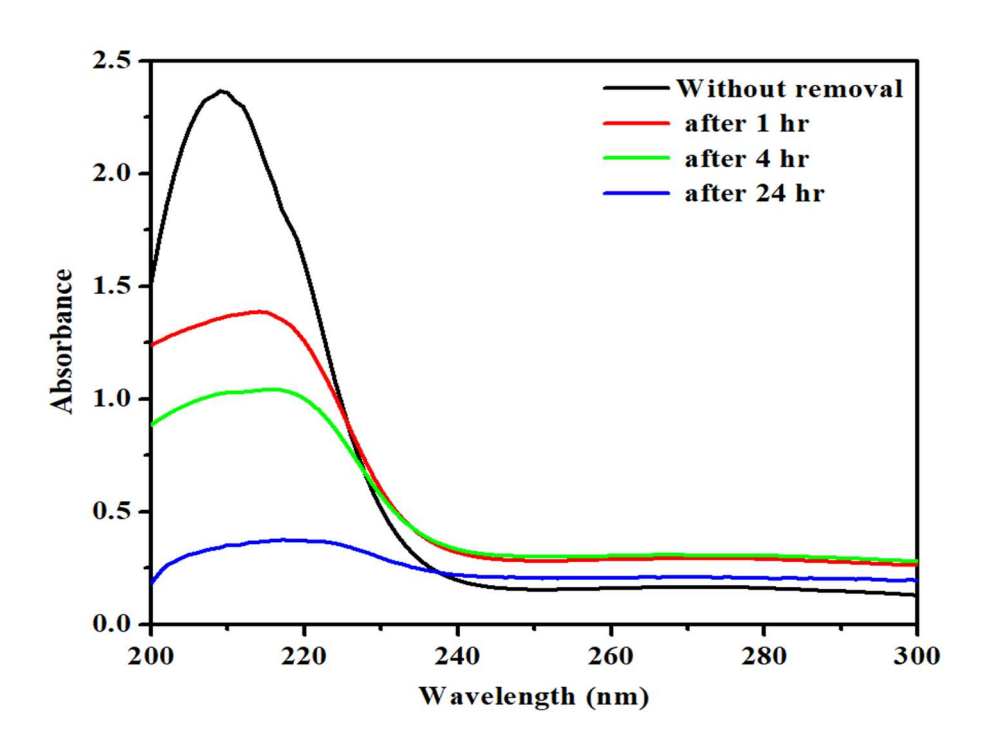


Fig. 48. UV-visible spectra representing detection and removal of  $Pb^{2+}$  ion in aqueous solution

From the graph, it can be seen that with an increase in the duration of the contact time of the adsorbent with the Pb<sup>2+</sup> ion solution, more of these ions get adsorbed on the electrode surface, resulting in a decrease in the concentration of the Pb<sup>2+</sup> ion in the solution.

Table 8: Removal efficiency of Pb<sup>2+</sup> ion by PGM 1composite with time

S. No	Contact time	% Removal		
1	1 hr	41.78		
2	4 hr	56.12		
3	24 hr	84.89		

#### 5.1. Conclusion:

The research work on the synthesis and applications of polypyrrole (PPY) based ternary nanocomposite (PGXs) for electrochemical detection and removal of heavy metals has been carried out successfully. The following conclusion has been drawn from this research work.

The preparation of polypyrrole has been carried out using oxidative chemical polymerization using the oxidant ferric chloride. Graphene oxide has been synthesized using the modified hammer method. The successful synthesis of PPY and GO was confirmed using FT-IR, XRD, SEM, and TGA analysis. The transition metal oxides (ZnO and MnO<sub>2</sub>) have been prepared from the working laboratory and characterized using the above techniques.

The Ex-situ method was employed for the preparation of binary (PPY/GO) and ternary (PPY/GO/ZnO and PPY/GO/MnO<sub>2</sub>) composites at different weight ratios. Each binary and ternary composites were optimized in terms of showing better electrochemical response using cyclic voltammetry. The structural, Morphological, and thermal studies of optimized binary (PG 1) and ternary (PGZ 2 and PGM 1) carried out by FT-IR, XRD SEM, and TGA analysis, are also in good agreement with the literature.

Electrochemical (CV) and EIS studies show the enhanced electrochemical response of binary and ternary composites, which may be due to the synergetic effect between the individual materials in their composites, facilitating the fast electron transfer process. The electrochemical response of the PG 1 composite is higher compared to the other composites (PG 2, PG 3, and PG4). Which is may be due to the reason that an increase in the amount of GO results in the agglomeration of PPY and GO leads to the formation of a small amount of nanocomposite material on the surface of CPE that slows the electron transport processes.

Further the electrochemical response of the PGZ 2 compared to (PGZ 1, PGZ 3,) and PGM 1 composite compared to (PGM 2, PGM 3,) is higher. This may be ascribed due

to the pseudo-capacitor behavior of ZnO, and MnO<sub>2</sub> up to a certain amount providing a smooth surface for the fast electron transport within the electrode material.

The optimized PG 1 and ternary (PGZ 2, and PGM 1) were analyzed for the sensing of Pb<sup>2+</sup> ion using the DPASV. The sensing response for the Pb<sup>2+</sup> ion on the surface of the ternary nanocomposite is higher compared to that of the binary composite. The increased surface area due to GO and pseudo capacitive behavior of PPY ZnO, and MnO<sub>2</sub> making the electron transfer process more feasible in ternary composite compared to PG 1. Secondly, negatively charged functional groups in PPY, GO, and ZnO, in PGZ 2 PPY, GO, and MnO<sub>2</sub>, in case of PGM 1 act as binding sites for the Pb<sup>2+</sup> ions, resulting in the formation of complexes through coordinate bonds. This results in enhancing the selective sites for the accumulation of metal on its surface in the case of PGZ 2 and PGM 1 thus increasing the stripping peak current response. A LOD of 0.05 μM for PGZ 2 and LOD of 0.03 μM for PGM 1 within the concentration range of 0.3-3.0 Pb<sup>2+</sup> μM Pb<sup>2+</sup> ions was obtained. The developed sensors also show a good selectivity for the detection of Pb<sup>2+</sup> ions in presence of other interfering ions (Cd<sup>2+</sup> and Cu<sup>2+</sup>)

The detection of the  $Pb^{2+}$  ions by the prepared electrodes and are also helpful in the removal of  $Pb^{2+}$  ions, which has been carried out by UV-visible spectroscopy. PGZ 2 and PGM 1 electrodes show a removal efficiency of 86.92 % and 84.89 % for  $Pb^{2+}$  ions, respectively, after 24 hours of contact.

The results for the sensing of Pb<sup>2+</sup> ions on the surface of working electrodes (PGZ 2 and PGM 1) are summarized in the **Table 9** 

**Table 9:** Results for the sensing of Pb<sup>2+</sup> ions on the surface of working electrodes

Material	Concentration	LOD	Sensitivity	Reproducibility	Stability	Interference
	range (μM)	(µM)	$(mA/\mu M)$	(RSD %)	(RSD%)	
PPY/GO/ZnO	0.3-3.0	0.05	0.0127	1.089%	3.67%	Cd <sup>2+</sup> , Cu <sup>2+</sup>
(PGZ 2)						
PPY/GO/MnO <sub>2</sub>	0.3-3.0	0.03	0.0373	4.12 %	6.99 %	Cd <sup>2+</sup> , Cu <sup>2+</sup>
(PGM 1)						

## 5.2. Future perspectives

The use of PPY/GO/ZnO (PGZs) and PPY/GO/MnO<sub>2</sub> (PGMs) ternary nanocomposites for sensing heavy metals holds significant promise for future developments in environmental monitoring and analytical chemistry. The combination of PPY, GO, and ZnO/MnO<sub>2</sub> in the ternary composite results in improving the properties of the composite, which improves the sensitivity and selectivity for the sensing of heavy metals. By optimizing the composite's structure and composition, it may be possible to fine-tune its response to specific heavy metals, enhancing selectivity. The composite could be integrated into systems designed for in-situ environmental monitoring.

\_\_\_\_\_

Akhtar, M., Tahir, A., Zulfiqar, S., Hanif, F., Warsi, M. F., Agboola, P. O., and Shakir, I. (2020). Ternary hybrid of polyaniline-alanine-reduced graphene oxide for electrochemical sensing of heavy metal ions. Synthetic Metals, 265, 116410.

Ali, Z.R., and Dawood, A. F., (2022). Structural and Electrical characterizations of new synthesized PVA/PoPDA-rGO-ZnO Nanocomposite. Egypt. J. Chem. 65(4) 761 – 770.

Arulraj, A. D., Devasenathipathy, R., Chen, S. M., Vasantha, V. S., and Wang, S. F. (2016). Femtomolar detection of mercuric ions using polypyrrole, pectin and graphene nanocomposites modified electrode. Journal of colloid and interface science, 483, 268-274.

Arumugam, C., Kandasamy, S. K., and Subramaniam, T. K. (2023). Enhancing supercapacitor performance using ZnO embedded on GO/PPy composite as versatile electrodes. High Energy Chemistry, 57(1), 69-76..

Ates, M., Caliskan, S., and Gazi, M. (2018). Ternary nanocomposites of graphene / TiO2 /polypyrrole for energy storage applications. Fullerenes, Nanotubes and Carbon Nanostructures, 26(10), 631–642.

Ates, M., Mizrak, I., Kuzgun, O., and Aktas, S. (2020). Synthesis, characterization, and supercapacitor performances of activated and inactivated rGO/MnO2 and rGO/MnO2/PPy nanocomposites. Ionics, 26(9), 4723-4735.

Bai, H., and Shi, G. (2007). Gas sensors based on conducting polymers. Sensors, 7(3), 267-307.

Bansod, B., Kumar, T., Thakur, R., Rana, S., and Singh, I. (2017). A review on various electrochemical techniques for heavy metal ions detection with different sensing platforms. Biosensors and Bioelectronics, 94, 443-455.

Batool, A., Kanwal, F., Imran, M., Jamil, T., and Siddiqi, S. A. (2012). Synthesis of polypyrrole/zinc oxide composites and study of their structural, thermal and electrical properties. Synthetic Metals, 161(23-24), 2753–2758.

Birniwa, A. H., Mahmud, H. N. M. E., Abdullahi, S. S. A., Habibu, S., Jagaba, A. H., Ibrahim, M. N. M., ... and Umar, K. (2022). Adsorption behavior of methylene blue cationic dye in aqueous solution using polypyrrole-polyethylenimine nanoadsorbent. Polymers, 14(16), 3362

Blaise, N., Gomdje Valéry, H., Maallah, R., Oubaouz, M., Tigana Djonse Justin, B., Andrew Ofudje, E., and Chtaini, A. (2022). Simultaneous electrochemical detection of Pb and Cd by carbon paste electrodes modified by activated clay. Journal of Analytical Methods in Chemistry, 2022(1), 6900839

Bose, S., Kuila, T., Uddin, M. E., Kim, N. H., Lau, A. K. T., and Lee, J. H. (2010). In-situ synthesis and characterization of electrically conductive polypyrrole/graphene nanocomposites. Polymer, 51(25), 5921–5928.

Chang, J., Zhou, G., Christensen, E. R., Heideman, R., and Chen, J. (2014). Graphene-based sensors for detection of heavy metals in water: a review. Analytical and bioanalytical chemistry, 406, 3957-3975.

Chee, W. K., Lim, H. N., Harrison, I., Chong, K. F., Zainal, Z., Ng, C. H., and Huang, N. M. (2015). Performance of flexible and binderless polypyrrole/graphene oxide/zinc oxide supercapacitor electrode in a symmetrical two-electrode configuration. Electrochimica Acta, 157, 88-94.

Chen, L., Li, Z., Meng, Y., Zhang, P., Su, Z., Liu, Y., Huang, Y., Zhou, Y., Xie, Q., and Yao, S. (2014). Sensitive square wave anodic stripping voltammetric determination of Cd2+ and Pb2+ ions at Bi/Nafion/overoxidized 2-mercaptoethanesulfonate-tethered polypyrrole/glassy carbon electrode. Sensors and Actuators B Chemical, 191, 94–101.

Chitte, H. K., Shinde, G. N., Bhat, N. V., and Walunj, V. E. (2011). Synthesis of Polypyrrole Using Ferric Chloride (FeCl3) as Oxidant Together with Some Dopants for Use in Gas Sensors. Journal of Sensor Technology, 01(02), 47–56.

Chougule, M. A., Pawar, S. G., Godse, P. R., Mulik, R. N., Sen, S., and Patil, V. B. (2011). Synthesis and Characterization of Polypyrrole (PPy) Thin Films. Soft Nanoscience Letters, 01(01), 6–10.

Chougule, M. A., Sen, S., and Patil, V. B. (2012). Facile and efficient route for preparation of polypyrrole-ZnO nanocomposites: microstructural, optical, and charge transport properties. Journal of Applied Polymer Science, 125(S1), E541-E547.

Cui, L., Wu, J., and Ju, H. (2015). Electrochemical sensing of heavy metal ions with inorganic, organic and bio-materials. Biosensors and Bioelectronics, 63, 276-286.

Dai, H., Wang, N., Wang, D., Ma, H., and Lin, M. (2016). An electrochemical sensor based on phytic acid functionalized polypyrrole/graphene oxide nanocomposites for simultaneous determination of Cd (II) and Pb (II). Chemical Engineering Journal, 299, 150-155.

Diédhiou, I., Fall, B., Gaye, C., Sall, M. L., Diaw, A. K. D., Gningue-Sall, D., ... and Raouafi, N. (2023). Preparations and applications of organic conducting polymers/graphene composites in heavy metal ion sensing: A review. International Journal of Materials Research, 114(2), 79-99.

Ding, C., Qian, X., Yu, G., and An, X. (2010). Dopant effect and characterization of polypyrrole-cellulose composites prepared by in situ polymerization process. Cellulose, 17(6), 1067–1077

Ding, R., Cheong, Y. H., Ahamed, A., and Lisak, G. (2021). Heavy Metals Detection with Paper-Based Electrochemical Sensors. Analytical Chemistry, 93(4), 1880–1888.

Dong, Y., Ding, Y., Zhou, Y., Chen, J., and Wang, C. (2014). Differential pulse anodic stripping voltammetric determination of Pb ion at a montmorillonites/polyaniline

nanocomposite modified glassy carbon electrode. Journal of Electroanalytical Chemistry, 717-718, 206–212.

El Sikaily, A., Ghoniem, D. G., Ramadan, O., El-Nahrery, E. M., Shahat, A., and Hassan, R. Y. (2025). Highly Selective Detection of Heavy Metal Ions in Food and Water Using a 5-BHAHS@NC/MnO2-Based Electrochemical Sensor. Biochemical Engineering Journal, 109660.

Engwa, G. A., Ferdinand, P. U., Nwalo, F. N., and Unachukwu, M. N. (2019). Mechanism and Health Effects of Heavy Metal Toxicity in Humans. Edited by Karcioglu O. and Arslan B. Poisoning in the modern world: new tricks for an old dog?, In *IntechOpen eBooks*. https://doi.org/10.5772/intechopen.82511

Fourati, N., Blel, N., Lattach, Y., Ktari, N., & Zerrouki, C. (2016). Chemical and Biological Sensors from Conducting and Semiconducting Polymers. Reference Module in Materials Science and Materials Engineering. doi:10.1016/b978-0-12-803581-8.01733-1

Ghanbari, K., and Bonyadi, S. (2018). An electrochemical sensor based on reduced graphene oxide decorated with polypyrrole nanofibers and zinc oxide–copper oxide p–n junction heterostructures for the simultaneous voltammetric determination of ascorbic acid, dopamine, paracetamol, and tryptophan. New Journal of Chemistry, 42(11), 8512–8523.

Guerrero-Contreras, J., and Caballero-Briones, F. (2015). Graphene oxide powders with different oxidation degrees, prepared by synthesis variations of the Hummers method. Materials Chemistry and Physics, 153, 209–220

Han, G., Liu, Y., Kan, E., Tang, J., Zhang, L., Wang, H., and Tang, W. (2014). Sandwich-structured MnO2/polypyrrole/reduced graphene oxide hybrid composites for high-performance supercapacitors. RSC Adv., 4(20), 9898–9904

Harlin, A., and Ferenets, M. (2006). Introduction to conductive materials. In Intelligent textiles and clothing. Woodhed Puhlishing in Textiles (217-237).

Hu, S., Gao, G., Liu, Y., Hu, J., Song, Y., and Zou, X. (2019). An electrochemical sensor based on ion-imprinted PPy/rGO composite for Cd (II) determination in water. International Journal of Electrochemical Science, 14(12), 10714-10730.

Islam, S., Shaheen Shah, S., Naher, S., Ali Ehsan, M., Aziz, M. A., and Ahammad, A. S. (2021). Graphene and carbon nanotube-based electrochemical sensing platforms for dopamine. Chemistry–An Asian Journal, 16(22), 3516-3543.

Ismardi, A., Gunawan, T. D., Suhendi, A., and Fathona, I. W. (2024). Study of graphene incorporation into ZnO-PVA nanocomposites modified electrode for sensitive detection of cadmium. Heliyon, 10(11).

Jin, M., Yuan, H., Liu, B., Peng, J., Xu, L., and Yang, D. (2020). Review of the distribution and detection methods of heavy metals in the environment. Analytical methods, 12(48), 5747-5766.

Joseph, A., Subramanian, S., Ramamurthy, P. C., Sampath, S., Kumar, R. V., and Schwandt, C. (2014). Iminodiacetic acid functionalized polypyrrole modified electrode as Pb (II) sensor: synthesis and DPASV studies. Electrochimica Acta, 137, 557-563.

Karthik, R., and Thambidurai, S. (2017). Synthesis of cobalt doped ZnO/reduced graphene oxide nanorods as active material for heavy metal ions sensor and antibacterial activity. Journal of Alloys and Compounds, 715, 254-265.

Kausar, H., Khan, Y., Ahmad, A., Ahmad, S. I., and Nami, S. A. (2021). Synthesis and characterization of zirconium (IV) molybdosulphosalicylate, multi-walled carbon nanotubes and polypyrrole based ternary nanocomposites: Adsorption and lead sensing studies. Synthetic Metals, 274, 116730.

Koller, M., and Saleh, H. M. (2018). Introductory chapter: Introducing heavy metals. Heavy metals, 1, 3-11.

Konwer, S., Boruah, R., and Dolui, S. K. (2011). Studies on conducting polypyrrole/graphene oxide composites as supercapacitor electrode. Journal of electronic materials, 40, 2248-2255.

Krasovska, M., Gerbreders, V., Mihailova, I., Ogurcovs, A., Sledevskis, E., Gerbreders, A., and Sarajevs, P. (2018). ZnO-nanostructure-based electrochemical sensor: Effect of nanostructure morphology on the sensing of heavy metal ions. Beilstein Journal of Nanotechnology, 9, 2421–2431.

Kulandaivalu, S., Suhaimi, N., and Sulaiman, Y. (2019). Unveiling high specific energy supercapacitor from layer-by-layer assembled polypyrrole/graphene oxide polypyrrole/manganese oxide electrode material. Scientific reports, 9(1), 4884.

Kumar, A., Kumar, A., Mudila, H., and Kumar, V. (2020, May). Synthesis and thermal analysis of polyaniline (PANI). In Journal of Physics: Conference Series 1531(1), 012108.

Kumar, M., and Puri, A. (2012). A review of permissible limits of drinking water. Indian journal of occupational and environmental medicine, 16(1), 40-44.

Le, T. H., Kim, Y., and Yoon, H. (2017). Electrical and electrochemical properties of conducting polymers. Polymers, 9(4), 150.

Lee, S., Oh, J., Kim, D., and Piao, Y. (2016). A sensitive electrochemical sensor using an iron oxide/graphene composite for the simultaneous detection of heavy metal ions. Talanta, 160, 528–536.

Li, L., Xia, K., Li, L., Shang, S., Guo, Q., and Yan, G. (2012). Fabrication and characterization of free-standing polypyrrole/graphene oxide nanocomposite paper. Journal of Nanoparticle Research, 14, 1-8.

Li, S., Lu, X., Xue, Y., Lei, J., Zheng, T., and Wang, C. (2012). Fabrication of Polypyrrole/Graphene Oxide Composite Nanosheets and Their Applications for Cr(VI) Removal in Aqueous Solution. PLoS ONE, 7(8), e43328.

Liang, F., Liu, Z., and Liu, Y. (2017). Enhanced electrochemical properties of MnO2/PPy nanocomposites by miniemulsion polymerization. Journal of Materials Science: Materials in Electronics, 28, 10603-10610.

Liao, J., Song, Y., Wang, R., Zeng, Y., Si, H., Ge, C., and Lin, S. (2021). A synergistic promotion strategy for selective trapping and sensing of lead (II) by oxygen-vacancy and surface modulation of MnO2 nanoflowers. Sensors and Actuators B: Chemical, 345, 130384.

Lo, M., Diaw, A. K., Gningue-Sall, D., Aaron, J. J., Oturan, M. A., and Chehimi, M. M. (2018). Tracking metal ions with polypyrrole thin films adhesively bonded to diazonium-modified flexible ITO electrodes. Environmental Science and Pollution Research, 25, 20012-20022.

Luyen, N. D., Trang, H. T., Khang, P. Y., Thanh, N. M., Vu, H. X. A., Phong, N. H., and Khieu, D. Q. (2024). Simultaneous determination of Pb (II) and Cd (II) by electrochemical method using ZnO/ErGO-modified electrode. Journal of Applied Electrochemistry, 54(4), 917-933.

Masindi, V., and Muedi, K. L. (2018). Environmental contamination by heavy metals. *Heavy metals*, 10(4), 115-133.

Mitra, S., Chakraborty, A. J., Tareq, A. M., Emran, T. B., Nainu, F., Khusro, A., ... and Simal-Gandara, J. (2022). Impact of heavy metals on the environment and human health: Novel therapeutic insights to counter the toxicity. Journal of King Saud University-Science, 34(3), 101865.

Mudila, H., Prasher, P., Kumar, M., Kapoor, H., Kumar, A., Zaidi, M. G. H., and Verma, A. (2019). An insight into Cadmium poisoning and its removal from aqueous sources by Graphene Adsorbents. International Journal of Environmental Health Research, 29(1), 1-21.

Mudila, H., Zaidi, M. G. H., Rana, S., Joshi, V., and Alam, S. (2013). Enhanced electrocapacitive performance of graphene oxide polypyrrole nanocomposites. International Journal of Chemical and Analytical Science, 4(3), 139–145.

Muralikrishna, S., Nagaraju, D. H., Balakrishna, R. G., Surareungchai, W., Ramakrishnappa, T., and Shivanandareddy, A. B. (2017). Hydrogels of polyaniline with graphene oxide for highly sensitive electrochemical determination of lead ions. Analytica chimica acta, 990, 67-77.

Namsheer, K., and Rout, C. S. (2021). Conducting polymers: a comprehensive review on recent advances in synthesis, properties and applications. RSC advances, 11(10), 5659-5697.

Naveen, M. H., Gurudatt, N. G., and Shim, Y. B. (2017). Applications of conducting polymer composites to electrochemical sensors: A review. Applied materials today, 9, 419-433.

Ningaraju, S., Jagadish, K., Srikantaswamy, S., Prakash, A. G., and Ravikumar, H. B. (2019). Synthesis of graphite oxide nanoparticles and conductivity studies of PSF/GO and PSAN/GO polymer nanocomposites. Materials Science and Engineering: B, 246, 62-75.

Niu, T., Li, J., Qi, Y., Huang, X., and Ren, Y. (2021). Preparation and electrochemical properties of α-MnO2/rGO-PPy composite as cathode material for zinc-ion battery. Journal of Materials Science, 56(29), 16582–16590.

Oularbi, L., Turmine, M., and El Rhazi, M. (2017). Electrochemical determination of traces lead ions using a new nanocomposite of polypyrrole/carbon nanofibers. Journal of Solid State Electrochemistry, 21, 3289-3300.

Palanisamy, S., Thangavelu, K., Chen, S. M., Velusamy, V., Chang, M. H., Chen, T. W., ... and Ramaraj, S. K. (2017). Synthesis and characterization of polypyrrole decorated graphene/β-cyclodextrin composite for low-level electrochemical detection of mercury (II) in water. Sensors and Actuators B: Chemical, 243, 888-894.

Palsaniya, S., Nemade, H. B., and Dasmahapatra, A. K. (2021). Hierarchical PANI-RGO-ZnO ternary nanocomposites for symmetric tandem supercapacitor. Journal of Physics and Chemistry of Solids, 154, 110081

Promphet, N., Rattanarat, P., Rangkupan, R., Chailapakul, O., and Rodthongkum, N. (2015). An electrochemical sensor based on graphene/polyaniline/polystyrene nanoporous fibers modified electrode for the simultaneous determination of lead and cadmium. Sensors and Actuators B: Chemical, 207, 526-534.

Pruna, A., Shao, Q., Kamruzzaman, M., Zapien, J. A., and Ruotolo, A. (2016). Enhanced electrochemical performance of ZnO nanorod core/polypyrrole shell arrays by graphene oxide. Electrochimica Acta, 187, 517-524.

Qian, W. U., Hong-Mei, B. I., and Xiao-Jun, H. A. N. (2021). Research progress of electrochemical detection of heavy metal ions. Chinese Journal of Analytical Chemistry, 49(3), 330-340.

Quintana, H., Ramírez, J. L., Rubio, E. F., Marquez, E., González, G., González, G., and Uruchurtu, J. (2013). Electrochemical sensor based on polypyrrole for the detection of heavy metals in aqueous solutions. ECS Transactions, 47(1), 265.

Ramachandran, T., and Dhayabaran, V. V. (2019). Utilization of a MnO2/polythiophene/rGO nanocomposite-modified glassy carbon electrode as an electrochemical sensor for methyl parathion. Journal of Materials Science: Materials in Electronics, 30(13), 12315–12327.

Ramalechume, C., Keerthana, S., and Mercy Andrew Swamidoss, C. (2020). Electrochemical detection of heavy metals using carbon quantum dots modified with metal oxides. Materials Today: Proceedings. doi:10.1016/j.matpr.2020.10.693

Rehman, A. U., Ikram, M., Kan, K., Zhao, Y., Zhang, W. J., Zhang, J., ... and Shi, K. (2018). 3D interlayer nanohybrids composed of reduced graphenescheme oxide/SnO2/PPy grown from expanded graphite for the detection of ultra-trace Cd2+, Cu2+, Hg2+ and Pb2+ ions. Sensors and Actuators B: Chemical, 274, 285-295.

Rong, R., Zhao, H., Gan, X., Chen, S., and Quan, X. (2017). An electrochemical sensor based on graphene-polypyrrole nanocomposite for the specific detection of Pb (II). Nano, 12(01), 1750008.

Ruecha, N., Rodthongkum, N., Cate, D. M., Volckens, J., Chailapakul, O., and Henry, C. S. (2015). Sensitive electrochemical sensor using a graphene–polyaniline nanocomposite for simultaneous detection of Zn (II), Cd (II), and Pb (II). Analytica chimica acta, 874, 40-48.

Sanyal, K., Chappa, S., Bahadur, J., Pandey, A. K., and Mishra, N. L. (2020). Arsenic quantification and speciation at trace levels in natural water samples by total reflection X-ray fluorescence after pre-concentration with N-methyl-d-glucamine functionalized quartz supports. Journal of Analytical Atomic Spectrometry, 35(11), 2770-2778.

Sebastian, N., Yu, W. C., Hu, Y. C., Balram, D., and Yu, Y. H. (2022). Morphological evolution of nanosheets-stacked spherical ZnO for preparation of GO-Zn/ZnO ternary nanocomposite: A novel electrochemical platform for nanomolar detection of antihistamine promethazine hydrochloride. Journal of Alloys and Compounds, 890, 161768.

Seenivasan, R., Chang, W. J., and Gunasekaran, S. (2015). Highly sensitive detection and removal of lead ions in water using cysteine-functionalized graphene oxide/polypyrrole nanocomposite film electrode. ACS applied materials and interfaces, 7(29), 15935-15943.

Sharif, M., Heidari, A., and Aghaeinejad Meybodi, A. (2021). Polythiophene/zinc oxide/graphene oxide ternary photocatalyst: synthesis, characterization and application. Polymer-Plastics Technology and Materials, 60(13), 1450-1460.

Singh, G., Gupta, N., Kumar, A., Prasher, P., and Mudila, H. (2025). Systematic development of PPY/GO/ZnO hybrid composite for electrochemical detection of Pb2+ in aqueous solution. Ionics, 1-15.

Singh, G., Nisha, A. K., and Mudila, H. (2023). Comparative study on the electrochemical performance of PPY/GO binary and PPY-GO/ZnO ternary nanocomposites. Bulgarian Chemical Communications, 55(A), 37-43

Singh, G., Nisha, Kumar, A., Prasher, P., and Mudila, H. (2022). Assessment of toxicity and electrochemical sensing of arsenic in aqueous sources. Journal of Environmental Engineering and Science, 18(1), 10-23.

Smarzewska, S., and Ciesielski, W. (2015). Application of a graphene oxide—carbon paste electrode for the determination of lead in rainbow trout from central Europe. Food Analytical Methods, 8, 635-642.

Song, J., Wang, X., and Chang, C. T. (2014). Preparation and characterization of graphene oxide. Journal of Nanomaterials, 2014(1), 276143.

Song, Y., Bian, C., Hu, J., Li, Y., Tong, J., Sun, J., ... and Xia, S. (2019). Porous polypyrrole/graphene oxide functionalized with carboxyl composite for electrochemical sensor of trace cadmium (II). Journal of The Electrochemical Society, 166(2), B95.

Sosa Lissarrague, M. H., Alshehri, S., Alsalhi, A., Lassalle, V. L., and López Corral, I. (2023). Heavy metal removal from aqueous effluents by TiO2 and ZnO nanomaterials. Adsorption Science & Technology, 2023, 2728305.

Sun, H., Wang, C., Xu, Y., Dai, D., Deng, X., and Gao, H. (2019). A novel electrochemical sensor based on A glassy carbon electrode modified with GO/MnO2 for simultaneous determination of trace Cu (II) and Pb (II) in environmental water. ChemistrySelect, 4(40), 11862-11871.

Suvina, V., Krishna, S. M., Nagaraju, D. H., Melo, J. S., and Balakrishna, R. G. (2018). Polypyrrole-reduced graphene oxide nanocomposite hydrogels: A promising electrode material for the simultaneous detection of multiple heavy metal ions. Materials Letters, 232, 209-212.

Tchounwou, P. B., Yedjou, C. G., Patlolla, A. K., and Sutton, D. J. (2012). Heavy metal toxicity and the environment. Molecular, clinical and environmental toxicology: volume 3: environmental toxicology, 133-164.

Velempini, T., Pillay, K., Mbianda, X. Y., and Arotiba, O. A. (2018). Application of a polypyrrole/carboxy methyl cellulose ion imprinted polymer in the electrochemical detection of mercury in water. Electroanalysis, 30(11), 2612-2619.

Verma, S., Bhatt, P., Verma, A., Mudila, H., Prasher, P., and Rene, E. R. (2021). Microbial technologies for heavy metal remediation: effect of process conditions and current practices. Clean Technologies and Environmental Policy, 1-23.

Wanekaya, A., and Sadik, O. A. (2002). Electrochemical detection of lead using overoxidized polypyrrole films. Journal of Electroanalytical Chemistry, 537(1-2), 135-143.

Xu, T., Dai, H., and Jin, Y. (2020). Electrochemical sensing of lead (II) by differential pulse voltammetry using conductive polypyrrole nanoparticles. *Microchimica Acta*, 187, 1-7.

Yadav, V. B., Gadi, R., and Kalra, S. (2019). Adsorption of lead on clay-CNT nanocomposite in aqueous media by UV-Vis-spectrophotometer: kinetics and thermodynamic studies. Emergent Materials, 2, 441-451.

Yukird, J., Kongsittikul, P., Qin, J., Chailapakul, O., and Rodthongkum, N. (2018). ZnO@ graphene nanocomposite modified electrode for sensitive and simultaneous detection of Cd (II) and Pb (II). Synthetic Metals, 245, 251-259.

Yussuf, A., Al-Saleh, M., Al-Enezi, S., and Abraham, G. (2018). Synthesis and characterization of conductive polypyrrole: the influence of the oxidants and monomer on the electrical, thermal, and morphological properties. International Journal of Polymer Science, 2018(1), 4191747...

Zhang, H., Li, Y., Zhang, Y., Wu, J., Li, S., and Li, L. (2023). A disposable electrochemical sensor for lead ion detection based on in situ polymerization of conductive polypyrrole coating. Journal of Electronic Materials, 52(3), 1819-1828.

Zhang, Q. X., Wen, H., Peng, D., Fu, Q., and Huang, X. J. (2015). Interesting interference evidence of electrochemical detection of Zn (II), Cd (II) and Pb (II) on three different morphologies of MnO2 nanocrystals. Journal of Electroanalytical Chemistry, 739, 89-96.

Zhou, H., Yan, Z., Yang, X., Lv, J., Kang, L., and Liu, Z.-H. (2016). RGO/MnO2 /polypyrrole ternary film electrode for supercapacitor. Materials Chemistry and Physics, 177, 40–47

Zhou, X. (2024). Electrochemical detection of heavy metal ions in water using MWCNT/ZnO nanocomposite. International Journal of Electrochemical Science, 19(5), 100559.

Zhu, X., Tong, J., Bian, C., Gao, C., and Xia, S. (2017). The polypyrrole/multiwalled carbon nanotube modified au microelectrode for sensitive electrochemical detection of trace levels of Pb2+. Micromachines, 8(3), 86.

Zhuang, Y., Zhao, M., He, Y., Cheng, F., and Chen, S. (2018). Fabrication of ZnO/rGO/PPy heterostructure for electrochemical detection of mercury ion. Journal of Electroanalytical Chemistry, 826, 90-95.

#### **RESEARCH**



# Systematic development of PPY/GO/ZnO hybrid composite for electrochemical detection of Pb<sup>2+</sup> in aqueous solution

Goverdhan Singh<sup>1</sup> · Nisha Gupta<sup>1</sup> · Anil Kumar<sup>1</sup> · Parteek Prasher<sup>2</sup> · Harish Mudila<sup>1</sup>

Received: 26 October 2024 / Revised: 9 December 2024 / Accepted: 5 January 2025 © The Author(s), under exclusive licence to Springer-Verlag GmbH Germany, part of Springer Nature 2025

#### **Abstract**

The accumulation of heavy metals in water sources at levels exceeding acceptable limits poses a serious risk to human health and the environment. Various electrochemical methods and electroactive materials have been employed to identify and measure these metal ions. However, effective, low-cost, sensitive, and stability, with low detection limit and high reproducibility, are the major requirements of such sensing materials. In this regard, an enhanced hybrid ternary composite PGT based on polypyrrole, GO, and ZnO (PPY/GO/ZnO) has been fabricated and is reportedly being used for the first time to identify lead (Pb<sup>2+</sup>) ions at the trace level in aqueous solutions. The ternary composite was characterized using Fourier transform-infrared spectroscopy (FTIR), X-ray diffraction (XRD), X-ray photoelectron spectroscopy (XPS), scanning electron microscopy (SEM), and thermogravimetric analysis (TGA) to study its structural, morphological, and thermal properties. The electrochemical response of the composite material was analyzed using cyclic voltammetry (CV) and electron impedance spectroscopy (EIS) in potassium ferricyanide as a redox probe. The sensitivity, selectivity, and reproducibility of the PGT were studied via the differential pulse anodic stripping voltammetry (DPASV) technique. The electrode material shows a good linear response ( $R^2 = \sim 0.98$ ) with a limit of detection of 0.05  $\mu$ M for Pb<sup>2+</sup> ions within the concentration range of 0.3 to 3  $\mu$ M. The reproducibility RSD (relative standard deviation, 1.089%), stability RSD (3.67%), and interference of the working electrode in the presence of other metal ions (Cd<sup>2+</sup> and Cu<sup>2+</sup>) show a good response. These results represent the possibilities of employing the PGT electrode to effectively detect other heavy metal ions from aqueous sources.

**Keywords** Polypyrrole · Graphene oxide · Heavy metal ion · DPASV · Zinc oxide · Pollution

#### Introduction

Numerous anthropogenic and natural sources discharge heavy metals (HMs) into the different strata (air, soil, and water) of the environment. Through their excess concentration in the environment, these HMs lead to retard the environment's ability to promote life. This directs toward threatening the health of plants, animals, and humans [1, 2]. HM toxicity to organisms is influenced by various factors such as the nature of HMs, the organism exposed to HMs, and the duration of exposure [3]. HMs like Pb, Cu, As, Zn, Hg, and Cr are reported as the most prevailing environmental

pollutants by the United States Environmental Protection Agency (USEPA) report [4]. Among the variety of HMs, lead (Pb) is considered a hazardous environmental pollutant, affecting both human and animal neurological, immunological, reproductive, and digestive systems. Furthermore, Pb<sup>2+</sup> ion buildup in the body has a serious negative impact on children's neurobehavioral development, raises blood pressure, damages the kidneys, and results in anemia [5]. Various organizations viz. environmental protection agency (EPA, 0.015 mg/L), World Health Organization (WHO, 0.01 mg/L), and Central Pollution Control Board (CPCB, 0.01 mg/L) have set certain permissible limits of concentrations of Pb<sup>2+</sup> ion to be present in various potable waters [6]. Therefore, the detection and determination of Pb<sup>2+</sup> ions present in the various samples is of supreme importance in monitoring the environmental quality.

A variety of techniques ranging from analytical to electrochemical are employed for the detection of these HM (including Pb<sup>2+</sup>) contaminants from various sources.

Published online: 11 January 2025



Harish Mudila harismudila@gmail.com

Department of Chemistry, Lovely Professional University, Punjab 144411, India

<sup>&</sup>lt;sup>2</sup> Department of Chemistry, UPES, Dehradun 248007, India

## Comparative study on the electrochemical performance of PPY/GO binary and PPY-GO/ZnO ternary nanocomposites

G. Singh, Nisha, A. Kumar, H. Mudila\*

Department of Chemistry, Lovely Professional University, Phagwara, Punjab-144411, India

Received: April 03, 2023; Revised: April 27, 2023

PPY/GO binary nanocomposites (PGs) and PPY-GO/ZnO ternary nanocomposites (PGZs) as electrode material were synthesized *via* the *ex-situ* method. The PGs, prepared by varying the proportions of GO (%w/w) in PPY, were characterized by FTIR, XRD, TGA, and electrochemical measurements. The PGs were analyzed by cyclic voltammetry (CV) for their electrochemical performance. The binary composite (PG5) having the highest specific capacitance (Cs=391.3 F/g) value was preferred for the preparation of ternary composites, i.e., PGZs with ZnO in different ratios (%w/w) by the *ex-situ* method. The highest specific capacitance of 352.1 F/g was obtained for PGZ-1 at 1 mV/s which is lower than for its binary counterpart (PG5) but was higher than those of ZnO, PPY, and GO. The incorporation of GO has enhanced the electrochemical performance of PGs, however, the encapsulation of ZnO in PG was found to decrease the electrochemical response of PGZs. The result suggested this to occur due to the disorder caused in the PPY chains by ZnO.

**Keywords:** Conducting polymer; Composites; Capacitance; Graphene oxide; Transition metal oxide, Clean energy.

#### INTRODUCTION

Conventional energy sources are largely employed to encounter the need for the energy required in various aspects of life. The use of these energy sources at a tremendous rate is the major contributor to climate changes such as air pollution, global warming, etc. [1]. To overcome these issues there is a great need to develop energy techniques that are readily available and environmentally friendly. Among the various energy sources, electrochemical supercapacitors are considered the potent candidates widely used in power inventors, electrochemical actuators, power supplies, etc. The mechanism of charge storage in supercapacitors is based on (a) electrochemical double-layer capacitors (EDLC) or (b) fast and reversible redox reactions that take place on the interface of electrodes and electrolytes (pseudo capacitors) [1, 2]. Various types of electroactive material, viz., carbonaceous material, conducting polymers (CPs), and transition metal oxides (TMOs) are employed as the electrode material in supercapacitors. CPs are appropriate as an electrode because of their high porosity, storage ability, and reversibility but they lack cyclic stability charging-discharging rate. drawbacks can be improved by entering structural changes in CPs by hybridizing them with other electroactive materials [2-4]. CPs with carbonaceous material like graphene oxide (GO) show a synergetic effect and produce an electrode with high capacitance behavior [5].

TMOs having pseudo capacitive behavior act as a filler between the CPs and carbonaceous material that may improve the electrolyte-electrode interaction resulting in the fast diffusion of ions and hence improving the capacitive behavior of the electrode material [3, 6]. However, some studies show a decrease in performance with the addition of TMO in the matrix [4]. Nowadays a variety of CPs (polypyrrole, polyaniline, etc.) are hybridized with carbonaceous material (GO, rGO, etc.), and TMOs (ZnO, V<sub>2</sub>O<sub>5</sub>, and others) to form ternary composites used in supercapacitors for the storage of the electrochemical energy [7, 8]. This work presents the fabrication of PPY/GO binary nanocomposites (PGs) and PPY-GO/ZnO ternary nanocomposites (PGZs). The as-fabricated PGs and PGZs were further studied for their electrochemical performance by cyclic voltammetry (CV).

#### MATERIALS AND METHODS

#### Materials

Monomer pyrrole (PY, >99%, Spectrochem), graphite powder, potassium permanganate (KMnO<sub>4</sub>), sulfuric acid (H<sub>2</sub>SO<sub>4</sub>), hydrogen peroxide (H<sub>2</sub>O<sub>2</sub>), and hydrochloric acid (HCl) were acquired from Loba Chemie. Ferric chloride (FeCl<sub>3</sub>), and PVDF (polyvinylidene fluoride) were from Sigma Aldrich, N- cetyl -N, N, N- trimethyl ammonium bromide (CTAB), and ascorbic acid were obtained from S D Fine Chem. Ltd.

<sup>\*</sup> To whom all correspondence should be sent: E-mail: harismudila@gmail.com



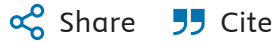
### Journal of the Indian Chemical Society

Volume 102, Issue 6, June 2025, 101718

# rGO/ZnO modified polyaniline hybrid ternary nanocomposite as highly sensitive electrode for Pb<sup>2+</sup> detection in aqueous sources

Nisha a, Goverdhan Singh a, Anil Kumar a, Parteek Prasher b, Harish Mudila A 🖰 🖾

Show more ✓





https://doi.org/10.1016/j.jics.2025.101718 7 Get rights and content  $\pi$ 

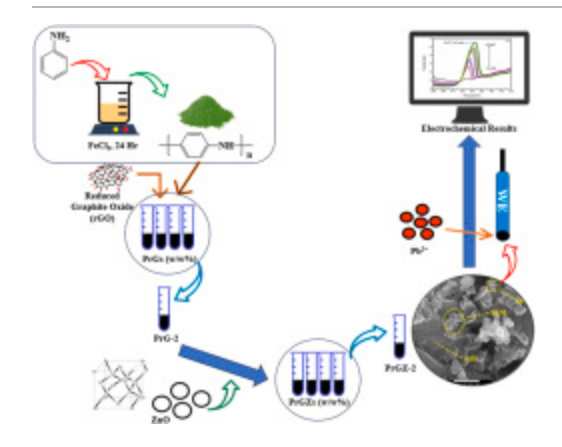
## **Highlights**

- PrGZ-2 represents a high sensitivity with a LOD of 0.3μM and excellent linearity (R<sup>2</sup>) 0.994.
- PrGZ-2 reveals an improved electron transfer, low resistance, and enhanced Pb<sup>2+</sup> detection efficiency.
- The ternary hybrid composite exhibits a low RSD (2.13%) and strong repeatability and stability, ensuring reliable Pb<sup>2+</sup> detection.
- PrGZ-2 maintains high sensitivity and selectivity in the presence of Cd<sup>2+</sup> and Cu<sup>2+</sup>, marking its suitability for environmental monitoring.

#### **Abstract**

This research work demonstrates the effective determination of Pb<sup>2+</sup> ions from aqueous sources using systematically developed ternary nanocomposites (PrGZs). These nanocomposites were synthesized through a judicious combination of Polyaniline (PANI), reduced Graphene Oxide (rGO), and Zinc Oxide (ZnO). The physical properties of PrGZs were characterized using techniques such as Fourier Transform Infrared Spectroscopy (FTIR), Xray Diffraction (XRD), Thermogravimetric Analysis (TGA), Differential Scanning Calorimetry (DSC), and Scanning Electron Microscopy (SEM). The electrochemical performance of PrGZs was evaluated using Electrochemical Impedance Spectroscopy (EIS) and Differential Pulse Anodic Stripping Voltammetry (DPASV) with a carbon paste electrode (CPE). Notably, PrGZ-2 exhibited significantly improved detection and sensitivity compared to the individual components and binary composite, attributed to its low resistance, pseudo-capacitive behaviour, and enhanced electron transfer properties. The calculated limits of detection (LOD) and quantification (LOQ) for PrGZ-2 were 0.3μM and 1.16μM, respectively, within a Pb<sup>2+</sup> ion concentration range of 1μM–5.5μM. This indicates good sensitivity for low concentration detection, with an R<sup>2</sup> value of 0.994. The relative standard deviation (RSD) for PrGZ-2 was 2.13%, confirming acceptable repeatability and precision of the measurements on the working electrode at a scan rate of 0.01 V/s. Furthermore, the composite material displayed good results in the presence of interfering metals and demonstrated appreciable repeatability and stability. These findings suggest that the material holds significant potential and could be evaluated for detecting other toxic heavy metals, expanding its application for environmental monitoring without interference from lead.

## Graphical abstract



Download: Download high-res image (221KB)

Download: Download full-size image

## Synthesis of PANI-GO and PANI-rGO nanocomposites and their electrochemical performance

Nisha<sup>1</sup>, G. Singh<sup>1</sup>, A. Kumar<sup>1</sup>, P. Prasher<sup>2</sup>, H. Mudila<sup>1\*</sup>

<sup>1</sup>Department of Chemistry, Lovely Professional University, Phagwara, Punjab-144411, India <sup>2</sup>Department of Chemistry, UPES, Dehradun, 248007, India

Received: March 27, 2023; Revised: April 30, 2023

In this work, a series of binary nanocomposites (PGs and PGRs) were synthesized by adding a varying percentage of GO and rGO to the matrix of polyaniline (PANI). PANI was synthesized by the chemical oxidative method, while GO was synthesized through the modified Hummers method and was further reduced to rGO. All the individual material and composite materials were analyzed through FTIR, XRD, TGA-DSC, and SEM analysis. The electrochemical performance was studied *via* cyclic voltammetry for the PANI, GO, PGs, and PGRs in the potential range of -0.5 to 0.5 V at varying scans (1 to 500 mV/s). The specific capacitance of PANI, GO, and rGO was found to be 169.57, 248.69, and 279.34 F/g while the maximum specific capacitance for the binary composites for PG-5 and PGR-5 was found to be 367 and 1231 F/g respectively.

Keywords: Polyaniline, Reduced graphene oxide, Electrochemical sensor, Clean energy, Cyclic voltammetry.

#### INTRODUCTION

Conductive polymers (CPs) are of great interest because of their incomparable properties like high surface area, multi-redox reaction, thermal resistance, and chemical stability. Out of various CPs, polyaniline (PANI) possesses a wide range of electrical properties and is a great choice because of its ease of synthesis [1, 2]. Apart from the CPs, nowadays carbon-containing materials like graphite oxide (GO) and reduced graphite oxide (rGO) provide a capable preliminary material for the fabrication of composites with CPs due to defects and potential functionalization [1, 2]. GO is a single sheet having oxygen-containing functional groups like -OH, C-O-C, and -COOH groups [3] whereas rGO has extraordinary physical and chemical properties, a 2D form of graphite, sp<sup>2</sup> hybridization, great mechanical properties, electron transport, high surface area, and great conductivity. rGO has a honeycomb-like structure in which one strong bond C-C is present in the plane and another  $\pi$ -bond is present out of the plane having a delocalized network, this structure is important for the availability of electrons for conduction [2, 3]. Numerous improvements have been made to CPs and carbon-containing compounds to form their composites for the reason that they provide low cost, save time, and give a better result of conductivity by acting as electroactive material [4-6].

In this experimental work, systematic studies have been carried out on the fabrication and electrochemical activity of the PANI-GO (PGs) and

PANI-rGO (PGR) composites. The present work involves the formation of a binary composite with different ratios of PANI with GO and rGO (w/w %) by a simple route of *ex-situ* polymerization. The fabricated composites were characterized using FTIR, XRD, TGA, DSC, and SEM. These composites were found to have great electroactive properties when studied for their specific capacitance determined by cyclic voltammetry (CV).

#### MATERIALS AND METHOD

#### Materials

Chemicals like aniline (p=1.021 g/ml, LOBA Chemie), SDS (sodium dodecyl sulfate, Qualikems Fine chem.) ferric chloride (Alpha Chemika), graphite (LOBA Chemie Pvt Ltd), sulfuric acid (Avantor Performance Materials India Ltd), potassium permanganate (Hi-Media Laboratories Pvt. Ltd.), sodium nitrate (Avarice Industries), hydrogen peroxide, hydrochloric acid, hydrazine hydrate and ethanol were procured from LOBA Chemie Pvt Ltd and the chemicals were not further purified because all chemicals were of analytical quality.

#### Preparation of PANI, GO, and rGO

Preparation of PANI from aniline was carried out by the process mentioned by Bangade *et al. 2020*, in the presence of an anionic surfactant and an oxidant FeCl<sub>3</sub> [7]. GO was formed by the modified Hummers method as explained by Mudila *et al. 2014* [8]. In a beaker deionized water (250 ml) was taken to which

<sup>\*</sup> To whom all correspondence should be sent: E-mail: harismudila@gmail.com

Article Volume 14, Issue 4, 2024, 90 https://doi.org/10.33263/BRIAC144.090

## Studies on Optical Band Gap and Optical Conductivity of Ex-situ Fabricated rGO:V<sub>2</sub>O<sub>5</sub> Composites

Aanchal Sharma <sup>1</sup>, Pawan Sharma <sup>1</sup>, Nandan Singh Karki <sup>2</sup>, Manisha Bisht <sup>2</sup>, Goverdhan Singh <sup>1</sup>, Anil Kumar <sup>1</sup>, and Harish Mudila <sup>1,\*</sup>

- Department of Chemistry; Lovely Professional University, Punjab-144411, India
- Department of Chemistry, L.S.M.G.P.G.C., Pithoragarh-262502, Uttarakhand-262501 India
- \* Correspondence: harismudila@gmail.com;

Scopus Author ID 56372911400

Received: 22.11.2023; Accepted: 20.12.2024; Published: 20.07.2024

**Abstract:** In this present study, Graphene oxide (GO) is synthesized by modified Hummer's method. The GO formed is further used to prepare V<sub>2</sub>O<sub>5</sub> embellished reduced graphene oxide (rGO) composites (rGO: V<sub>2</sub>O<sub>5</sub>) in varying ratios via an in-situ process. UV-Vis spectroscopy was employed to study optical properties such as band gap and optical conductivity of the composites and individual species. rGO synthesized was studied to have a narrow band gap of 1.93 eV, which was much lower than the metal oxide used. Thus, rGO enticing material is to be used to modify the band gap of the prepared composites, thus lowering the optical band gap to 1.32 eV for rGO: V<sub>2</sub>O<sub>5</sub>(2:1) and enhancing the optical conductivity to 5.34×10<sup>10</sup> S.cm<sup>-1</sup>. Characterization of the compound is done using various analytical techniques, including FTIR, SEM, XRD, and TGA. All these studies designate the successful fabrication of the required composites with specific properties. Thus, it is concluded from the study that rGO:V<sub>2</sub>O<sub>5</sub> in 2:1 can be used as a potent material in optoelectronic applications.

**Keywords**: Clean and affordable energy, optical conductivity, optical band gap, reduced graphene oxide,  $V_2O_5$ .

© 2024 by the authors. This article is an open-access article distributed under the terms and conditions of the Creative Commons Attribution (CC BY) license (https://creativecommons.org/licenses/by/4.0/).

#### 1. Introduction

In recent years, the study of the optical properties of material has been an interesting area of research due to the increasing demand for advanced materials with unique electronic and optical properties [1]. In current studies, rGO and V<sub>2</sub>O<sub>5</sub> synthesize a hybrid material with better optical activity than the individual material.

V<sub>2</sub>O<sub>5</sub> was chosen for the research due to its remarkable properties, such as good adsorption in visible regions, electrical conductivity, and great electrochemical performance. Along with this, V<sub>2</sub>O<sub>5</sub> is an easily available and efficacious material [2-4]. rGO has been used due to its ability to act as a supporting material for charge transport. rGO consists of many important properties, such as electrical conductivity, large surface area, and good optical properties [5-8].

Various studies have been done to investigate the optical properties of rGO: V<sub>2</sub>O<sub>5</sub> composites that are obtained by the *ex-situ* fabrication method. One of the important optical properties of these materials is the optical band gap, which measures the energy required to excite the electrons from the valance band to the conduction band. This is a significant property

Singh G, Nisha, Kumar A, Prasher P and Mudila H Assessment of toxicity and electrochemical sensing of arsenic in aqueous sources. Journal of Environmental Engineering and Science, https://doi.org/10.1680/jenes.22.00011 Research Article Paper 2200011 Received 07/02/2022; Accepted 28/09/2022

ICE Publishing: All rights reserved

#### Journal of Environmental Engineering and Science



# Assessment of toxicity and electrochemical sensing of arsenic in aqueous sources

#### Goverdhan Singh PhD

Research Scholar, Department of Chemistry, Lovely Professional University, Phagwara, India

#### Nisha PhD

Research Scholar, Department of Chemistry, Lovely Professional University, Phagwara, India

#### Anil Kumar PhD

Assistant Professor, Department of Chemistry, Lovely Professional University, Phagwara, India

#### Parteek Prasher PhD

Assistant Professor, Department of Chemistry, UPES, Dehradun, India

#### Harish Mudila PhD

Assistant Professor, Department of Chemistry, Lovely Professional University, Phagwara, India (corresponding author: harismudila@gmail.com)





A variety of contaminants present in potable water, including heavy metals, cause numerous health hazards. Arsenic (As) is studied as one of the chief heavy elements hazardous to human beings and other categories of life. Arsenic as a natural constituent of the earth's crust is present in mineral rocks, which are deposited through various natural processes. Moreover, arsenic is also added to groundwater anthropogenically through the burning of fossil fuels, arsenical agrochemicals, wood preservatives and so on. Arsenic (III) (As<sup>III</sup>) and arsenic (V) (As<sup>V</sup>) are toxic inorganic forms in aqueous solution and are responsible for cancer, arsenicosis, vascular diseases and toxicity related to genes, cells, epidemiology and so on. In view of these problems, it is necessary to detect and decontaminate arsenic contamination in potable water. In this paper, brief descriptions are given of the most significant electrochemical methods, due to their advantages such as robustness, speed, accuracy and simplicity. Moreover, techniques such as differential pulse voltammetry, square-wave voltammetry (SWV), stripping chronopotentiometry, anodic stripping voltammetry and cyclic voltammetry (CV) have kept the electrochemical method as a diverse and advanced technique for the sensing process. Furthermore, details of the determination and decontamination of arsenic in potable water through an electrochemical process with a particular focus on SWV and CV are discussed.

**Keywords:** arsenic/cyclic voltammetry/decontamination/electrochemical method/ground water/heavy metals/square-wave voltammetry/ toxicity/UN SDG 3: Good health and well-being/UN SDG 6: Clean water and sanitation

#### **Notation**

 $\begin{array}{ll} E_{\rm step} & \text{potential step} \\ I_1, \ I_2 & \text{current} \\ V & \text{potential} \\ \Delta E & \text{pulse amplitude} \\ \tau & \text{time (s)} \end{array}$ 

#### Introduction

Water, which covers 70% of the earth's crust, is one of the most important natural resources necessary for the good health and well-being and survival of life on earth. As a wonderful natural component, it can dissolve numerous constituents (organic and inorganic chemicals and various other substances) in varying concentrations (Mudila *et al.*, 2018; Obinnaa and Ebere, 2019). The chemicals dissolved in potable water could be beneficial as well as hazardous to the living community consuming that water. A large part of the world is suffering from public health emergencies of incredible proportions due to the scarcity of potable water, while a large community of the world is under threat due to chemical poisoning and contaminants present in groundwater consumed as drinking water (Hussam, 2013; Pooja *et al.*, 2020). Contaminants in

potable water are undesired and may be foreign particles and so on, which are responsible for influencing the normal functioning of a system, and could be of different forms and can be generated from a variety of sources (Sharma and Bhattacharya, 2017). These contaminants, regardless of the source, are hazardous to the ecosystem and hence to all the forms of life present there, particularly humans (Gleick, 2002). According to the report of the World Health Organization (WHO) on potable water for the year 2022, nearly 2 billion people all over the globe depend on contaminated sources, which leads to various waterborne diseases (cholera, diarrhoea, dysentery and typhoid) and other health hazards (Luvhimbi *et al.*, 2022).

A variety of contaminants are present in water coming from different sources. Microbial contamination mainly includes pathogens such as bacteria, parasites, viruses and worms. These pathogens knowingly or unknowingly can reach water sources through human and animal wastes, thus causing distinctive problems in water. Poor water quality, poor hygiene and food sources play a significant role in pathogen exposure leading to the outbreak of waterborne infections such as diarrhoea, dysentery and cholera. Infections caused by

# A comprehensive review on material and techniques used for heavy metal detection in potable water $\bigcirc$

Nisha; Goverdhan; Harish Mudila ➡; Anil Kumar; Parteek Prasher



AIP Conf. Proc. 2800, 020186 (2023) https://doi.org/10.1063/5.0162879





CrossMark

#### Articles You May Be Interested In

Completing the dark matter solutions in degenerate Kaluza-Klein theory

J. Math. Phys. (April 2019)

Gibbs measures based on 1d (an)harmonic oscillators as mean-field limits

J. Math. Phys. (April 2018)

An upper diameter bound for compact Ricci solitons with application to the Hitchin-Thorpe inequality. II

J. Math. Phys. (April 2018)

oril 2018)

500 kHz or 8.5 GHz? And all the ranges in between.

ock-in Amplifiers for your periodic signal measurement







